THE UNIVERSITY OF CALGARY

A Novel Low-Complexity IF-Sampling Receiver

by

Chun Yeung Hung

A THESIS

SUBMITTED TO THE FACULTY OF GRADUATE STUDIES

IN PARTIAL FULFILMENT OF THE REQUIREMENTS FOR

THE DEGREE OF MASTER OF SCIENCE

DEPARTMENT OF ELECTRICAL AND

COMPUTER ENGINEERING

CALGARY, ALBERTA

December, 1996

Abstract

As advances in technology provide faster and cheaper digital hardwares, it is becoming more feasible to implement a receiver in the digital domain. One widely adopted architecture is the IF-sampling receiver which samples the intermediate-frequency signal and recovers the transmitted information in the digital domain. By restricting the modulation to be linear, such as quadrature phase shift keying (QPSK), this thesis proposes a new receiver architecture which employs the minimum sampling rate of 2 samples per symbol and trivial digital processing to recover the inphase and quadrature symbols. In addition to the new receiver architecture, this thesis also presents the design of a zero intersymbol interference signalling pulse specifically for this new receiver. With the new pulse and the new receiver, the effect of sampling timing error on the system performance is investigated. Simulation results indicate that the bit error rate becomes irreducible when the timing error is greater than 15% of the symbol period. Two systems are proposed to combat the timing error problem. The first system is a direct sequence spread spectrum system using 11 chip Barker sequence. This system uses the autocorrelation of the Barker sequence to suppress the intersymbol interference. The second system takes a different approach in which the intersymbol interference is greatly avoided by simply increasing the sampling rate to 4 samples per symbol and making slight changes in the digital structure of the receiver. Simulation results are also obtained to show the performance of the two systems.

Acknowledgments

I would like to thank Dr. M. Fattouche, my supervisor, for his support and guidance in the successful completion of this project. Besides, I would also like to express gratitude to Dr. B.R. Petersen and Dr. S.T. Nichols for their technical expertise. Also I am grateful for the financial supports from both TRLabs and University of Calgary in the form of scholarship and teaching assistantship. Finally, I am deeply indebted to my family for their great support of my education in Canada.

Table of Contents

Approval Page ..... **ii**

Abstract ..... **iii**

Acknowledgments ..... **iv**

Table of Contents ..... **v**

List of Tables ..... **vii**

List of Figures ..... **viii**

Chapter 1 Introduction **1**

1.1 Advantages of Digital Communications 1

1.2 Overview of Receiver Architectures 2

1.3 Thesis Structure 4

Chapter 2 Two Important Concepts for IF-sampling Receiver **5**

2.1 $F_s/4$ Downconversion 5

2.2 Sampling Theorems 14

2.2.1 Nyquist Sampling Theorem 14

2.2.2 Bandpass Sampling Theorem 16

2.2.3 Sampling Theorem for Linearly Modulated Signals with Zero Intersymbol Interference 21

2.3 Summary 25

Chapter 3 The Proposed IF-sampling Receiver **26**

3.1 The Transmitter 26

3.2 The Channel 32

3.3 The Proposed IF-sampling Receiver 35

3.4 Signal Design for the Proposed IF-sampling Receiver 41

3.5 Summary 52

Chapter 4 Performance of the Proposed IF-sampling Receiver **53**
4.1 DQPSK Modulator and Differential DQPSK Detector 53
4.2 The Effect of Bandpass White Noise on the Proposed IF-sampling Receiver 57
4.3 The Equivalent Discrete-time Model 70
4.3.1 The Equivalent Discrete-time Model for Any Signalling Pulse 70
4.3.2 The Equivalent Discrete-time Model for Truncated 100% Excess Bandwidth Duobinary Pulse 74
4.4 Simulation of the IF-sampling system with 100% Excess Bandwidth Duobinary Pulse 84
4.5 Summary 97

Chapter 5 Two Solutions and Their Performance **98**
5.1 Solution 1 : Direct-Sequence Spread-Spectrum IF-sampling System .. 98
5.1.1 Autocorrelation of Barker Sequence 99
5.1.2 The DS-SS IF-sampling Transmitter 101
5.1.3 The Channel 103
5.1.4 The DS-SS IF-sampling Receiver 104
5.1.5 Performance of the DS-SS IF-sampling system 114
5.2 Solution 2 : IF-sampling System with 4 Samples Per Symbol 117
5.2.1 IF-sampling Receiver with 4 Samples Per Symbol 118
5.2.2 Performance of the IF-sampling system with 4 Samples Per Symbol 131
5.3 Summary 133

Chapter 6 Conclusion and Future Work **135**

References **138**

List of Tables

4.3.1 Table of tap weights A, B and C for $0 \le t_d \le 0.25T_p$ 79

4.3.2 Table of tap weights E, F and G for $-0.25T_p \le t_d \le 0$ 83

5.1.1 Values of $y[n]$ for different time offsets n 101

5.1.2 Table of tap weights A_s, B_s and C_s for $0 \le t_d \le 0.25T_c$ 109

5.1.3 Table of tap weights E_s, F_s and G_s for $-0.25T_c \le t_d \le 0$ 112

5.2.1 Values of A_4 and B_4 for $0 \le t_d \le 0.25T_p$ 123

5.2.2 Values of C_4 and D_4 for $-0.25T_p \le t_d \le 0$ 129

List of Figures

2.1.1 Analog quadrature downconverter 5

2.1.2 Graphical representation on the effect of sampling on the cosine and sine carriers with $F_s = 4 \cdot f_{IF}$ 6

2.1.3 Structure of recovering inphase and quadrature samples with $F_s/4$ downconversion. Note that δ[n] denotes the discrete-time delta function 8

2.1.4a Spectrum of $r_{IF}(t)$ 9

2.1.4b Periodic spectrum of $r_{IF}[n]$ 9

2.1.4c Periodic spectrum of the mixed signal 9

2.1.4d Periodic spectrum of the decimated signal 9

2.2.1a Spectrum of the original bandpass signal 15

2.2.1b Spectrum of the sampled bandpass signal with $F_s \geq 2f_{IF} + W$ 15

2.2.2a Spectrum of the continuous-time bandpass signal 19

2.2.2b Spectrum of the sampled signal with $F_s = 4f_o$. A 100% spectral overlap occurs 19

2.2.2c Spectrum of the sampled signal with $F_s = 5f_o$. Spectral overlap is marginally avoided 19

2.2.2d Spectrum of the sampled signal with $F_s = 11f_o$. Spectral overlap occurs 19

2.2.3 Spectrum of the discrete pulse $g(t = nT_p)$ with the sampling of 1 sample per symbol 24

3.1 Block diagram of the bandpass communication system model 27

3.1.1 Detailed block diagram representation of the modulator 28

3.2.1 Power density spectrum of the bandpass white noise 33

3.2.2a Power density spectra of $x(t)$ and $y(t)$ 35

3.2.2b Autocorrelation functions of $x(t)$ and $y(t)$ 35

3.3.1 Architecture of the IF-sampling receiver 35

3.3.2a Spectrum of the RF signal with 100% excess bandwidth 37

3.3.2b Spectrum of the IF signal for $f_{IF} = \frac{0.5}{T_p}$ 37

3.4.1a Time domain zero ISI criterion 47

3.4.1b Frequency domain zero ISI criterion (magnitude response only) 47

3.4.2a Magnitude spectrum of $g(t)$ 48

3.4.2b Magnitude spectrum of the periodic replication of $G(f)$ 48

3.4.3 Magnitude spectrum of zero ISI signalling pulse for $W = \frac{2}{T_p}$ 49

3.4.4 Block diagram of reconstruction process 50

3.4.5 The minimum bandwidth zero ISI signalling pulse 51

4.1.1 Signal constellation showing the relationship between the relative phase shift and the dibit 54

4.1.2 Constellation showing all four possible transmit signal points 55

4.1.3 Differential detection for DQPSK symbols 55

4.2.1 Relationship between $\phi_{xx}(\tau)$ and $\phi_{z_i z_i}[k]$. The same relationship applies between $\phi_{yy}(\tau)$ and $\phi_{z_q z_q}[k]$ 61

4.2.2 Autocorrelation functions $\phi_{xx}(\tau)$ and $\phi_{yy}(\tau)$ for 0% excess bandwidth 62

4.2.3a Power density spectra of $x(t)$ and $y(t)$ for 0% excess bandwidth 63

4.2.3b Power density spectra of $z_i[n]$ and $z_q[n]$ for 0% excess bandwidth 63

4.2.4 Autocorrelation functions of $\phi_{xx}(\tau)$ and $\phi_{yy}(\tau)$ for 50% excess bandwidth 64

4.2.5a Power density spectra of $x(t)$ and $y(t)$ for 50% excess bandwidth..... 65

4.2.5b Power density spectra of $z_i[n]$ and $z_q[n]$ for 50% excess bandwidth..... 65

4.2.6 Autocorrelation functions $\phi_{xx}(\tau)$ and $\phi_{yy}(\tau)$ for 100% excess bandwidth..... 66

4.2.7a Power density spectra of $x(t)$ and $y(t)$ for 100% excess bandwidth..... 67

4.2.7b Power density spectra of $z_i[n]$ and $z_q[n]$ for 100% excess bandwidth..... 67

4.3.1 Equivalent discrete-time model for any signalling pulse..... 72

4.3.2 Equivalent discrete-time model for both original and truncated 100% excess bandwidth duobinary pulse and $t_d = 0$ 76

4.3.3 Equivalent discrete-time model for truncated 100% excess bandwidth duobinary pulse and $0 \le t_d \le 0.25T_p$ 78

4.3.4 Equivalent discrete-time model for truncated 100% excess bandwidth duobinary pulse and $-0.25T_p \le t_d \le 0$ 82

4.4.1 Bit error rate curves for different timing errors. For all cases, $\phi = 0$ 90

4.4.2 Bit error rate curves for different timing errors t_d and phase shifts ϕ 94

4.4.3 Top-left : Constellation of rotated symbols for $\phi = 0^o$ and $t_d = 0$ 96

4.4.3 Top-right : Constellation of asymmetric ISI channel output for $\phi = 0^o$ and $t_d = 0.15T_p$ 96

4.4.3 Bottom-left : Constellation of rotated symbols for $\phi = 45^o$ and $t_d = 0$ 96

4.4.3 Bottom-right : Constellation of asymmetric ISI channel output for $\phi = 45^o$ and $t_d = 0.15T_p$ 96

5.1.1 Transmitter in direct-sequence spread-spectrum IF-sampling system $M = 11$ and $p[n]$ is the 11 chip Barker sequence 102

5.1.2 Architecture of the IF-sampling receiver for DS-SS system 105

5.1.3 Discrete-time Model of the DS-SS IF-sampling system..... 106

5.1.4 Simulated performance of the DS-SS IF-sampling system. Note that the phase shift, $-(\pi t_d / T_c) + \theta$, is zero for all cases 115

5.2.1 Illustration of the safe region for 100% excess bandwidth duobinary pulse..... 117

5.2.2 Architecture of the IF-sampling receiver with 4 samples per symbol and $0 \le t_d \le 0.25T_p$ 118

5.2.3 Equivalent discrete-time model for IF-sampling system with 4 samples per symbol and $0 \le t_d \le 0.25T_p$ 122

5.2.4 Architecture of the IF-sampling receiver with 4 samples per symbol and $-0.25T_p \le t_d \le 0$ 126

5.2.5 Equivalent discrete-time model for IF-sampling system with 4 samples per symbol and $-0.25T_p \le t_d \le 0$ 128

5.2.6 Simulated performance of the IF-sampling system with 4 samples per symbol. Note that $\phi = 0$ 132

Chapter 1 Introduction

In the early days of wireless communications, most commercial systems employed analog modulation techniques for the transmission of voice and video. There were two reasons behind this choice. Unlike digital modulation which requires precise timing information in the receiver, analog modulation does not have this requirement and therefore the receiver architecture for analog modulation tended to be simpler. Secondly, due to a higher availability of analog hardware over digital hardware, it was much easier to implement an analog communications system with off-the-shelf components. Therefore analog modulation was an affordable solution for wireless communications. In the last two decades, digital hardware technology has undergone significant changes. Devices like analog-to-digital (A/D) converters and digital signal processing (DSP) chips have been improved to offer better performance while their size and cost have been reduced due mainly to advances in integrated circuit technology. For such reasons, digital modulation has become a feasible solution for wireless communications.

1.1 Advantages of Digital Communications

There are several benefits exclusively offered by digital communications. Firstly a digital communications system provides a unified means for transmission of any kind of information. From an engineering point of view, information originates in either the analog (eg. voice) or the digital format (eg. computer data). Since information in the digital format is already represented by binary digits, no conversion is necessary and the binary digits can be directly transmitted through the system. On the other hand, in order to transmit analog signals through a digital communications system, an analog-to-digital conversion is required in the transmitter. This conversion is achieved by sampling

followed by quantization and encoding. Although the signal is distorted by the quantization noise, this kind of distortion can be made negligibly small. Once the digital representation of the signal is obtained, a digital communications system can be used to transmit the information and digital-to-analog conversion is performed on the receiver side to reconstruct the original analog signal.

Furthermore, a digital communications system allows system engineers to increase the robustness of the system against natural and man-made disturbances. For example, channel coding is known to be effective in reducing the effect of noise while digital voice encryption protects the conversation against eavesdropping. Lastly a digital system can easily store information for later transmission. This feature makes time division multiple access (TDMA) possible.

1.2 Overview of Receiver Architectures

The architectures of most digital communications receivers can be categorized into three groups [27] : superheterodyne, direct conversion, and IF-sampling receivers.

The superheterodyne receiver is a traditional architecture being used for a long time in analog system. The main idea is to downconvert the received radio frequency (RF) signal into an intermediate frequency (IF) signal through single or multiple stages of mixing and filtering. This idea is extended into a digital system in which the RF signal is first downconverted into an IF signal which is then processed by quadrature downconverter to extract the inphase and quadrature signals. A great virtue of this approach is that the intermediate frequency is fixed. This allows optimization of circuit parameters to operate at the fixed IF. Also standardization can be imposed on the intermediate frequencies so that manufacturers can produce integrated chips (ICs)

operating on those standard intermediate frequencies in large quantities. However, due to the presence of the two analog branches in the quadrature downconverter, phase and gain imbalances [3][28] are introduced on the inphase and quadrature signals, thereby degrading the system performance.

Unlike the superheterodyne architecture, a direct conversion receiver employs a single analog quadrature downconverter to downconvert the RF signal into baseband inphase and quadrature signals in one step. This approach results in lower chip count (that is less complexity) and lower cost . However, as mentioned in [11], this simplicity is deceptive. Some of the realization challenges are the requirement of high-gain low-noise mixer and high-dynamic range baseband channel filters. Also the inphase and quadrature signals suffer gain and phase imbalances.

The third architecture is commonly known as IF-sampling receiver. Similar to the superheterodyne architecture, the IF-sampling receiver downconverts the RF signal to a fixed IF. Thus the virtue of a fixed IF remains in the IF-sampling receiver. After being downconverted, the IF signal is directly sampled and processed in the digital domain to extract the inphase and quadrature signals. Since the analog quadrature downconverter no longer exists in the receiver chain, both amplitude and phase imbalances are completely eliminated. In addition, the IF-sampling receiver requires only one sampler (instead of two in the other two architectures) and thereby reduces cost and power consumption. This architecture has been widely adopted in several projects and papers [4][7][10]. In fact, there are chips [30][31] available using this architecture.

The major difference between the conventional IF-sampling receiver and the one proposed in this thesis is that the receiver architecture in this thesis is specifically designed for linear digital modulation schemes, such as quadrature phase shift keying (QPSK) and quadrature amplitude modulation (QAM). By having this restriction, the

receiver architecture is shown to be much simpler than the generic structure which preserves the inphase and quadrature signals regardless of the type of modulation used.

1.3 Thesis Structure

This thesis is mainly divided into three parts. The first part deals with the design of the newly proposed IF-sampling receiver. Two important concepts, namely $F_s/4$ downconversion and the sampling theorems, are covered in chapter 2. In chapter 3, the complete IF-sampling communications system including the transmitter, channel and receiver architectures is explained in detail. Also with the novel receiver architecture, a new requirement on the signalling pulse for zero intersymbol interference (IS) is found and the derivation is described in chapter 3.

The second part of the thesis focuses on the performance of the novel IF-sampling receiver in the presence of timing error. An equivalent discrete-time model is derived in chapter 4 to provide a better understanding of the distortion. Computer simulation results are also presented in chapter 4 to show the severe degradation caused by the timing error.

In the third part of the thesis, two solutions are proposed to combat the timing error. The first solution is a direct-sequence spread-spectrum system. The second solution takes a different approach in which the timing error distortion is significantly avoided by exploiting the pulse shape of the new zero ISI signalling pulse. Detailed analysis and simulated performances of both solutions are presented in chapter 5.

Finally a summary of the entire thesis and future work is provided in chapter 6.

Chapter 2 Two Important Concepts for IF-sampling Receivers

This chapter presents a detailed review of two important concepts, namely $F_s/4$ downconversion and the sampling theorems, for the design of IF-sampling receivers. These two concepts serve as the foundation on which any IF-sampling receiver is designed. As will be shown in this chapter, the $F_s/4$ downconversion requires a specific relationship between the intermediate frequency and the sampling rate while the sampling theorems govern the minimum sampling rate of the IF-sampling receiver.

2.1 $F_S/4$ Downconversion

In a superheterodyne receiver, the downconversion process is performed by mixing the intermediate frequency (IF) signal with cosine and sine carriers, followed by filtering each channel using a lowpass filter in order to remove the double frequency components. The filtered signals are then sampled by two samplers to obtain samples of the inphase and quadrature signals. This structure is commonly known as analog quadrature downconverter [3][8] and is shown in Figure 2.1.1.

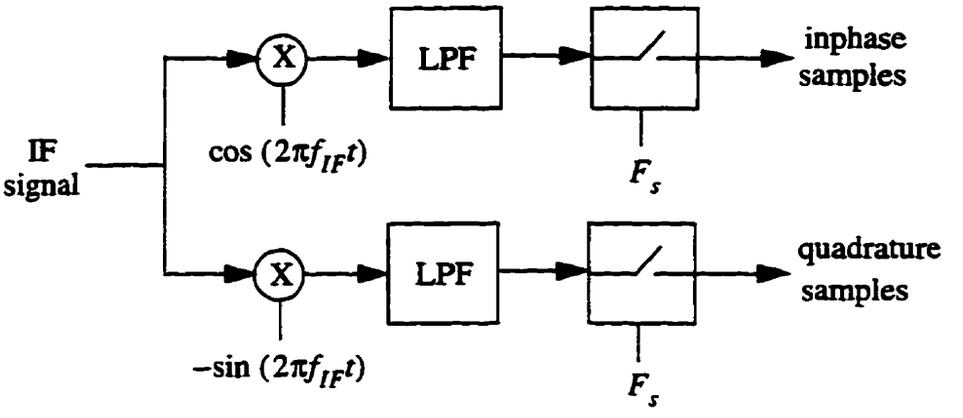

Figure 2.1.1 Analog quadrature downconverter.

A similar outcome can be achieved in the digital domain by sampling the IF signal with at least the Nyquist rate and then mixing it with digitally synthesized cosine and sine carriers. In this case, unlike the analog implementation, a large amount of simplification can be obtained when a technique known as $F_s/4$ downconversion [7][9][10] is used. This technique exploits the fact that when the 2 carriers, $\cos(2\pi f_{IF}t)$ and $\sin(2\pi f_{IF}t)$, are sampled at the specific sampling rate of $F_s = 4 \cdot f_{IF}$ and at the precise sampling times of $t = n/(4f_{IF})$ where $n = 0, 1, 2, \ldots$, the two sampled carriers are periodic sequences taking the values : +1, 0 and -1, that is,

$$\cos(2\pi f_{IF}t)\Big|_{t=\frac{n}{4f_{IF}}} = \cos\left(n\frac{\pi}{2}\right) = \{1, 0, -1, 0, \ldots\} \tag{2.1.1}$$

and

$$\sin(2\pi f_{IF}t)\Big|_{t=\frac{n}{4f_{IF}}} = \sin\left(n\frac{\pi}{2}\right) = \{0, 1, 0, -1, 0, \ldots\} \tag{2.1.2}$$

where f_{IF} is the IF carrier frequency.

These two sampling processes are also shown graphically in Figure 2.1.2 .

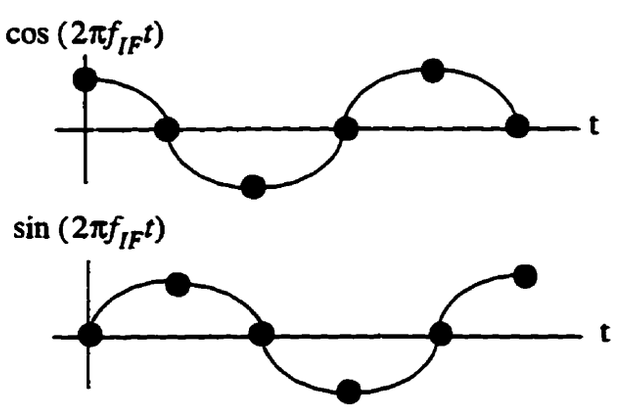

Figure 2.1.2 Graphical representation on the effect of sampling on the cosine and sine carriers with $F_s = 4 \cdot f_{IF}$.

In Figure 2.1.2, the dots represent the sampling points. The frequencies of both cosine and sine carriers are $F_s/4$. Also notice that at the sampling instants of time, whenever the cosine carrier is nonzero (either 1 or -1), the sine carrier must be zero. Similarly, when the sine carrier is nonzero (either 1 or -1), the cosine carrier must be zero. Therefore, when $F_s = 4 \cdot f_{IF}$ and when the sampler precisely samples at the correct instants of time, the sampled sine and cosine carriers are orthogonal.

Assuming that the continuous-time IF signal takes the form,

$$r_{IF}(t) = I(t) \cdot \cos(2\pi f_{IF} t) - Q(t) \cdot \sin(2\pi f_{IF} t) \qquad (2.1.3)$$

where $I(t)$ and $Q(t)$ are the inphase and quadrature signals respectively, then when $r_{IF}(t)$ is sampled by one sampler at a sampling rate of $F_s = 4 \cdot f_{IF}$ and at the precise sampling times of $t = n/(4f_{IF})$, the sampled sequence consists of samples of $I(t)$ interleaved by samples of $Q(t)$ with sign inversions introduced on some of the samples. Mathematically, the sampled IF signal can be represented as,

$$r_{IF}[n] = r_{IF}(t)\Big|_{t=\frac{n}{4f_{IF}}} = \{I_d[0], -Q_d[1], -I_d[2], Q_d[3], \ldots\} \quad (2.1.4)$$

where $I_d[n] = I\left(t = \frac{n}{4f_{IF}}\right)$ and $Q_d[n] = Q\left(t = \frac{n}{4f_{IF}}\right)$

The first sample of $r_{IF}[n]$ corresponds solely to a sample from $I(t)$ while the second sample of $r_{IF}[n]$ corresponds solely to a sample from $Q(t)$. The third sample comes from $I(t)$ and the fourth sample comes from $Q(t)$. So the orthogonality property ensures that when the IF signal is sampled by one sampler, each sample contains information about either the inphase or the quadrature signal, but not about both.

Therefore, with $F_s = 4 \cdot f_{IF}$ or $f_{IF} = F_s/4$, samples of $I(t)$ and $Q(t)$ can be obtained by properly sorting the samples into corresponding I/Q channels and correcting the sign inversions. The whole process is illustrated in Figure 2.1.3.

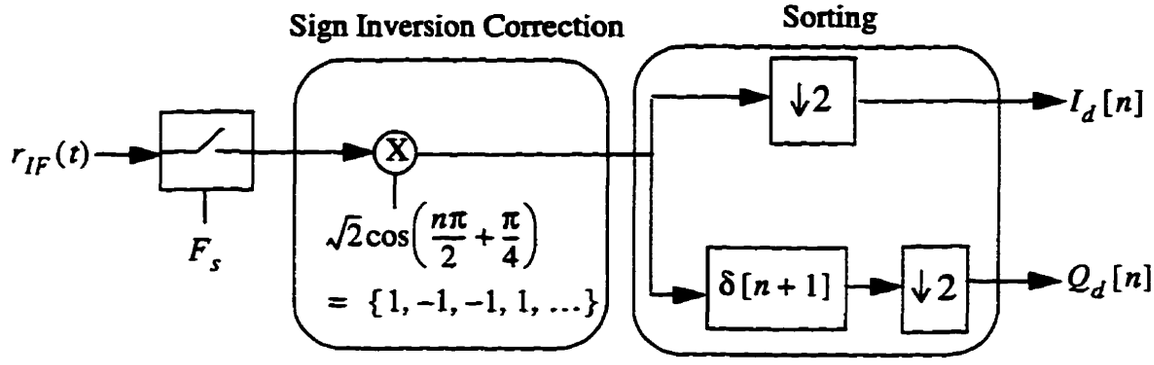

Figure 2.1.3 Structure of recovering inphase and quadrature samples with $F_s/4$ downconversion. Note that δ[n] denotes the discrete-time delta function.

So far $F_s/4$ downconversion has been shown to be an efficient technique to obtain the inphase and the quadrature samples out of an analog IF signal. The price for this simplification however [4][11] is the timing misalignment between the inphase (I) and the quadrature (Q) signals. This timing misalignment problem was addressed by Saulnier et al. [4] who propose to use Hilbert transform to relax it. However, in our design, this problem is solved using a different approach and the solutions are given in Chapter 3.

In addition to the time domain, the architecture (given in Figure 2.1.3) can also be examined in the frequency domain as shown in Figure 2.1.4. Both the spectrum of an analog IF signal $r_{IF}(t)$ and its version $r_{IF}[n]$ are shown in Figure 2.1.4(a) and 2.1.4 (b) respectively.

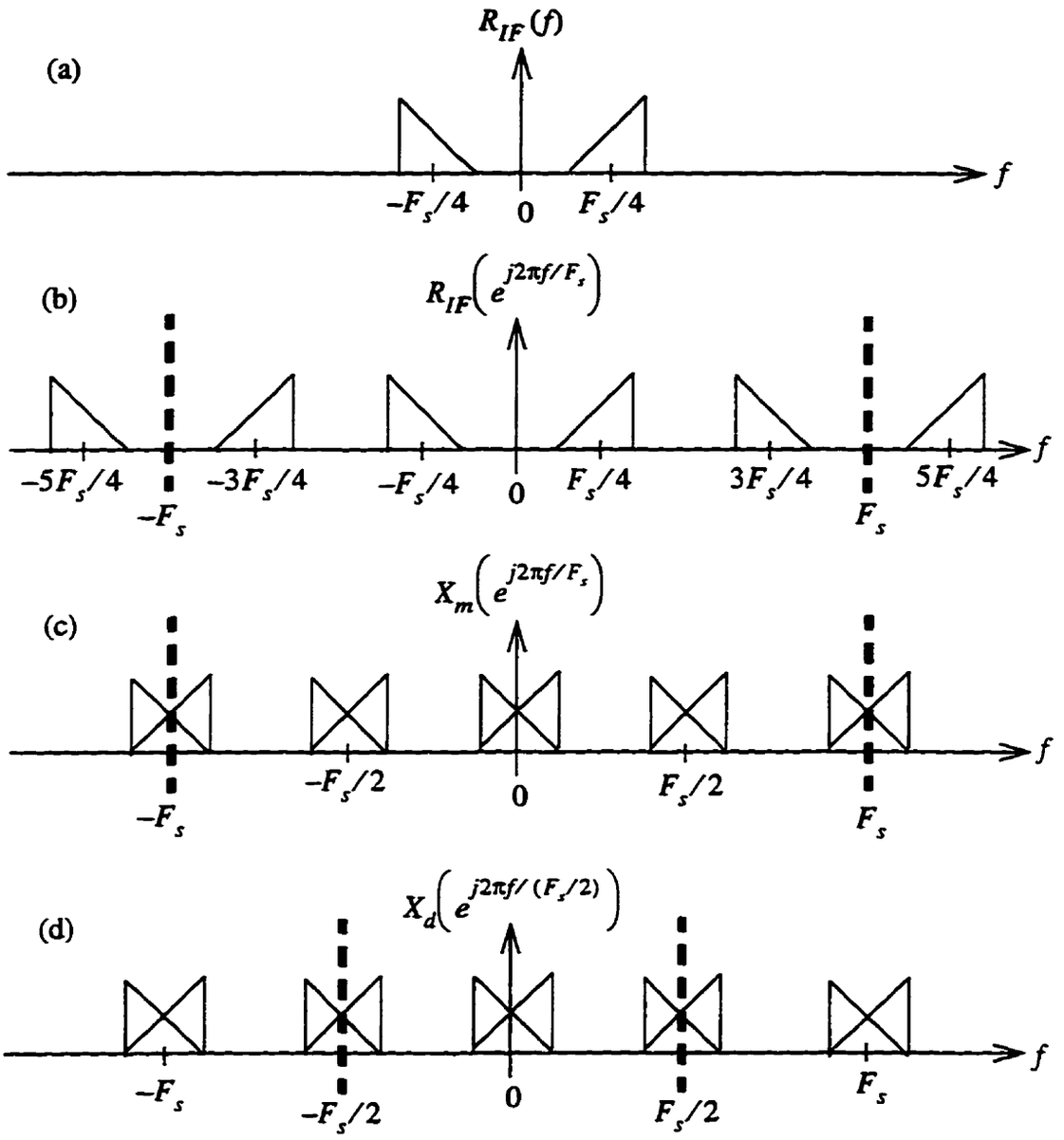

Figure 2.1.4 (a) Spectrum of $r_{IF}(t)$.

(b) Periodic spectrum of $r_{IF}[n]$.

(c) Periodic spectrum of the mixed signal.

(d) Periodic spectrum of the decimated signal.

Here it is assumed that the bandwidth of $r_{IF}(t)$ is small enough such that spectrum overlap is avoided in the sampling process. At the output of the sampler, the sampled sequence is multiplied by $\sqrt{2}\cos\left(\frac{n\pi}{2}+\frac{\pi}{4}\right)$ to correct the sign inversion. Equivalently, this multiplication can also be viewed as mixing in which the spectrum of $r_{IF}[n]$ is convolved with $\frac{\sqrt{2}}{2}\cdot\delta\left(f-\frac{F_s}{4}\right)\cdot e^{j\frac{\pi}{4}}+\frac{\sqrt{2}}{2}\cdot\delta\left(f+\frac{F_s}{4}\right)\cdot e^{-j\frac{\pi}{4}}$ in the frequency domain. The periodic spectrum of the mixed signal is shown in Figure 2.1.4(c). Finally the mixed signal is decimated by a factor of 2 and the output of the decimation contains samples of the inphase signal with a sampling rate of $F_s/2$. In the frequency domain, the spectra of the mixed and decimated signals are related by

$$X_d\left(e^{j2\pi\frac{f}{F_s'}}\right) = \frac{1}{2}\cdot X_m\left(e^{j2\pi\frac{f}{F_s}}\right) + \frac{1}{2}\cdot X_m\left(e^{j2\pi\frac{f-0.5F_s}{F_s}}\right) \qquad (2.1.5)$$

where $X_d\left(e^{j2\pi\frac{f}{F_s'}}\right)$ and $X_m\left(e^{j2\pi\frac{f}{F_s}}\right)$ are the discrete-time Fourier transforms of the decimated signal and mixed signal respectively and $F_s' = \frac{F_s}{2}$. As mentioned in [4], the double-frequency terms resulting from the mixing operation coincide with the sampling images and therefore,

$$X_d\left(e^{j2\pi\frac{f}{F_s'}}\right) = X_m\left(e^{j2\pi\frac{f}{F_s}}\right) \qquad (2.1.6)$$

and their only difference is the period at which the spectrum must repeat. For the mixed signal, the sampling rate is F_s and therefore its spectrum is required to repeat every F_s. On the other hand, the sampling rate of the decimated signal is $F_s/2$ and therefore its

spectrum must repeat every $F_s/2$. Unlike analog downconversion, lowpass filtering is not required in $F_s/4$ downconversion to remove the double-frequency terms. Instead, a decimation-by-2 of the mixed signal removes the double-frequency terms and yields the real part of the spectrum of the sampled inphase signals as shown in Figure 2.1.4(d).

For the recovery of quadrature samples, since $\sqrt{2}\cos\left(\frac{n\pi}{2}+\frac{\pi}{4}\right) = -\sqrt{2}\sin\left(\frac{n\pi}{2}-\frac{\pi}{4}\right)$, the sign correction sequence $\sqrt{2}\cos\left(\frac{n\pi}{2}+\frac{\pi}{4}\right)$ can be replaced by $-\sqrt{2}\sin\left(\frac{n\pi}{2}-\frac{\pi}{4}\right)$. By making this modification on the architecture, a similar approach to the one shown in Figure 2.1.4 can be used to illustrate the recovery of quadrature samples in the frequency domain.

So far the analog downconversion from RF to IF is assumed to be coherent. However, from an implementation viewpoint, it is easier to build a noncoherent downconverter. The phase error resulting from noncoherent downconversion can be characterized by θ and the resulting IF signal is,

$$\hat{r}_{IF}(t) = I(t) \cdot \cos(2\pi f_{IF} t + \theta) - Q(t) \cdot \sin(2\pi f_{IF} t + \theta) \qquad (2.1.7)$$

By replacing $r_{IF}(t)$ with $\hat{r}_{IF}(t)$ in Figure 2.1.3, the sampled sequence $\hat{r}_{IF}[n]$ can be obtained as,

$$\begin{aligned} \hat{r}_{IF}[n] &= \hat{r}_{IF}\left(t = \frac{n}{4f_{IF}}\right) \\ &= \{\ I_d[0] \cdot \cos\theta - Q_d[0] \cdot \sin\theta\ , \\ &\quad -I_d[1] \cdot \sin\theta - Q_d[1] \cdot \cos\theta\ , \\ &\quad -I_d[2] \cdot \cos\theta + Q_d[2] \cdot \sin\theta\ , \\ &\quad I_d[3] \cdot \sin\theta + Q_d[3] \cdot \cos\theta\ ,\ldots\ \} \end{aligned} \qquad (2.1.8)$$

where $I_d[n] = I\left(t = \frac{n}{4f_{IF}}\right)$ and $Q_d[n] = Q\left(t = \frac{n}{4f_{IF}}\right)$

By processing $\hat{r}_{IF}[n]$ using the structure shown in Figure 2.1.3, the two output sequences $\hat{I}_d[n]$ and $\hat{Q}_d[n]$ are found to be,

$$\hat{I}_d[n] = I_d[2n] \cdot \cos\theta - Q_d[2n] \cdot \sin\theta \tag{2.1.9}$$

$$\hat{Q}_d[n] = I_d[2n+1] \cdot \sin\theta + Q_d[2n+1] \cdot \cos\theta \tag{2.1.10}$$

Notice that $\hat{I}_d[n]$ no longer contains samples from $I(t)$ alone. Instead $\hat{I}_d[n]$ contains contributions from both $I(t)$ and $Q(t)$. Same result applies to $\hat{Q}_d[n]$ which also contains samples from both $I(t)$ and $Q(t)$. This implies that the cosine and sine carriers are no longer orthogonal at the desired sampling times and this loss of orthogonality introduces crosstalk between the inphase and the quadrature samples.

However, notice that if

$$I_d[2n] = I_d[2n+1] \tag{2.1.11}$$

and

$$Q_d[2n] = Q_d[2n+1] \tag{2.1.12}$$

then $\hat{I}_d[n]$ and $\hat{Q}_d[n]$ can be represented in a matrix form as follows,

$$\begin{bmatrix} \hat{I}_d[n] \\ \hat{Q}_d[n] \end{bmatrix} = \begin{bmatrix} \cos\theta & -\sin\theta \\ \sin\theta & \cos\theta \end{bmatrix} \cdot \begin{bmatrix} I_d[2n] \\ Q_d[2n] \end{bmatrix} \tag{2.1.13}$$

Or equivalently, in complex numbers notation,

$$\hat{I}_d[n] + j\hat{Q}_d[n] = (I_d[2n] + jQ_d[2n]) \cdot e^{j\theta} \qquad (2.1.14)$$

Both equations 2.1.13 and 2.1.14 indicate that the crosstalk can be viewed as a rotation of the inphase and the quadrature samples in the complex plane provided that assumptions 2.1.11 and 2.1.12 are valid. It will be shown in chapter 4 that these two assumptions are valid for a special family of signalling pulses. In this case, the crosstalk does indeed have the effect of rotation of the inphase and quadrature symbols.

In addition to $F_s/4$ as the intermediate frequency, an addition of any integer multiple of F_s to $F_s/4$ also yields an intermediate frequency suitable for $F_s/4$ downconversion. This is mainly due to the fact that the spectrum of any discrete-time signal is periodic in frequency with period F_S. Thus the first group of suitable IF frequencies is,

$$\text{1st group of suitable IF} = \{\frac{F_s}{4}, \frac{5F_s}{4}, \frac{9F_s}{4}, \ldots\} \qquad (2.1.15)$$

Besides $F_s/4$, it is found that $3F_s/4$ is also a suitable IF. The only difference between the two IF frequencies : $F_s/4$ and $3F_s/4$, is that the sign inversion on the Q channel takes place at different positions. Therefore with $3F_s/4$ as the IF center frequency, the sampled sequence $r_{IF}[n]$ should be multiplied by $\sqrt{2}\cos\left(\frac{n\pi}{2} - \frac{\pi}{4}\right)$ to correct the sign inversion. The second group of suitable IF frequencies is,

$$\text{2nd group of suitable IF} = \{\frac{3F_s}{4}, \frac{7F_s}{4}, \frac{11F_s}{4}, \ldots\} \qquad (2.1.16)$$

By combining the 1st and 2nd groups of the suitable IF frequencies, it follows that any

odd integer multiple of $F_s/4$ is appropriate for $F_s/4$ downconversion, that is

$$\text{suitable IF} = (2n+1)\cdot\frac{F_s}{4} \qquad \text{where n} = 0,1,2,\ldots \tag{2.1.17}$$

So $F_s/4$ downconversion restricts the choice of IF frequencies to ones that satisfy Equation 2.1.17. The suitable IF can be as high as desired, while the minimum IF is $F_s/4$.

2.2 Sampling Theorems

In order to achieve $F_s/4$ downconversion, the IF frequency must satisfy Equation 2.1.17. Since the suitable IF is given in terms of the sampling rate of the sampler, it is also required to specify the sampling rate. The objective of this section is to find the minimum sampling rate for demodulation of the received signal.

2.2.1 Nyquist Sampling Theorem

The most well-known criterion for choosing a sampling rate is the Nyquist Sampling Theorem [1, pp. 86] which can be stated as follows : Let $x_c(t)$ be a bandlimited signal with

$$X_c(f) = 0 \qquad for |f| \geq f_h \tag{2.2.1}$$

where $X_c(f)$ is the continuous-time Fourier transform of $x_c(t)$. Then $x_c(t)$ is uniquely determined by its samples $x[n] = x_c(n/F_s)$ where F_s is the sampling rate and, $n = 0, \pm1, \pm2, \ldots$ if

$$F_s \geq 2f_h \tag{2.2.2}$$

In other words, any sampling rate greater than twice the highest frequency component guarantees that spectral overlap does not occur in the sampling process. Therefore no information is lost in the sampling process. Since the Nyquist Sampling Theorem is valid for any bandlimited signal, this theorem is also applicable to a bandpass IF signal. Let $y_c(t)$ be a bandpass IF signal with bandwidth of W Hz and an intermediate frequency of f_{IF} Hz, then

$$Y_c(f) = 0 \begin{cases} \text{for } f > 0 \text{ and } |f - f_{IF}| \geq \frac{W}{2} \\ \text{for } f < 0 \text{ and } |f + f_{IF}| \geq \frac{W}{2} \end{cases} \tag{2.2.3}$$

where $Y_c(f)$ is the continuous-time Fourier transform of $y_c(t)$. The highest frequency component of $y_c(t)$ is at $f = f_{IF} + W/2$ Hz. Therefore, according to the Nyquist Sampling Theorem, the sampling rate must satisfy

$$F_s \geq 2 \cdot \left(f_{IF} + \frac{W}{2} \right) \tag{2.2.4}$$

in order to avoid spectral overlap of $y_c(t)$. The frequency domain representation of the sampling process is shown in Figure 2.2.1.

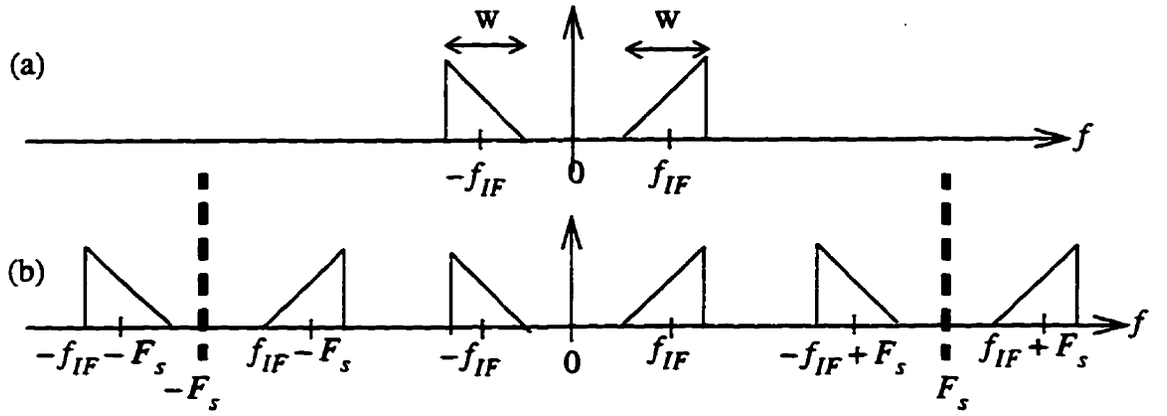

Figure 2.2.1 (a) Spectrum of the original bandpass signal.

(b) Spectrum of the sampled bandpass signal with $F_s \geq 2f_{IF} + W$.

From Equation 2.2.4, it is clear that the Nyquist sampling rate depends on both the intermediate frequency and the bandwidth, W, of the IF signal. The higher the intermediate frequency, the higher the required Nyquist sampling rate. The same argument applies for the bandwidth. As a result even if the information signal occupies a small bandwidth centered at a high intermediate frequency, the sampling rate must be significantly higher than the bandwidth for avoiding spectral overlap.

2.2.2 Bandpass Sampling Theorem

For the bandpass signal shown in Figure 2.2.1(a), there is an unoccupied spectrum in the low frequency region from $-f_{IF}+\frac{W}{2}$ to $f_{IF}-\frac{W}{2}$. Thus it may be possible to use this unoccupied spectrum to accommodate the spectral images resulting from the sampling process. This idea results in a more efficient sampling of the bandpass signal known as the bandpass sampling theorem [5, pp. 321-337] [11] , which is a special case of the Nyquist Sampling Theorem for the sampling of bandpass signal.

The bandpass sampling theorem states that if a bandpass signal, $x_s(t)$, has its frequency content confined from f_l to f_h , that is

$$X_s(f) = 0 \qquad for\ |f| > f_h \text{ or } |f| < f_l \tag{2.2.5}$$

where $X_s(f)$ is the continuous-time Fourier transform of $x_s(t)$, f_h is the highest (positive) frequency component and f_l is the lowest (positive) frequency component, then the bandpass signal can be reproduced from its samples provided that the sampling rate F_s satisfies the relationship

$$\frac{2f_h}{n} \le F_s \le \frac{2f_l}{n-1} \qquad \text{where n is integer valued and } 2 \le n \le \frac{f_h}{f_h - f_l} \quad (2.2.6)$$

In other words, the condition stated by Equation 2.2.6 ensures that spectral overlap does not occur in the sampling process.

Several important points about the bandpass sampling theorem can be inferred from Equation 2.2.6 :

(a) In Nyquist Sampling Theorem, as long as the continuous-time signal is bandlimited, there always exists a sampling rate for avoiding spectral overlap. However in bandpass sampling, it is possible that even if the continuous-time signal is a bandpass signal, there may exist no sampling rate suitable for bandpass sampling. The condition for the existence of a suitable F_s comes from the condition on the index n,

$$2 \le n \le \frac{f_h}{f_h - f_l} \quad (2.2.7)$$

Thus, a suitable sampling rate does not exist if

$$\frac{f_h}{f_h - f_l} < 2 \qquad or \qquad f_h > 2f_l \quad (2.2.8)$$

On the contrary, if

$$\frac{f_h}{f_h - f_l} \ge 2 \qquad or \qquad f_h \le 2f_l \quad (2.2.9)$$

then there exists a set of sampling rates suitable for bandpass sampling.

(b) Unlike the Nyquist Sampling Theorem in which only the lower limit of the sampling rate is restricted (that is the sampling rate can be as high as desired), both lower and upper limits of the sampling rate are restricted in the bandpass sampling theorem. The sampling rate cannot be too high or too low and only a certain range of sampling rates are suitable for bandpass sampling to avoid spectral overlap. An example is illustrated in Figure 2.2.2. Here f_l and f_h are assumed to be $5f_o$ and $7f_o$. The spectrum of this bandpass signal is shown in Figure 2.2.2a. With these values of f_l and f_h, the range of n is found to be $2 \le n \le 3.5$, that is n can be 2 or 3. By substituting these values of f_l, f_h and n = 2 into Equation 2.2.6, it follows that the sampling rate F_s falls in the range,

$$7f_o \le F_s \le 10f_o \tag{2.2.10}$$

On the other hand, with $n = 3$,

$$4.66f_o \le F_s \le 5f_o \tag{2.2.11}$$

Thus, in this example, the minimum sampling rate is $4.66f_o$ and the highest sampling rate is $10f_o$. There is a gap between these two sets of F_s, that is F_s cannot be in the range from $5f_o$ (exclusive) to $7f_o$ (exclusive). The aliasing effects for different sampling rates are shown in Figure 2.2.2 (b), (c) and (d). Firstly, F_s is chosen to be $4f_o$ which is lower than required. In this case, the spectrum (shown in Figure 2.2.2a) is repeated periodically every $4f_o$. The aliased spectrum is shown in Figure 2.2.2b and a 100% spectral overlap occurs with this low sampling rate. Next F_s is chosen to be $5f_o$ which is a suitable sampling rate for bandpass sampling and the spectrum of the sampled signal is shown in Figure

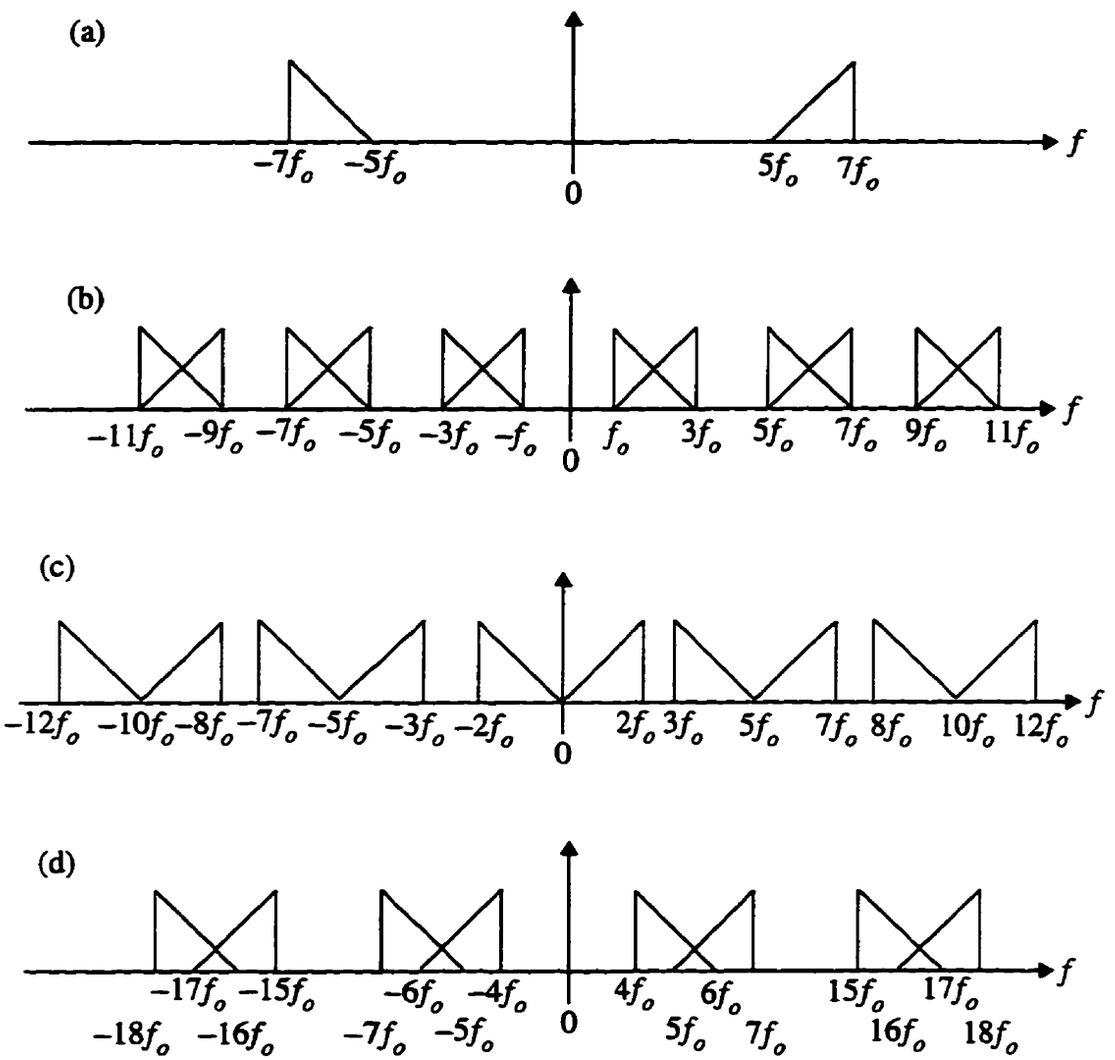

Figure 2.2.2

(a) Spectrum of the continuous-time bandpass signal.

(b) Spectrum of the sampled signal with $F_s = 4f_o$. A 100% spectral overlap occurs.

(c) Spectrum of the sampled signal with $F_s = 5f_o$. Spectral overlap is marginally avoided.

(d) Spectrum of the sampled signal with $F_s = 11f_o$. Spectral overlap occurs.

2.2.2c. Spectral overlap is marginally avoided with this sampling rate. Finally F_s is chosen to be $11f_o$ which is greater than the highest sampling rate. The aliased spectrum is shown in Figure 2.2.2d. Again, since the sampling rate is not included in the bandpass sampling theorem, spectral overlap occurs.

(c) The maximum and minimum sampling rates can be derived from Equation 2.2.6. In order to obtain the maximum sampling rate, F_s is set to be the upper limit (i.e. $F_s = \frac{2f_l}{n-1}$) and n is chosen to be the minimum (i.e. $n = 2$). Therefore the maximum sampling rate is found to be

$$F_{s,max} = 2f_l \qquad (2.2.12)$$

Notice that the maximum sampling rate for bandpass sampling is still lower than the Nyquist sampling rate which is $2f_h$. To obtain the minimum sampling rate, F_s is set to be the lower limit (i.e. $f_s = \frac{2f_h}{n}$) and n is set to the maximum value. Therefore if n is equal to $\frac{f_h}{f_h - f_l}$ with the assumption that $\frac{f_h}{f_h - f_l}$ is an integer greater than or equal to 2, then the minimum sampling rate is found to be

$$F_{s,min} = 2(f_h - f_l) \qquad (2.2.13)$$

Thus, for bandpass sampling, the minimum sampling rate is twice the bandwidth of the bandpass signal. This is analogous to the Nyquist Sampling Theorem which requires the minimum sampling rate to be twice the highest frequency component.

In addition to the above three points, there are other properties about the bandpass sampling theorem which can be found in [5, pp. 321-337]. The most important knowledge drawn from the bandpass sampling theorem is stated in Equation (2.2.13) which specifies the minimum sampling rate to be twice the signal bandwidth. If the bandpass IF signal $y_c(t)$ has a frequency content confined within $f_{IF} \pm \frac{W}{2}$, that is

$$Y_c(f) = 0 \qquad for \ |f - f_{IF}| > \frac{W}{2} \tag{2.2.14}$$

then the minimum sampling rate for avoiding spectral overlap is

$$F_s \geq 2W \tag{2.2.15}$$

provided that $\frac{f_h}{f_h - f_l}$, or equivalently $\frac{f_{IF} + \frac{W}{2}}{W}$ is an integer greater than or equal to 2. In other words, f_{IF} must satisfy the following condition

$$f_{IF} = (1.5 + k) \cdot W \qquad where \ k = 0, 1, 2, \ldots \tag{2.2.16}$$

So there exists a restriction on the intermediate frequency for achieving minimum sampling rate in bandpass sampling.

2.2.3 Sampling Theorem for Linearly Modulated Signals with Zero Intersymbol Interference

Both the Nyquist sampling theorem and the bandpass sampling theorem deal with general lowpass and bandpass signals. The objective of these two theorems is to determine the criterion of the sampling rate for avoiding spectral overlap in the sampling process. In other words, in the derivation of the two theorems, spectral overlap is treated as a destructive phenomenon to be avoided at all price. However, in the design of a

digital communication receiver, a certain form of spectral overlap at some point of the receiver chain is desirable. One example is the downconversion of an IF (or RF) signal to baseband. It is found that the downconverted signal is a result of a 100% overlap of the positive and negative spectra of the IF signal.

Another example, which is the main concern of this section, is the recovery of the information-bearing inphase (I) and quadrature (Q) symbols from their corresponding baseband signals without intersymbol interference. Here the digital modulation scheme is assumed to be linear, such as quadrature phase shift keying (QPSK) and quadrature amplitude modulation (QAM). Since both the I and Q symbols are discrete-time signals and the two baseband signals are continuous-time waveforms, the recovery process can be carried out by sampling the two analog baseband signals using proper sampling rates. Mathematically, the two linearly modulated lowpass signals can be lumped into one complex-valued lowpass equivalent signal $u(t)$ represented as

$$u(t) = \sum_{m=-\infty}^{\infty} (I_m + jQ_m) \cdot g(t - mT_p) \qquad (2.2.17)$$

where I_m and Q_m are the inphase and quadrature symbols respectively, T_p is the symbol period and $g(t)$ is the signalling pulse being modulated by the complex symbols $I_m + jQ_m$. Here the signalling pulse is assumed to be a Nyquist pulse which has a special property,

$$g(t)\big|_{t=nT_p} = \begin{cases} 1 & \text{for n} = 0 \\ 0 & \text{otherwise} \end{cases} \qquad (2.2.18)$$

A signalling pulse which satisfies Equation 2.2.18 is referred to as a Nyquist pulse. Assuming that this complex-valued signal is sampled at a sampling rate of 1 complex

sample per symbol, then the sampled sequence u_n can be obtained as,

$$u_n = u(t)\big|_{t=nT_p} \qquad \text{where n} = 0, \pm 1, \pm 2, \ldots \qquad (2.2.19)$$

Substituting Equations 2.2.17 and 2.2.18 into 2.2.19 yields

$$u_n = \sum_{m=-\infty}^{\infty} (I_m + jQ_m) \cdot g(nT_p - mT_p) = I_n + jQ_n \qquad (2.2.20)$$

Therefore, in the time domain, it is clear that the inphase and quadrature symbols can be recovered with no ISI by performing a complex-valued sampling of $u(t)$ with a sampling rate equal to the symbol rate.

The frequency domain interpretation can be obtained by taking the Fourier transform on both sides of Equation 2.2.18 which yields

$$G\left(e^{j2\pi fT_p}\right) = 1 \qquad \text{for all } f \qquad (2.2.21)$$

Equation (2.2.21) implies that in order to successfully recover the inphase and quadrature symbols with no ISI, the Fourier transform of the discrete-time signal $g(t = nT_p)$ must be 1 for all frequencies. One well-known family of pulses which satisfies this condition is the family of raised cosine pulses [2, pp. 546]. The raised cosine pulse is specified as

$$g(t) = \frac{\sin(\pi t/T_p)}{\pi t/T_p} \cdot \frac{\cos(\pi\beta t/T_p)}{1 - 4(\beta t/T_p)^2} \qquad (2.2.22)$$

where β is the roll-off factor taking any value from 0 (inclusive) to 1 (inclusive). Except for the case where the roll-off factor is zero, all raised cosine pulses have a bandwidth greater than half of the symbol rate. In other words, the highest frequency component of the pulse is greater than half of the sampling rate and therefore spectral overlap occurs in the sampling process. This is shown in Figure 2.2.3. It is important to note that the spectral overlap does not introduce any loss in the information of the transmitted symbols as long as Equation 2.2.21 is satisfied, that is, as long as the spectral overlap causes the spectrum of the discrete pulse $g\,(t = nT_p)$ to be flat.

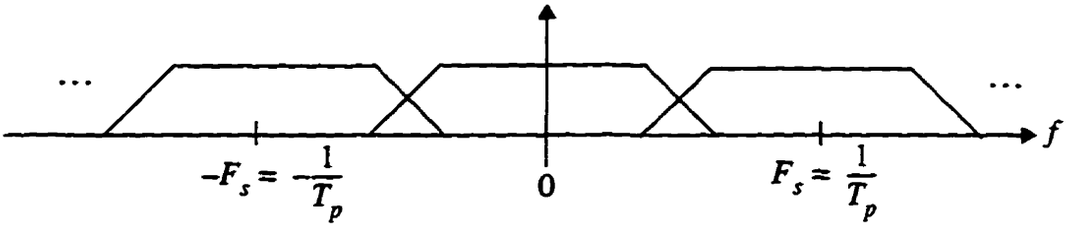

Figure 2.2.3 Spectrum of the discrete pulse $g\,(t = nT_p)$ with the sampling of 1 sample per symbol.

Two important points are derived from the above discussion. Firstly, as shown in Figure 2.2.3, a certain form of spectral overlap is constructive in the recovery of the information symbols and should not be avoided. Secondly, both inphase and quadrature symbols can be recovered by sampling the lowpass equivalent signal $u\,(t)$ (Equation 2.2.17) with one complex sample per symbol, or equivalently 2 real samples per symbol. Thus, with proper system design, the sampling rate can be as low as 2 real samples per symbol for the demodulation of a linearly modulated signal. Notice that this sampling rate is independent of the bandwidth of $u\,(t)$.

2.3 Summary

In summary, this chapter has provided an overview of a digital downconversion technique known as $F_s/4$ downconversion. In order to employ this technique, the system must be able to satisfy a special relationship between the intermediate frequency and the sampling rate stated in Equation 2.1.17. As shown in Figure 2.1.3, this technique allows the receiver to use a very simple digital structure to extract the inphase and quadrature samples from the continuous-time bandpass IF signal provided the sampling time is correct and the analog downconversion is coherent.

In addition to $F_s/4$ downconversion, a review of three sampling theorems was also presented. Both the Nyquist sampling theorem and the bandpass sampling theorem specify the sampling rate for avoiding spectral overlap in the sampling process. Since the Nyquist sampling theorem is valid for any bandlimited signal (either lowpass or bandpass) whereas the bandpass sampling theorem is only valid for bandpass signal, the Nyquist sampling rate is more general and therefore requires a higher sampling rate. On the other hand, the third sampling theorem only deals with the demodulation of linearly modulated signals with no ISI. Due to the constructive spectral overlap, a minimum sampling rate of 2 real samples per symbol can be employed for the recovery of the inphase and quadrature symbols. Such a sampling rate is adopted in the proposed IF-sampling receiver.

Chapter 3 The Proposed IF-sampling Receiver

This chapter presents the design of a bandpass digital communications system comprising a conventional transmitter, an additive bandpass white Gaussian noise channel and the proposed IF-sampling receiver. The complete system block diagram is shown in Figure 3.1. In a high level description, the modulator maps a group of information bits into one of the predefined bandpass waveforms. The selected waveform $s(t)$ is then transmitted through the additive bandpass white Gaussian noise channel and picked up by the receiver. The IF-sampling receiver produces two discrete-time sequences, namely the received inphase (I) symbols and the received quadrature (Q) symbols from the received signal. At the final stage, the detector processes the received I/Q symbols to generate an estimate of the transmitted information bits. All functions in Figure 3.1, except for the detector, are explained in detail in the following sections. In addition to the architecture of the system, the criterion for the signalling pulse achieving zero intersymbol interference (ISI) is also derived for the proposed IF-sampling receiver. Based on this criterion, one can obtain the minimum bandwidth for achieving zero ISI and the corresponding pulse shape.

3.1 The Transmitter

This section explains the details of the transmitter in Figure 3.1. Basically the transmitter consists of a modulator which accepts the information bits as input, generates the corresponding data symbols and produces a continuous-time signal carrying the information of the symbols. The block diagram of the modulator is illustrated in Figure 3.1.1 . In this project, the transmitter is restricted to implement only linear modulation scheme, such as QPSK and QAM. Other modulation schemes, such as continuous phase frequency shift keying (CPFSK), cannot be represented by the block diagram shown in

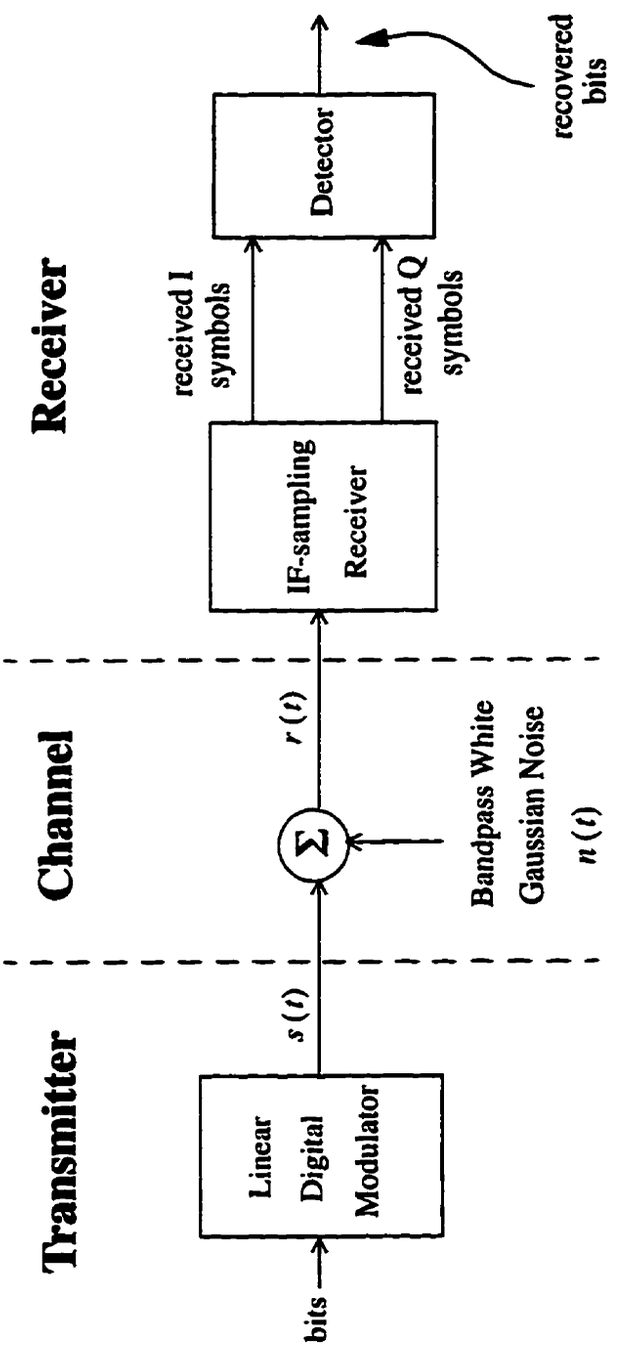

Figure 3.1 Block diagram of the bandpass communication system model

Figure 3.1.1 . Three operations are performed in the modulator : (1) symbol mapping, (2) pulse shaping and (3) frequency upconversion.

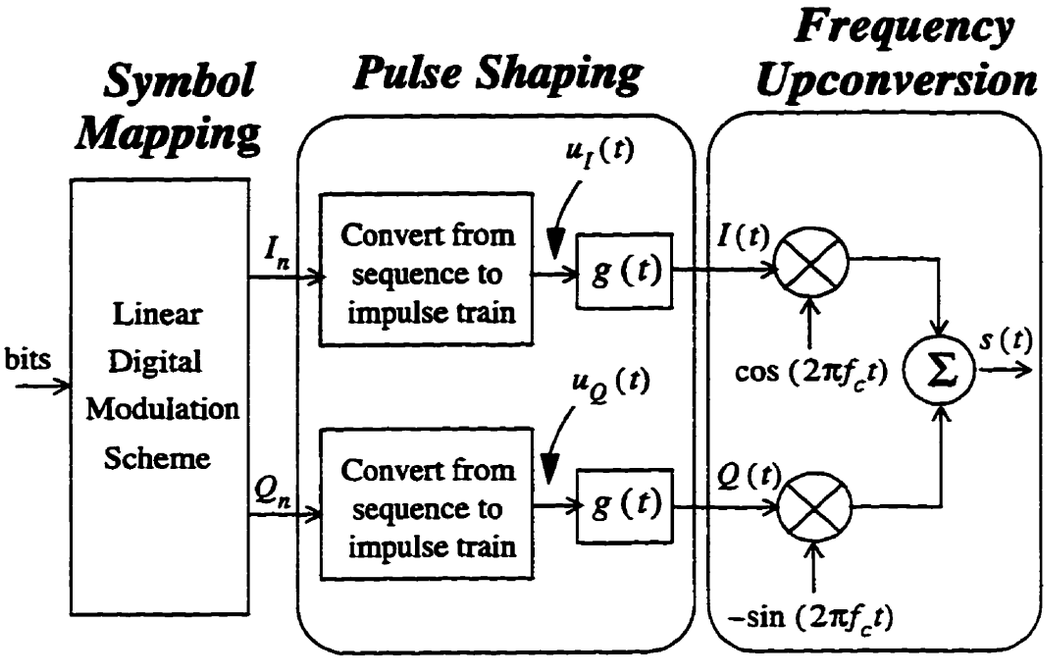

Figure 3.1.1 Detailed block diagram representation of the modulator.

Each element in the discrete-time sequence of the information bits is either a 1 or a 0. The process of symbol mapping is performed by a linear digital modulation scheme in which a group of k consecutive information bits is mapped into an M-ary complex symbol, where $M = 2^k$. In this way, a single M-ary complex symbol is used to carry k information bits. In general, the real and imaginary parts of the complex symbols are known as the inphase symbols, I_n, and the quadrature symbols, Q_n. If the rate of the information bits is R_b bit/sec, then the symbol rate R_s will be

$$R_s = \frac{R_b}{\log_2 M} = \frac{R_b}{k} \tag{3.1.1}$$

At the output of the digital modulation scheme, the two discrete-time sequences, I_n and Q_n, are converted by the pulse shaping block into two continuous-time baseband signals namely the inphase signal $I(t)$ and the quadrature signal $Q(t)$. This conversion process is similar to the reconstruction process of a bandlimited signal from its samples in the Nyquist sampling theorem [1, pp. 87]. The conversion process is performed in 2 steps : (1) conversion from a discrete-time sequence to an impulse train with a sampling rate of 1 sample per symbol and (2) filtering. To illustrate, given the two discrete-time sequences I_n and Q_n , one can obtain the two continuous-time signals $u_I(t)$ and $u_Q(t)$ by converting a sequence to an impulse train with a sampling rate of $1/T_p$, that is

$$u_I(t) = \sum_{m=-\infty}^{\infty} I_m \cdot \delta(t - mT_p) \tag{3.1.2}$$

$$u_Q(t) = \sum_{m=-\infty}^{\infty} Q_m \cdot \delta(t - mT_p) \tag{3.1.3}$$

where $\delta(t) \equiv$ Dirac delta function

$T_p \equiv$ symbol period $= 1/R_s$

From the expressions given in Equations 3.1.2 and 3.1.3, the signals $u_I(t)$ and $u_Q(t)$ can also be viewed as modulation of an impulse train $\sum_{m=-\infty}^{\infty} \delta(t - mT_p)$ by two discrete-time sequences I_m and Q_m respectively. These two modulated impulse trains are then passed into the two pulse shaping filters having the same impulse response denoted as $g(t)$. In practice, $g(t)$ is known as the signalling pulse. The outputs of the two filters are given as the convolution of $g(t)$ with $u_I(t)$ and $u_Q(t)$, that is

$$I(t) = u_I(t) \otimes g(t) = \sum_{m=-\infty}^{\infty} I_m \cdot g(t-mT_p) \tag{3.1.4}$$

$$Q(t) = u_Q(t) \otimes g(t) = \sum_{m=-\infty}^{\infty} Q_m \cdot g(t-mT_p) \tag{3.1.5}$$

where $\otimes$ denotes a convolution operation.

The two signals, $I(t)$ and $Q(t)$, are then used to amplitude-modulate (AM) the sine and cosine carriers respectively. Equivalently, in the frequency domain, the spectra of $I(t)$ and $Q(t)$ are frequency up-shifted by the cosine and sine carriers respectively to a carrier frequency f_c. By summing up these two AM signals, the linearly modulated bandpass signal, $s(t)$, is obtained as :

$$\begin{aligned} s(t) = & \sum_{m=-\infty}^{\infty} I_m \cdot g(t-mT_p) \cdot \cos(2\pi f_c t) \\ & - \sum_{m=-\infty}^{\infty} Q_m \cdot g(t-mT_p) \cdot \sin(2\pi f_c t) \end{aligned} \tag{3.1.6}$$

The required transmission bandwidth for the communication system is dictated by the bandwidth of the bandpass signal $s(t)$ which can also be represented by its complex-valued lowpass equivalent signal, $v(t)$, as

$$s(t) = Re\{v(t) \cdot e^{j2\pi f_c t}\} \tag{3.1.7}$$

$$\text{where } v(t) = \sum_{m=-\infty}^{\infty} (I_m + jQ_m) \cdot g(t-mT_p)$$

By taking the continuous-time Fourier transform of $s(t)$, the frequency domain

relationship between $s(t)$ and $v(t)$ is obtained as

$$S(f) = \frac{1}{2}\left[V(f-f_c) + V^*(-f-f_c)\right] \qquad (3.1.8)$$

where $S(f) \equiv$ continuous-time Fourier transform of $s(t)$

$V(f)$ = continuous-time Fourier transform of $v(t)$

and * represents a complex conjugate operation.

Equation 3.1.8 clearly indicates that the bandpass bandwidth of $s(t)$ is the same as the total lowpass bandwidth (including both positive and negative frequency spectra) of $v(t)$. Therefore the transmission bandwidth is the same as the total lowpass bandwidth of $v(t)$. The full derivation of the power density spectrum of $v(t)$ is given by [2, pp. 204] and the result is stated as follows.

If the encoded symbols, I_n and Q_n, are uncorrelated and have zero mean, that is

$$\phi_{IQ}[m] = E\{I_n \cdot Q_{n-m}\} = 0 \qquad \text{for all m} \qquad (3.1.9)$$

$$E\{I_n\} = E\{Q_n\} = 0 \qquad \text{for all n} \qquad (3.1.10)$$

where $E\{\ \}$ denotes the expectation operation.

then the lowpass equivalent signal is a cyclostationary process with average power density spectrum given by

$$\Phi_{vv}(f) = \frac{\sigma_i^2}{T_p} \cdot |G(f)|^2 \qquad (3.1.11)$$

$$\text{where } \sigma_i^2 = \frac{1}{2} \cdot E\{(I_n + jQ_n) \cdot (I_n + jQ_n)^*\} \qquad (3.1.12)$$

Therefore the lowpass equivalent of the linearly modulated signal has the same spectral shape as the magnitude response of the signalling pulse $g(t)$. If the bandwidth of $g(t)$ is equal to $W/2$ Hz, that is

$$|G(f)| = 0 \quad \text{for } |f| > \frac{W}{2} \text{ Hz} \tag{3.1.13}$$

then the bandwidth of the bandpass linearly modulated signal $s(t)$ is equal to W Hz.

3.2 The Channel

The second block in the system is a bandpass channel which is assumed to corrupt the transmitted bandpass signal $s(t)$ by the addition of the bandpass white Gaussian noise $n(t)$. By summing the transmitted signal and the noise, the received signal $r(t)$ is found to be,

$$\begin{aligned} r(t) = & \sum_{m=-\infty}^{\infty} I_m \cdot g(t-mT_p) \cdot \cos(2\pi f_c t) \\ & - \sum_{m=-\infty}^{\infty} Q_m \cdot g(t-mT_p) \cdot \sin(2\pi f_c t) \\ & + n(t) \end{aligned} \tag{3.2.1}$$

The noise is assumed to be a wide-sense stationary stochastic Gaussian process with zero mean,

$$E\{n(t)\} = 0 \qquad \text{for all time t} \tag{3.2.2}$$

Furthermore the noise is also assumed to have a flat real-valued power density spectrum

of $\frac{N_o}{2}$ in a frequency region with bandwidth of W Hz and centered at the carrier frequency. Thus if the power density spectrum of $n(t)$ is denoted as $\Phi_{nn}(f)$, then

$$\Phi_{nn}(f) = \begin{cases} \frac{N_o}{2} & |f-f_c| \le \frac{W}{2} \text{ or } |f+f_c| \le \frac{W}{2} \\ 0 & \text{otherwise} \end{cases} \qquad (3.2.3)$$

Due to this special property of the power density spectrum, this random process is commonly known as bandpass white noise. Figure 3.2.1 shows the sketch of the power density spectrum.

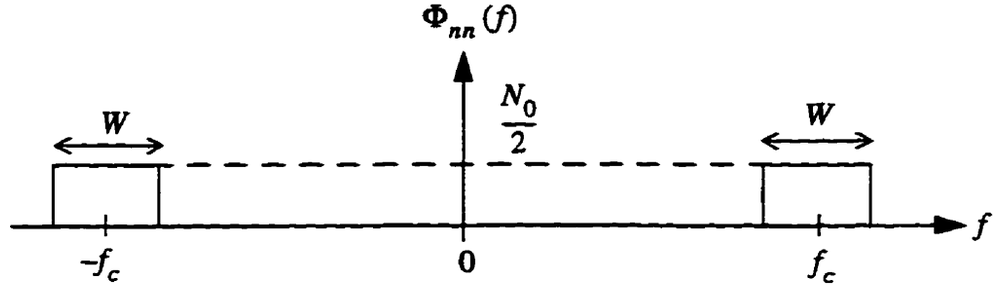

Figure 3.2.1 Power density spectrum of the bandpass white noise.

In general, any bandpass random process can be decomposed into two lowpass noise processes namely the inphase component $x(t)$ and the quadrature component $y(t)$. So $n(t)$ can also be written as

$$n(t) = x(t) \cdot \cos(2\pi f_c t) - y(t) \cdot \sin(2\pi f_c t) \qquad (3.2.4)$$

where $x(t) \equiv$ inphase component of $n(t)$

$y(t) \equiv$ quadrature component of $n(t)$

Since $n(t)$ is assumed to be a Gaussian process, it follows that both $x(t)$ and $y(t)$ are also zero-mean Gaussian random processes [2, pp. 162]. Thus

$$E\{x(t)\} = E\{y(t)\} = 0 \quad \text{for all time t} \tag{3.2.5}$$

Also due to the stationarity of the bandpass noise $n(t)$, the two components $x(t)$ and $y(t)$ are real-valued individually and jointly wide-sense stationary processes [2, pp.159]. The autocorrelation functions of $x(t)$ and $y(t)$ are exactly the same and given as,

$$\phi_{xx}(\tau) = E\{x(t) \cdot x(t-\tau)\} = N_0 \cdot \frac{\sin(\pi W\tau)}{\pi\tau} \tag{3.2.6}$$

$$\phi_{yy}(\tau) = E\{y(t) \cdot y(t-\tau)\} = N_0 \cdot \frac{\sin(\pi W\tau)}{\pi\tau} \tag{3.2.7}$$

It has been shown [2, pp. 159] that the two processes, $x(t)$ and $y(t)$, are also uncorrelated for all time shifts τ, therefore

$$\phi_{xy}(\tau) = E\{x(t)\} \cdot E\{y(t-\tau)\} \quad \text{for all time shifts } \tau \tag{3.2.8}$$

Therefore, since $x(t)$ and $y(t)$ are Gaussian processes, they are statistically independent. Substituting Equation 3.2.5 into Equation 3.2.8 yields

$$\phi_{xy}(\tau) = E\{x(t) \cdot y(t-\tau)\} = 0 \quad \text{for all time shifts} \tau \tag{3.2.9}$$

Therefore the cross-correlation function of $x(t)$ and $y(t)$ is always zero and $x(t)$ and $y(t)$ are orthogonal. The power density spectra $\Phi_{xx}(f)$ and $\Phi_{yy}(f)$ are obtained by taking the Fourier transform of $\phi_{xx}(\tau)$ and $\phi_{yy}(\tau)$. Hence

$$\Phi_{xx}(f) = \Phi_{yy}(f) = \begin{cases} N_o & |f| < \frac{W}{2} \\ 0 & otherwise \end{cases} \tag{3.2.10}$$

Both the autocorrelation functions and the power density spectra are also sketched in Figure 3.2.2.

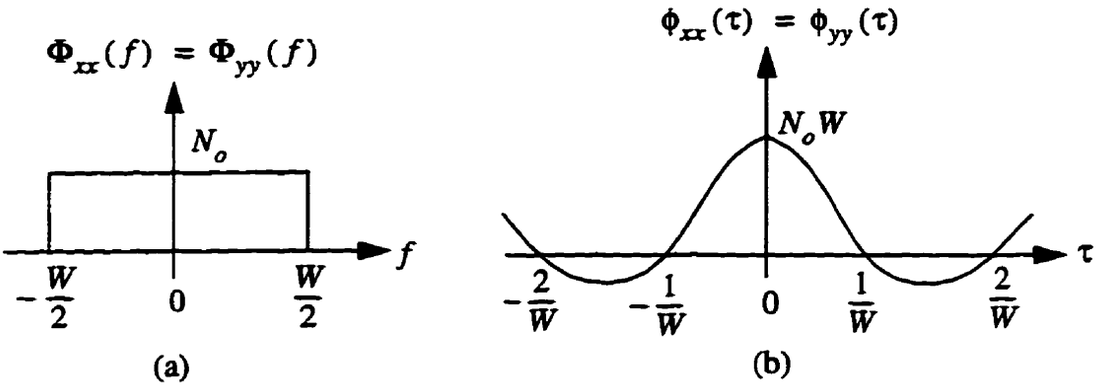

Figure 3.2.2 (a) Power density spectra of $x(t)$ and $y(t)$.

(b) Autocorrelation functions of $x(t)$ and $y(t)$.

3.3 The Proposed IF-sampling Receiver

The architecture of the proposed IF-sampling receiver is based on the concepts of $F_s/4$ downconversion and the sampling theorem for linearly modulated signal. The receiver employs the minimum sampling rate of 2 samples per symbol and a simple digital structure (similar to Figure 2.1.3) to recover the transmitted information symbols from the sampled IF signal. The proposed receiver architecture is shown in Figure 3.3.1 .

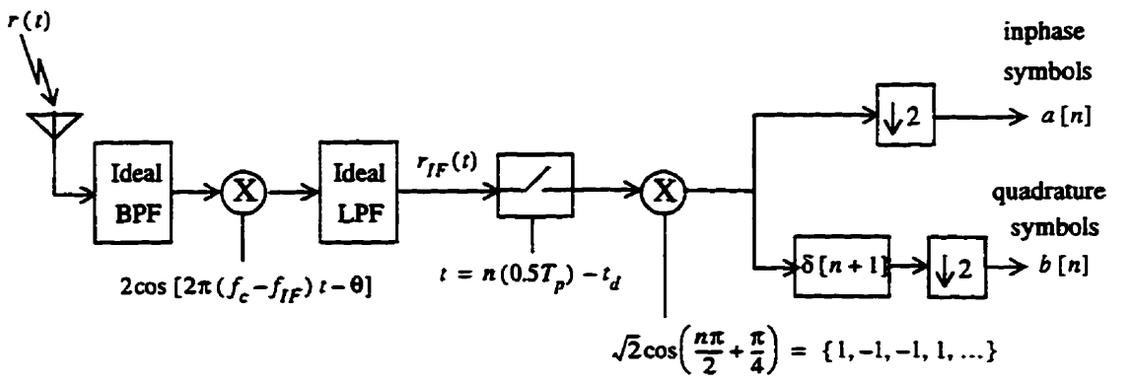

Figure 3.3.1 Architecture of the IF-sampling receiver.

The received radio frequency (RF) signal, $r(t)$, is given as

$$\begin{aligned} r(t) = & \sum_{m=-\infty}^{\infty} I_m \cdot g(t-mT_p) \cdot \cos(2\pi f_c t) \\ & - \sum_{m=-\infty}^{\infty} Q_m \cdot g(t-mT_p) \cdot \sin(2\pi f_c t) \\ & + x(t) \cdot \cos(2\pi f_c t) \\ & - y(t) \cdot \sin(2\pi f_c t) \end{aligned} \qquad (3.3.1)$$

This RF signal is first filtered by the ideal bandpass filter (BPF) which eliminates any signal and noise outside the transmission band. The filtered signal is then mixed with a local oscillator, $2\cos[2\pi(f_c - f_{IF})t - \theta]$ where f_c is the RF carrier frequency and f_{IF} is the intermediate frequency. It is assumed that a perfect estimate of the carrier frequency is available in the receiver. However there exists an unknown phase offset between the received signal and the local oscillator. This phase offset is characterized by the unknown constant θ in the local oscillator output. At the output of the mixer, the signal is filtered by an ideal lowpass filter (LPF) to remove the double-frequency component. In order to perform $F_s/4$ downconversion, the intermediate frequency must satisfy the condition,

$$f_{IF} = (2n+1) \cdot \frac{F_s}{4} \qquad \text{where n} = 0,1,2,\ldots \qquad (3.3.2)$$

Since a low intermediate frequency can ease the input bandwidth requirement of the sampler, the minimum intermediate frequency $F_s/4$ is used. Therefore the sampling rate (F_s) and the intermediate frequency (f_{IF}) are selected to be,

$$F_s = \frac{2}{T_p} \quad Hz \qquad (3.3.3)$$

$$f_{IF} = \frac{F_s}{4} = \frac{0.5}{T_p} \quad Hz \tag{3.3.4}$$

The bandwidth of the ideal lowpass filter must be large enough to pass the IF signal without any distortion. Therefore the frequency response of the ideal lowpass filter $LPF(f)$ is given as

$$LPF(f) = \begin{cases} 1 & |f| < \frac{0.5}{T_p} + \frac{W}{2} \\ 0 & otherwise \end{cases} \tag{3.3.5}$$

Depending on the bandwidth of the signalling pulse and the intermediate frequency being selected in the receiver, spectral overlap can happen at both the input and output of the sampler. Firstly, if the minimum intermediate frequency is employed, then the negative and positive spectra of the IF signal (at the input of the sampler) partially overlap with each other. This is illustrated in Figure 3.3.2 with the assumption of a 100% excess bandwidth signalling pulse.

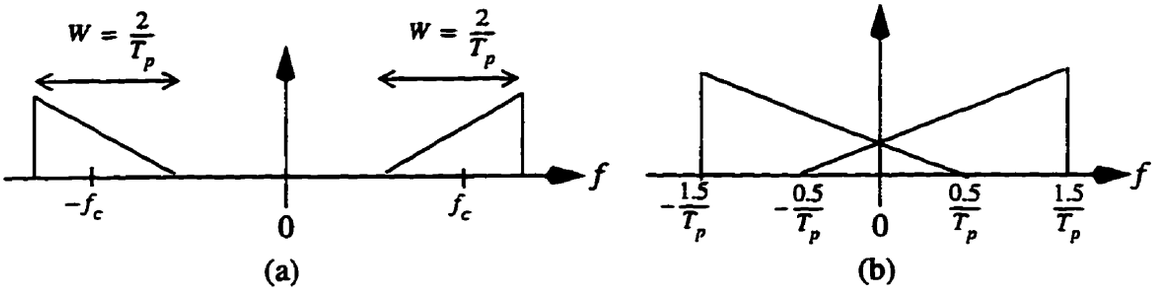

Figure 3.3.2 (a) Spectrum of the RF signal with 100% excess bandwidth.

(b) Spectrum of the IF signal for $f_{IF} = \frac{0.5}{T_p}$.

Figure 3.3.2a shows the hypothetical RF spectrum with a 100% excess bandwidth and Figure 3.3.2b shows the corresponding IF spectrum at the output of the ideal lowpass filter (LPF). There is an exceptional case in which the spectral overlap is marginally avoided. This special situation occurs when either the signalling pulse has a 0% excess bandwidth or a higher intermediate frequency is chosen from Equation 3.3.2 . It should be noted that if a higher intermediate frequency is used, then the ideal lowpass filter should be replaced by a bandpass filter.

Secondly, spectral overlap can also occur in the sampling process (or equivalently at the output of the sampler) depending on the excess bandwidth of the signalling pulse. Unless the signalling pulse has a 0% excess bandwidth, spectral overlap always occurs when sampling. This spectral overlap is independent of the intermediate frequency. It is important to note that these two forms of spectral overlap are constructive in making both the IF-to-baseband downconversion and the demodulation of the waveform signal into I/Q symbols to be performed in one step — the sampling process.

Whether the two spectral overlaps occur or not, the downconverted IF signal can always be represented as

$$\begin{aligned} r_{IF}(t) = & \sum_{m=-\infty}^{\infty} I_m \cdot g(t-mT_p) \cdot \cos(2\pi f_{IF} t + \theta) \\ & - \sum_{m=-\infty}^{\infty} Q_m \cdot g(t-mT_p) \cdot \sin(2\pi f_{IF} t + \theta) \\ & + x(t) \cdot \cos(2\pi f_{IF} t + \theta) \\ & - y(t) \cdot \sin(2\pi f_{IF} t + \theta) \end{aligned} \qquad (3.3.6)$$

The IF signal is sampled by one sampler with a sampling rate of 2 samples per symbol.

The sampler is assumed to have infinite resolution such that quantization error is ignored. However, due to the imperfection in the synchronization circuit, there exits an offset (error) in the actual sampling timing. Thus the actual sampling time is given as

$$t = n\frac{T_p}{2} - t_d \tag{3.3.7}$$

where t_d represents the sampling timing error. Note that t_d is always in the range from $-0.25T_p$ to $0.25T_p$, that is

$$-0.25T_p \le t_d \le 0.25T_p \tag{3.3.8}$$

A positive value of t_d corresponds to the sampling point off to the left ; whereas a negative value of t_d corresponds to the sampling point off to the right. By substituting Equations 3.3.4 and 3.3.7 into Equation 3.3.6, the sampled IF sequence $r_{IF}[n]$ is found to be

$$\begin{aligned} r_{IF}[n] = & \sum_{m=-\infty}^{\infty} I_m \cdot g\left(n\frac{T_p}{2} - t_d - mT_p\right) \cdot \cos\left(\frac{n\pi}{2} - \frac{\pi t_d}{T_p} + \theta\right) \\ & - \sum_{m=-\infty}^{\infty} Q_m \cdot g\left(n\frac{T_p}{2} - t_d - mT_p\right) \cdot \sin\left(\frac{n\pi}{2} - \frac{\pi t_d}{T_p} + \theta\right) \\ & + x\left(n\frac{T_p}{2} - t_d\right) \cdot \cos\left(\frac{n\pi}{2} - \frac{\pi t_d}{T_p} + \theta\right) \\ & - y\left(n\frac{T_p}{2} - t_d\right) \cdot \sin\left(\frac{n\pi}{2} - \frac{\pi t_d}{T_p} + \theta\right) \end{aligned} \tag{3.3.9}$$

It is important to emphasize that if both the timing error and the phase offset are zero and the signalling pulse satisfies certain conditions (which will be discussed in the next section), then $r_{IF}[n]$ contains interleaved inphase and quadrature symbols with sign inversions introduced on some of the symbols. Mathematically, this can be stated as

$$\{I_o, -Q_o, -I_1, Q_1, I_2, -Q_2, -I_3, Q_3, \ldots\} \tag{3.3.10}$$

where I_n and Q_n are the transmitted inphase and quadrature symbols. In other words, the proposed IF-sampling receiver can directly extract the I/Q symbols from the analog IF signal without the need for recovering the two baseband continuous-time I/Q signals using decimation filters.

As shown in Figure 3.3.1, the recovered inphase symbols $a[n]$ can be obtained from the sampled IF sequence by multiplying $r_{IF}[n]$ with the sign correction sequence $\sqrt{2}\cos\left(\frac{n\pi}{2}+\frac{\pi}{4}\right)$ and decimating the multiplication output sequence by a factor of 2. Thus the received inphase symbol is

$$\begin{aligned} a[n] = & \sum_{m=-\infty}^{\infty} I_m \cdot g(nT_p - t_d - mT_p) \cdot \cos\left(-\frac{\pi t_d}{T_p} + \theta\right) \\ & - \sum_{m=-\infty}^{\infty} Q_m \cdot g(nT_p - t_d - mT_p) \cdot \sin\left(-\frac{\pi t_d}{T_p} + \theta\right) \\ & + x(nT_p - t_d) \cdot \cos\left(-\frac{\pi t_d}{T_p} + \theta\right) \\ & - y(nT_p - t_d) \cdot \sin\left(-\frac{\pi t_d}{T_p} + \theta\right) \end{aligned} \tag{3.3.11}$$

Similarly the recovered Q symbols can also be obtained by multiplying $r_{IF}[n]$ with the sign correction sequence $\sqrt{2}\cos\left(\frac{n\pi}{2}+\frac{\pi}{4}\right)$, time shifting the multiplication output sequence to the left by one sample and decimating the shifted sequence by a factor of 2. Thus the recovered quadrature symbol, $b[n]$, is

$$
\begin{aligned}
b[n] = & \sum_{m=-\infty}^{\infty} I_m \cdot g(nT_p + 0.5T_p - t_d - mT_p) \cdot \sin\left(-\frac{\pi t_d}{T_p} + \theta\right) \\
& + \sum_{m=-\infty}^{\infty} Q_m \cdot g(nT_p + 0.5T_p - t_d - mT_p) \cdot \cos\left(-\frac{\pi t_d}{T_p} + \theta\right) \\
& + x(nT_p + 0.5T_p - t_d) \cdot \sin\left(-\frac{\pi t_d}{T_p} + \theta\right) \\
& + y(nT_p + 0.5T_p - t_d) \cdot \cos\left(-\frac{\pi t_d}{T_p} + \theta\right)
\end{aligned}
\tag{3.3.12}
$$

3.4 Signal Design for the Proposed IF-sampling Receiver

From Equations 3.3.11 and 3.3.12, it is clear that both the recovered inphase symbols, $a[n]$, and the recovered quadrature symbols, $b[n]$, contain information about the transmitted I/Q symbols. In order to obtain a "clean" copy of the transmitted I/Q symbols under ideal conditions, the signalling pulse must satisfy certain conditions. This section focuses on the design of a bandlimited signalling pulse which allows the receiver to achieve zero intersymbol interference. The design procedures are similar to that of Nyquist criterion [2, pp. 543] and the generalized Nyquist criterion [13].

In the design of the signalling pulse, all distortions introduced either by the channel or by the nonideal receiver implementation are assumed to be zero. In other words, the timing error of the sampler, the phase offset and the two noise components (inphase and quadrature) are assumed to be zero :

$$t_d = 0 \tag{3.4.1}$$

$$\theta = 0 \tag{3.4.2}$$

$$x(t) = y(t) = 0 \qquad \text{for all t} \tag{3.4.3}$$

By substituting these four assumptions into Equations 3.3.11 and 3.3.12, the recovered inphase and quadrature symbols can be simplified as

$$a[n] = \sum_{m=-\infty}^{\infty} I_m \cdot g(nT_p - mT_p) \qquad (3.4.4)$$

and

$$b[n] = \sum_{m=-\infty}^{\infty} Q_m \cdot g(nT_p + 0.5T_p - mT_p) \qquad (3.4.5)$$

Notice that with both the timing error and the phase offset assumed to be zero, the recovered inphase symbols, $a[n]$, depend solely on the transmitted inphase symbols, I_m, and contain no contribution from the transmitted quadrature symbols, Q_m. The same observation applies to the recovered quadrature symbols, $b[n]$, which also depend only on the transmitted quadrature symbols, Q_m, and contain no contribution from the transmitted inphase symbols, I_m. In other words, no crosstalk is introduced between the inphase and quadrature channels if both timing error and phase offset are zero. In a practical communication system, it is very costly to make these two assumptions valid and therefore the effect of these two errors is discussed in chapter 4.

Although the crosstalk is removed, the effect of intersymbol interference (ISI) can still be introduced by an improper design of the signalling pulse. This is because both Equations 3.4.4 and 3.4.5 involve summation of all the transmitted I and Q symbols respectively. The first criterion for a zero ISI signalling pulse is derived from the I channel. Assume the k^{th} transmitted I symbol, I_k, is recovered at $n = k$, and the recovered symbol is denoted as $\hat{I}_k$, then Equation 3.3.4 can be written as,

$$\hat{I}_k = I_k \cdot g(0) + \sum_{\substack{m=-\infty \\ m \neq k}}^{\infty} I_m \cdot g(kT_p - mT_p) \qquad (3.4.6)$$

This equation is purposely separated into two terms to show the mathematical form of the intersymbol interference. The first term, $I_k \cdot g(0)$, is the desired inphase symbol scaled by $g(0)$. The second term, which is the summation of contribution of all inphase symbols other than I_k , represents the interference from other symbols within the inphase channel itself. Therefore the second term is denoted as the intersymbol interference term. In order to remove the ISI on inphase channel and retrieve I_k , the signalling pulse $g(t)$ must satisfy

$$g(t = nT_p) = \begin{cases} 1 & \text{for } n = 0 \\ 0 & \text{otherwise} \end{cases} \qquad (3.4.7)$$

Equation 3.4.7 is the criterion on the signalling pulse $g(t)$ for accomplishing zero ISI on the inphase channel.

To derive the criterion on the quadrature channel, the same procedure is applied. Again assume that the kth quadrature symbol, Q_k, is recovered at $n = k$ and the recovered symbol is denoted as $\hat{Q}_k$, then Equation 3.4.5 yields

$$\hat{Q}_k = Q_k \cdot g(0.5T_p) + \sum_{\substack{m=-\infty \\ m \neq k}}^{\infty} Q_m \cdot g(kT_p + 0.5T_p - mT_p) \qquad (3.4.8)$$

The same interpretation is made. The first term, $Q_k \cdot g(0.5T_p)$, is the desired quadrature symbol scaled by $g(0.5T_p)$. The second term, which is the summation of

contribution of all quadrature symbols other than Q_k, represents the intersymbol interference. Therefore, in order to remove the ISI on the quadrature channel and retrieve Q_k, the signaling pulse $g(t)$ must satisfy

$$g(t = 0.5T_p + nT_p) = \begin{cases} 1 & \text{for } n = 0 \\ 0 & \text{otherwise} \end{cases} \tag{3.4.9}$$

Equation 3.4.9 is the criterion on the signalling pulse $g(t)$ for obtaining zero ISI on the quadrature channel. Note that Equations 3.4.7 and 3.4.9 impose different restrictions on the same signalling pulse. In order to avoid ISI on both the inphase and quadrature channels, the signalling pulse must be able to simultaneously satisfy both equations. Therefore having zero ISI on both inphase and quadrature symbols requires $g(t)$ to be

$$g[n] = g(t = n0.5T_p) = \begin{cases} 1 & \text{for } n = 0,1 \\ 0 & \text{otherwise} \end{cases} \tag{3.4.10}$$

Equation 3.4.10 is the time-domain zero ISI criterion for a coherent IF-sampling receiver with perfect sampling timing. Notice that Equation 3.4.10 takes the same form as the conventional Nyquist criterion except that the sampling rate on $g(t)$ is $2/T_p$ and two nonzero samples are required. This is mainly due to the fact that the inphase and quadrature symbols are obtained at different times. Thus the timing misalignment problem is solved by imposing two conditions (Equations 3.4.7 and 3.4.9) instead of one on the signalling pulse.

In addition to the time domain representation, a frequency domain representation of the zero ISI criterion can also be obtained by taking the discrete-time Fourier transform (DTFT) of Equation 3.4.10 . In general, the DTFT of $g[n]$ is denoted as $G\left(e^{j\omega}\right)$ and the transform is defined as

$$G\left(e^{j\omega}\right) = \sum_{n=-\infty}^{\infty} g[n] \cdot e^{-j\omega n} \tag{3.4.11}$$

Substituting $g[n]$ from Equation 3.4.10 into Equation 3.4.11 yields

$$G\left(e^{j\omega}\right) = 1 + e^{-j\omega} = \left(2 \cdot \cos\frac{\omega}{2}\right) \cdot e^{-j\frac{\omega}{2}} \tag{3.4.12}$$

Applying the relationship between the normalized discrete-time frequency ω and the continuous-time frequency f : $\omega = 2\pi\frac{f}{F_s}$, and the relationship between F_s and T_p : $F_s = \frac{2}{T_p}$, Equation 3.4.12 reduces to

$$G\left(e^{j2\pi\frac{f}{F_s}}\right) = \left(2 \cdot \cos\frac{\pi f T_p}{2}\right) \cdot e^{-j\frac{\pi f T_p}{2}} \tag{3.4.13}$$

In general, the discrete-time Fourier transform, is related to the continuous-time Fourier transform, $G(f)$ by the sampling theorem as

$$G\left(e^{j2\pi\frac{f}{F_s}}\right) = F_s \cdot \sum_{k=-\infty}^{\infty} G(f - kF_s) \tag{3.4.14}$$

By combining equations 3.4.13 and 3.4.14, the restriction on $G(f)$ for zero ISI on both inphase and quadrature channels can be obtained as

$$\sum_{k=-\infty}^{\infty} G(f - kF_s) = T_p \cdot \cos\frac{\pi f T_p}{2} \cdot e^{-j\frac{\pi f T_p}{2}} \tag{3.4.15}$$

where $F_s = \frac{2}{T_p}$ Hz

Equation 3.4.15 is the frequency domain representation of the zero ISI criterion for a coherent IF-sampling receiver with perfect sampling timing. The criterion implies that in order to avoid ISI on both inphase and quadrature channels, the periodic replication of $G(f)$ must have a magnitude response of

$$\left| \sum_{k=-\infty}^{\infty} G(f-kF_s) \right| = T_p \cdot \left| \cos \frac{\pi f T_p}{2} \right| \tag{3.4.16}$$

and a phase response of

$$\arg\left\{ \sum_{k=-\infty}^{\infty} G(f-kF_s) \right\} = \begin{cases} -\frac{\pi f T_p}{2} & \text{if } \cos\frac{\pi f T_p}{2} > 0, \quad \text{for } |f| < \frac{1}{T_p} \\ -\frac{\pi f T_p}{2} + \pi & \text{if } \cos\frac{\pi f T_p}{2} < 0, \quad \text{for } |f| < \frac{1}{T_p} \end{cases} \tag{3.4.17}$$

Notice that, except at the points of phase discontinuity, the phase response is a linear function of frequency. Both the time domain and frequency domain zero ISI criterion are shown in Figure 3.4.1. Analysis of equation 3.4.15 leads to the bandwidth requirement of the signalling pulse. Assume W is the total lowpass bandwidth of the signalling pulse, then the study can be divided into 3 cases : $W < \frac{2}{T_p}$, $W = \frac{2}{T_p}$, $W > \frac{2}{T_p}$.

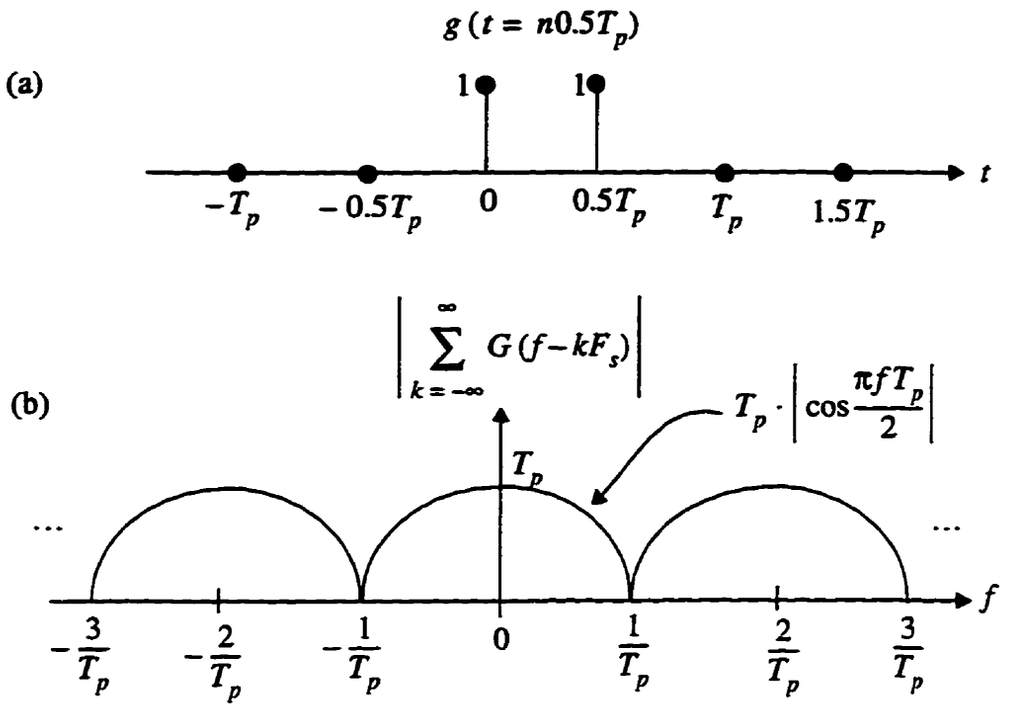

Figure 3.4.1 (a) Time domain zero ISI criterion.
(b) Frequency domain zero ISI criterion (magnitude response only).

Case 1 : $W < \frac{2}{T_p}$

Since W is less than $W < \frac{2}{T_p}$ and the sampling rate is $\frac{2}{T_p}$, then spectral overlap is avoided. Therefore as shown in Figure 3.4.2, it is impossible to fill in the spectral gaps to satisfy Equation 3.4.15 .

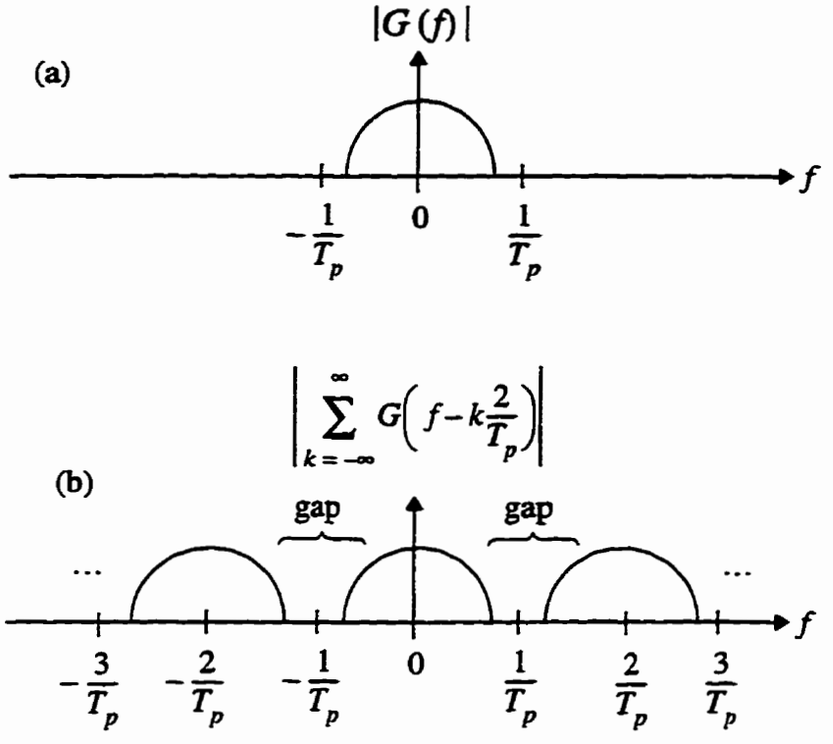

Figure 3.4.2 (a) Magnitude spectrum of $g(t)$.

(b) Magnitude spectrum of the periodic replication of $G(f)$.

Case 2 : $W = \frac{2}{T_p}$

When W is equal to $\frac{2}{T_p}$ and the sampling rate is $\frac{2}{T_p}$, frequency aliasing is marginally avoided. In this case, there exits only one solution of $g(t)$ which can satisfy the zero ISI criterion and the solution is

$$G(f) = \begin{cases} T_p \cdot \cos\frac{\pi f T_p}{2} \cdot e^{-j\frac{\pi f T_p}{2}} & \text{for } |f| < \frac{1}{T_p} \\ 0 & \text{otherwise} \end{cases} \qquad (3.4.18)$$

The magnitude spectrum is plotted in Figure 3.4.3.

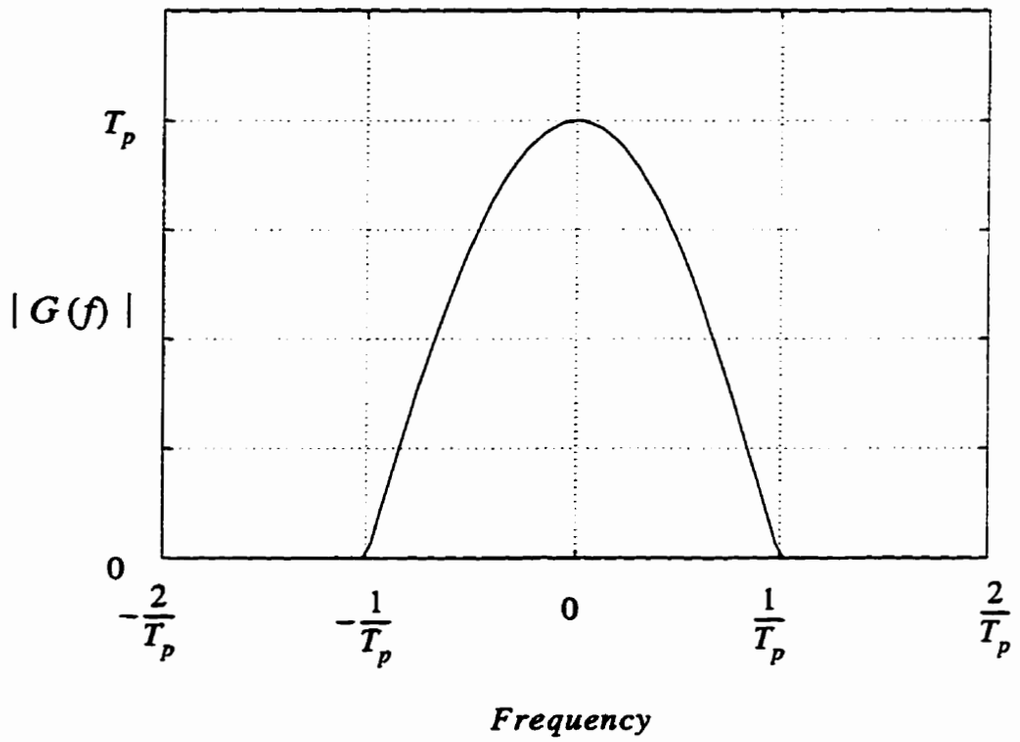

Figure 3.4.3 Magnitude spectrum of zero ISI signalling pulse for $W = \frac{2}{T_p}$.

The time domain zero ISI pulse, $g(t)$ can be obtained in two ways. The first approach is a direct application of the inverse continuous-time Fourier transform of $G(f)$ to obtain $g(t)$. The second approach involves the reconstruction of a

bandlimited continuous-time signal from its samples in the Nyquist sampling theorem. It is the second approach which is used in this thesis to obtain $g(t)$.

In general, a continuous-time signal, $g(t)$, can be constructed from a discrete-time signal, $g[n]$, in a process described as follows,

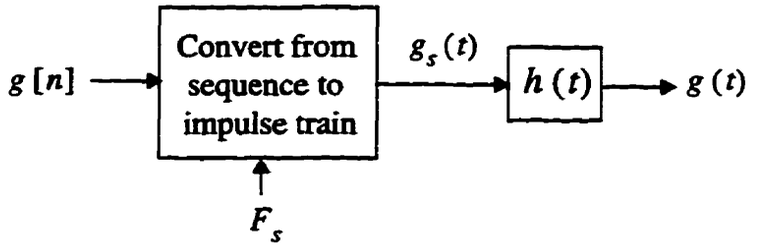

Figure 3.4.4 Block diagram of reconstruction process

By converting the sequences in $g[n]$ to an impulse train with a sampling rate of F_s, the modulated impulse train is found to be

$$g_s(t) = \sum_{k=-\infty}^{\infty} g[n] \cdot \delta\left(t - \frac{n}{F_s}\right) \qquad (3.4.19)$$

The impulse response of the ideal lowpass filter is given as

$$h(t) = \text{sinc pulse} = \frac{\sin(\pi t F_s)}{\pi t F_s} \qquad (3.4.20)$$

By convolving $g_s(t)$ with $h(t)$, the desired continuous-time signal is obtained as

$$g(t) = \sum_{k=-\infty}^{\infty} g[n] \cdot \frac{\sin[\pi(t-n/F_s)F_s]}{\pi(t-n/F_s)F_s} \qquad (3.4.21)$$

Substituting $g[n] = \begin{cases} 1 & \text{for } n=0,1 \\ 0 & \text{otherwise} \end{cases}$ and the sampling rate of $\frac{2}{T_p}$ Hz into Equation 3.4.21 produces the desired zero ISI signalling pulse,

$$\begin{aligned} g(t) &= \frac{\sin(2\pi t/T_p)}{2\pi t/T_p} + \frac{\sin[2\pi(t-0.5T_p)/T_p]}{2\pi(t-0.5T_p)/T_p} \\ &= \frac{0.25T_p^2 \cdot \sin(2\pi t/T_p)}{\pi t(0.5T_p - t)} \end{aligned} \qquad (3.4.22)$$

The pulse described by $g(t)$ is very similar to a duobinary pulse except that it has a 100% excess bandwidth. This pulse is plotted in Figure 3.4.5 . Notice that $g(t)$ can also be viewed as a sum of two sinc pulses with a time offset of $0.5T_p$.

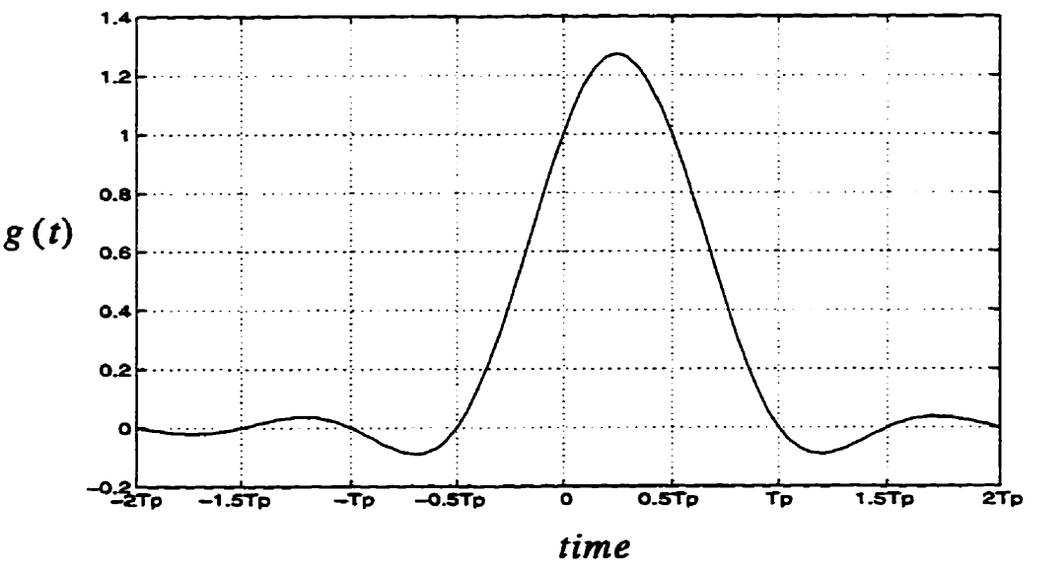

Figure 3.4.5 The minimum bandwidth zero ISI signalling pulse.

Case 3 : $W > \frac{2}{T_p}$

With $W > \frac{2}{T_p}$, the sampling rate is less than twice the highest frequency, As a result, frequency aliasing must occur. Therefore it is possible to have numerous choices of $g(t)$ to satisfy Equation 3.4.15 . However, since the transmission bandwidth should be kept as low as possible, the solution in case 2 is always better and no further study is pursued for this case.

As a result, for a coherent IF-sampling receiver with perfect sampling timing and a sampling rate of 2 samples per symbol, the minimum bandwidth for achieving zero intersymbol interference is $2/T_p$ Hz. Any signalling pulse with bandwidth less than $2/T_p$ Hz must generate ISI. In other words, an IF-sampling receiver requires a signalling pulse with at least a 100% excess bandwidth. When the bandwidth of $g(t)$ is greater than $2/T_p$ Hz , several choices of $g(t)$ can satisfy the zero ISI criterion stated in Equation 3.4.15 .

3.5 Summary

This chapter has described the details of the IF-sampling communications system. A linear modulation scheme is employed in the transmitter while the channel is assumed to be an additive bandpass white Gaussian noise channel. On the receiver side, the IF-sampling receiver is shown to be capable of extracting the inphase and quadrature symbols through the sampling process. With the proposed receiver architecture, both the time and frequency domains of the zero ISI criterion are derived. Also both the minimum bandwidth and the actual signalling pulse for achieving zero ISI are given in this chapter.

Chapter 4 Performance of the Proposed IF-sampling Receiver

In chapter 3, the proposed IF-sampling receiver was described. The receiver is general in the sense that any linear digital modulator and detector can be employed. However, in order to evaluate the performance of a communications system, a particular modulator and detector must be specified. In this project, differential quadrature phase shift keying (DQPSK) modulator and differential detector are adopted due to their simplicity and popularity. The whole system is simulated to obtain the bit error rate performance under the distortions of timing error, phase offset and noise. As will be shown in this chapter, the timing error can severely degrade the system performance and cause irreducible bit error rate. Also, due to the presence of the asymmetric intersymbol interference, the phase offset becomes an important factor on the system performance.

4.1 DQPSK Modulator and Differential DQPSK Detector

In recent years, a large amount of attention has been paid over digital mobile communication systems employing differential quadrature phase shift keying (DQPSK) [14]-[18]. One of the advantages of DQPSK modulation is its high bandwidth efficiency ranging from 2 bit/sec/Hz (for a 0% excess bandwidth signalling pulse) to 1 bit/sec/Hz (for a 100% excess bandwidth signalling pulse). The bandwidth efficiency is calculated using the bandpass bandwidth. In addition, a differential modulation scheme allows the use of noncoherent detectors which are of simpler implementation than coherent detectors. Due to these advantages, one particular form of DQPSK modulation, known as $\frac{\pi}{4}$ - DQPSK, has been adopted by both the North American and the Japanese digital cellular standards [16]. Consequently, DQPSK is also adopted throughout the thesis.

A DQPSK modulator takes two information bits at a time and produces one complex-valued symbol, $I_n + jQ_n$. These two bits are encoded using the phase difference between two consecutive complex symbols. If the two information bits (also known as dibits) are 00, 01, 11 or 10, then the phase changes relative to the previous symbol are 0°, 90°, 180° or 270° respectively. This encoding rule is shown graphically in Figure 4.1.1 .

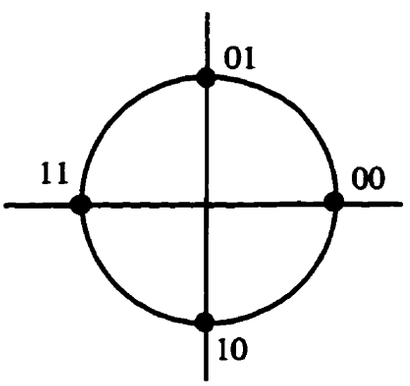

Figure 4.1.1 Signal constellation showing the relationship between the relative phase shift and the dibit.

Notice that the assignment of the relative phase change follows Gray coding [6, pp.201] such that all adjacent phase shifts only differ in one binary digit. The advantage of Gray coding is that since errors are most likely to be made to neighboring points in the signal constellation, only one bit is decoded incorrectly. This minimizes the number of errors resulting from the presence of distortion. In DQPSK modulation, an extra complex symbol is required at the beginning of the symbol sequence to provide a phase reference for the first dibit. This initial symbol is arbitrarily assumed to be $0.707 + j0.707$. By having the initial phase to be 45° and the encoding rule as shown in Figure 4.1.1, there are in total 4 possible transmit signal points in the signal constellation (Figure 4.1.2). All four points reside on the unit circle and their phases are 45°, 135°, 225° or 315° .

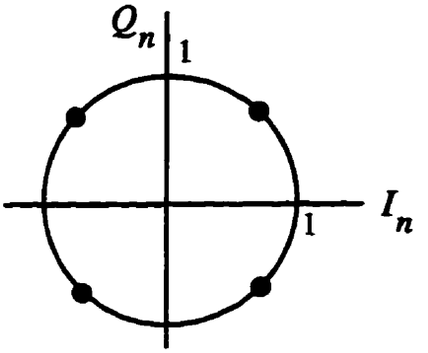

Figure 4.1.2 Constellation showing all four possible transmit signal points.

On the receiver side, the bandpass RF signal is processed by the IF-sampling receiver and a corresponding sequence of received complex symbols is generated at the output of the IF-sampling receiver. These distorted complex symbols, $a[n] + jb[n]$, are then decoded by the differential detector to recover the transmitted information bits. The distorted inphase and quadrature symbols are denoted by $a[n]$ and $b[n]$ respectively. A differential (or noncoherent) detector, which employs delay and conjugate multiplication [2, pp. 274], is adopted in this project. Several other types of differential detector can also be found in the literature [12], [14]. The block diagram of the differential detection is shown in Figure 4.1.3.

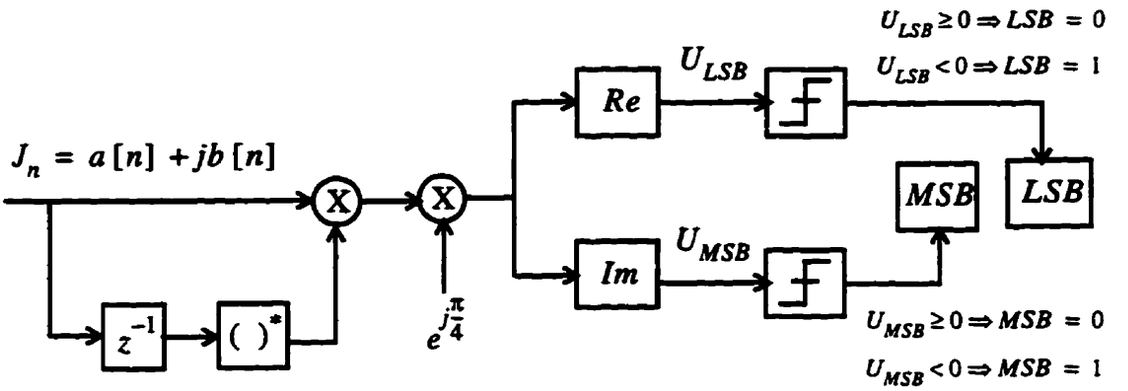

Figure 4.1.3 Differential detection for DQPSK symbols.

The received symbols are decoded according to the values of two decision variables whose derivations are based on the phase change between two consecutive complex symbols. This phase change is obtained by multiplying the present received complex symbol with the complex conjugate of the previous complex symbol. In Figure 4.1.3, there is a second multiplication of $e^{j\frac{\pi}{4}}$ which rotates the multiplication product by 45° in the counter-clockwise direction. This rotation causes the four signal points in Figure 4.1.1 to fall into the centers of the four quadrants. The decision variable for the most significant bit (MSB), U_{MSB}, is obtained as

$$U_{MSB} = Im\left(J[n] \cdot J^*[n-1] \cdot e^{j\frac{\pi}{4}} \right) \qquad (4.1.1)$$

where * denotes complex conjugate. The most significant bit is decoded as 0 if $U_{MSB} \geq 0$; otherwise it is a 1. On the other hand, the decision variable for the least significant bit (LSB), U_{LSB}, is determined as

$$U_{LSB} = Re\left(J[n] \cdot J^*[n-1] \cdot e^{j\frac{\pi}{4}} \right) \qquad (4.1.2)$$

Similarly, the least significant bit is decoded as 0 if $U_{LSB} \geq 0$; otherwise it is a 1. Notice that this differential detection scheme involves only multiplication and addition in the calculation of the decision variables. No complex operation, such as trigonometric function, is required.

4.2 The Effect of Bandpass White Noise on the Proposed IF-sampling Receiver

This section studies the propagation of the bandpass white noise through the IF-sampling receiver. It is assumed that the bandpass white noise has the same bandwidth as the information-bearing signal. Any out-of-band noise is filtered out by the front-end bandpass filter shown in Figure 3.3.1. Similar to the information signal, the bandpass white noise is also processed by the IF-sampling receiver which in turn produces the two corresponding discrete-time random sequences : $z_i[n]$ and $z_q[n]$. The subscript 'i' represents the inphase channel whereas the subscript 'q' refers to the quadrature channel. From the expressions of the received inphase and quadrature symbols derived in Equations 3.3.11 and 3.3.12, the inphase noise sequence $z_i[n]$ is found to be,

$$z_i[n] = x(nT_p - t_d) \cdot \cos\left(-\frac{\pi t_d}{T_p} + \theta\right) - y(nT_p - t_d) \cdot \sin\left(-\frac{\pi t_d}{T_p} + \theta\right) \qquad (4.2.1)$$

and the quadrature noise sequence $z_q[n]$ is,

$$z_q[n] = x(nT_p + 0.5T_p - t_d) \cdot \sin\left(-\frac{\pi t_d}{T_p} + \theta\right) + y(nT_p + 0.5T_p - t_d) \cdot \cos\left(-\frac{\pi t_d}{T_p} + \theta\right) \qquad (4.2.2)$$

Several statistical properties namely statistical means, autocorrelation functions, cross-correlation functions and probability density functions of these two noise sequences are investigated in this section. Throughout the whole investigation, both t_d and θ are treated as deterministic quantities.

The investigation starts with the statistical means of the two random processes. By taking ensemble expectation on $z_i[n]$ and $z_q[n]$, the statistical means are determined to be,

$$E\{z_i[n]\} = E\{x(nT_p - t_d)\} \cdot \cos\left(-\frac{\pi t_d}{T_p} + \theta\right) - E\{y(nT_p - t_d)\} \cdot \sin\left(-\frac{\pi t_d}{T_p} + \theta\right) \quad (4.2.3)$$

and

$$E\{z_q[n]\} = E\{x(nT_p + 0.5T_p - t_d)\} \cdot \sin\left(-\frac{\pi t_d}{T_p} + \theta\right) + E\{y(nT_p + 0.5T_p - t_d)\} \cdot \cos\left(-\frac{\pi t_d}{T_p} + \theta\right) \quad (4.2.4)$$

Since both $x(t)$ and $y(t)$ have zero means (Equation 3.2.5), it follows that both $z_i[n]$ and $z_q[n]$ also have zero means for all time, that is

$$E\{z_i[n]\} = E\{z_q[n]\} = 0 \quad \text{for all n} \quad (4.2.5)$$

The autocorrelation functions of both $z_i[n]$ and $z_q[n]$ are defined as,

$$\phi_{z_i z_i}[n; n-k] = E\{z_i[n] \cdot z_i[n-k]\} \quad (4.2.6)$$

$$\phi_{z_q z_q}[n; n-k] = E\{z_q[n] \cdot z_q[n-k]\} \quad (4.2.7)$$

By substituting the expression of $z_i[n]$ into Equation 4.2.6, the autocorrelation of

$z_i[n]$ is expanded as,

$$\begin{aligned}\phi_{z_i z_i}[n;n-k] &= E\left\{x(nT_p - t_d)\cdot x(nT_p - kT_p - t_d)\cdot \cos^2\left(-\frac{\pi t_d}{T_p}+\theta\right)\right\} \\ &-E\left\{x(nT_p - t_d)\cdot y(nT_p - kT_p - t_d)\cdot \cos\left(-\frac{\pi t_d}{T_p}+\theta\right)\cdot \sin\left(-\frac{\pi t_d}{T_p}+\theta\right)\right\} \\ &-E\left\{x(nT_p - kT_p - t_d)\cdot y(nT_p - t_d)\cdot \cos\left(-\frac{\pi t_d}{T_p}+\theta\right)\cdot \sin\left(-\frac{\pi t_d}{T_p}+\theta\right)\right\} \\ &+E\left\{y(nT_p - t_d)\cdot y(nT_p - kT_p - t_d)\cdot \sin^2\left(-\frac{\pi t_d}{T_p}+\theta\right)\right\}\end{aligned} \tag{4.2.8}$$

Since the cross-correlation between the two noise processes $x(t)$ and $y(t)$ is zero for all time shifts, the middle two terms are equal to zero and Equation 4.2.8 can be simplified as

$$\begin{aligned}\phi_{z_i z_i}[n;n-k] &= \phi_{xx}(\tau = kT_p)\cdot \cos^2\left(-\frac{\pi t_d}{T_p}+\theta\right) \\ &+\phi_{yy}(\tau = kT_p)\cdot \sin^2\left(-\frac{\pi t_d}{T_p}+\theta\right)\end{aligned} \tag{4.2.9}$$

Also due to the fact that $x(t)$ and $y(t)$ have the same autocorrelation function (Equations 3.2.6 and 3.2.7), the final expression for the autocorrelation of $z_i[n]$ is,

$$\phi_{z_i z_i}[n;n-k] = \phi_{z_i z_i}[k] = N_o \cdot \frac{\sin(\pi W k T_p)}{\pi k T_p} \tag{4.2.10}$$

Similarly the autocorrelation function of $z_q[n]$ can be obtained by repeating the above procedure. Substituting the expression for $z_q[n]$ into Equation 4.2.7 yields,

$$\phi_{z_q z_q}[n;n-k] =$$

$$E\{x(nT_p+0.5T_p-t_d)\cdot x(nT_p-kT_p+0.5T_p-t_d)\cdot \sin^2(\rho)\}$$

$$+E\{x(nT_p+0.5T_p-t_d)\cdot y(nT_p-kT_p+0.5T_p-t_d)\cdot \sin(\rho)\cdot\cos(\rho)\} \quad (4.2.11)$$

$$+E\{y(nT_p+0.5T_p-t_d)\cdot x(nT_p-kT_p+0.5T_p-t_d)\cdot \cos(\rho)\cdot\sin(\rho)\}$$

$$+E\{y(nT_p+0.5T_p-t_d)\cdot y(nT_p-kT_p+0.5T_p-t_d)\cdot \cos^2(\rho)\}$$

$$\text{where} \quad \rho = -\frac{\pi t_d}{T_p}+\theta \quad .$$

Applying the facts that the cross-correlation between $x(t)$ and $y(t)$ is always zero and that these two processes have the same autocorrelation function, the final expression for the autocorrelation of $z_q[n]$ is,

$$\phi_{z_q z_q}[n;n-k] = \phi_{z_q z_q}[k] = N_o \cdot \frac{\sin(\pi W k T_p)}{\pi k T_p} \quad (4.2.12)$$

Several observations can be made from Equations 4.2.10 and 4.2.12 . Firstly, both $z_i[n]$ and $z_q[n]$ have exactly the same autocorrelation function. Secondly, these two autocorrelation functions depend only on the difference of the two time indices. This suggests that both $z_i[n]$ and $z_q[n]$ are wide-sense stationary random processes. In addition, the relationship between $\phi_{xx}(\tau)$ and $\phi_{z_i z_i}[k]$ can be obtained through a sampling process described in Figure 4.2.1 . The same relationship applies between $\phi_{yy}(\tau)$ and $\phi_{z_q z_q}[k]$.

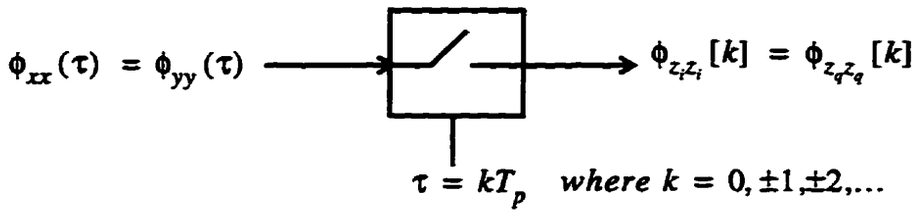

Figure 4.2.1 Relationship between $\phi_{xx}(\tau)$ and $\phi_{z_i z_i}[k]$. The same relationship applies between $\phi_{yy}(\tau)$ and $\phi_{z_q z_q}[k]$.

By applying the relationship shown in Figure 4.2.1 and the autocorrelation function and power density spectrum shown in Figure 3.2.2, it can be shown that the two discrete-time noise processes, $z_i[n]$ and $z_q[n]$, can be either white or non-white processes depending on the excess bandwidth of the signalling pulse. The proof is presented in the following three cases.

Case 1 : 0% excess bandwidth

With the signalling pulse having 0% excess bandwidth, the total lowpass bandwidth (W) is,

$$W = \frac{1}{T_p} \tag{4.2.13}$$

Then the autocorrelation functions, $\phi_{xx}(\tau)$ and $\phi_{yy}(\tau)$, become

$$\phi_{xx}(\tau) = \phi_{yy}(\tau) = N_o \cdot \frac{\sin\left(\pi \frac{\tau}{T_p}\right)}{\pi\tau} \tag{4.2.14}$$

These two functions are also sketched in Figure 4.2.2.

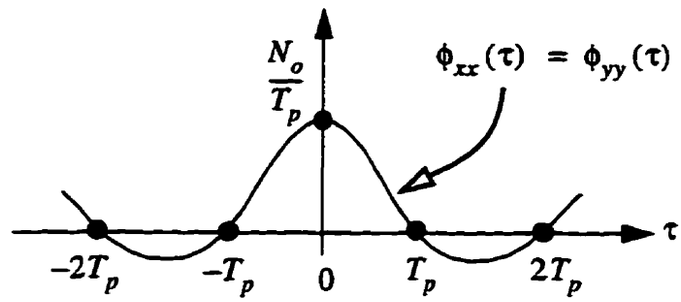

Figure 4.2.2 Autocorrelation functions $\phi_{xx}(\tau)$ and $\phi_{yy}(\tau)$ for 0% excess bandwidth.

By sampling this autocorrelation function with a sampling rate of $1/T_p$, one can obtain $\phi_{z_i z_i}[k]$ and $\phi_{z_q z_q}[k]$ as

$$\phi_{z_i z_i}[k] = \phi_{z_q z_q}[k] = \frac{N_o}{T_p} \cdot \delta[k] \qquad (4.2.15)$$

The sampling points are shown as dots in Figure 4.2.2. Since the discrete-time autocorrelation functions are zero except at k = 0, the two sequences, $z_i[n]$ and $z_q[n]$, are white random processes.

The same result can also be obtained in the frequency domain in which the power density spectra of $x(t)$ and $y(t)$ are given as,

$$\Phi_{xx}(f) = \Phi_{yy}(f) = \begin{cases} N_0 & |f| < \frac{1}{2T_p} \\ 0 & otherwise \end{cases} \qquad (4.2.16)$$

By periodically replicating $\Phi_{xx}(f)$ with a period of $1/T_p$ and multiplying the spectrum

by the sampling rate (i.e. $1/T_p$) , one can obtain the power density spectra of $z_i[n]$ and $z_q[n]$ as

$$\Phi_{z_i z_i}\left(e^{j2\pi fT_p}\right) = \Phi_{z_q z_q}\left(e^{j2\pi fT_p}\right) = \frac{N_o}{T_p} \tag{4.2.17}$$

All of these four power density spectra are shown in Figure 4.2.3.

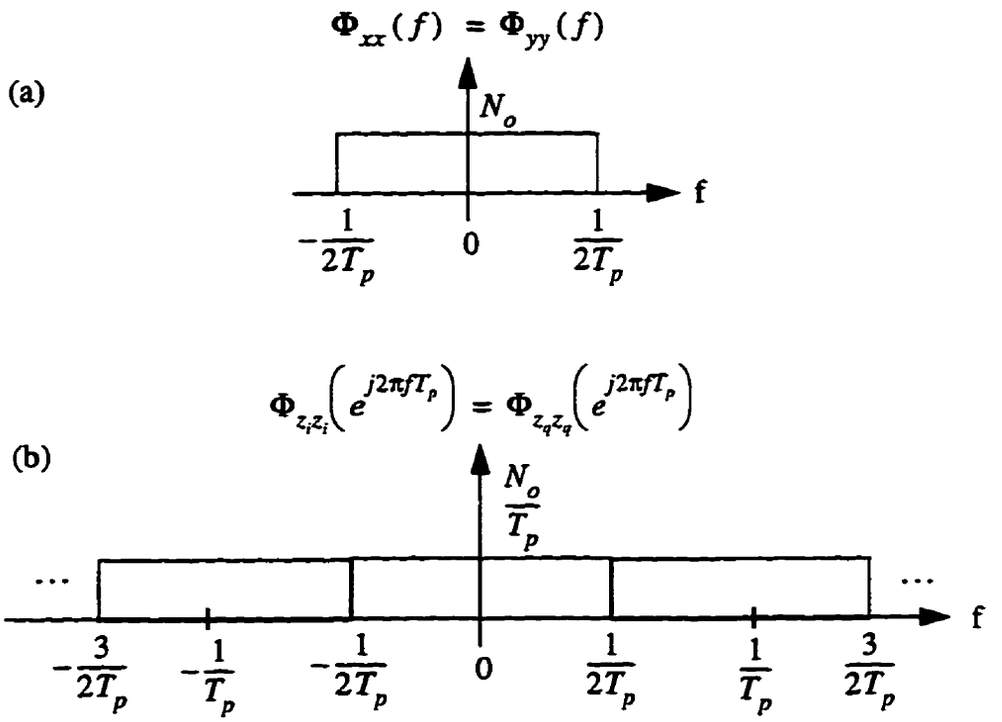

Figure 4.2.3 (a) Power density spectra of $x(t)$ and $y(t)$ for 0% excess bandwidth.
(b) Power density spectra of $z_i[n]$ and $z_q[n]$ for 0% excess bandwidth.

It is clear that both $z_i[n]$ and $z_q[n]$ have flat a power density spectra and as a result they are white processes.

Case 2 : 0% (exclusive) to 100% (exclusive) excess bandwidth

With the signalling pulse having 0% (exclusive) to 100% (exclusive) excess bandwidth, the total lowpass bandwidth (W) is in the range,

$$\frac{1}{T_p} < W < \frac{2}{T_p} \tag{4.2.18}$$

In general, the autocorrelation functions, $\phi_{xx}(\tau)$ and $\phi_{yy}(\tau)$ are given as,

$$\phi_{xx}(\tau) = \phi_{yy}(\tau) = N_o \cdot \frac{\sin(\pi W \tau)}{\pi \tau} \tag{4.2.19}$$

A special case of 50% excess bandwidth ($W = 1.5/T_p$) is used as an example and the corresponding autocorrelation functions of $\phi_{xx}(\tau)$ and $\phi_{yy}(\tau)$ are shown in Figure 4.2.4 .

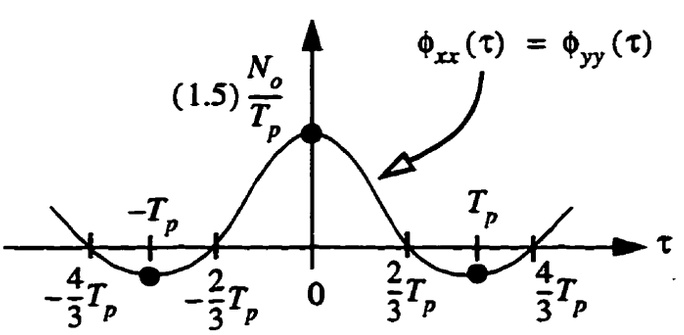

Figure 4.2.4 Autocorrelation functions of $\phi_{xx}(\tau)$ and $\phi_{yy}(\tau)$ for 50% excess bandwidth.

Mathematically, the autocorrelation functions of $z_i[n]$ and $z_q[n]$ are

$$\phi_{z_i z_i}[k] = \phi_{z_q z_q}[k] = N_o \cdot \frac{\sin(\pi 1.5k)}{\pi k T_p} \tag{4.2.20}$$

Notice that both $\phi_{z_i z_i}[k]$ and $\phi_{z_q z_q}[k]$ are no longer equal to a discrete-time delta

function. This implies that the two noise sequences are no longer white. The same observation can be made in the frequency domain. Both $\Phi_{xx}(f)$ and $\Phi_{yy}(f)$ are shown in Figure 4.2.5.

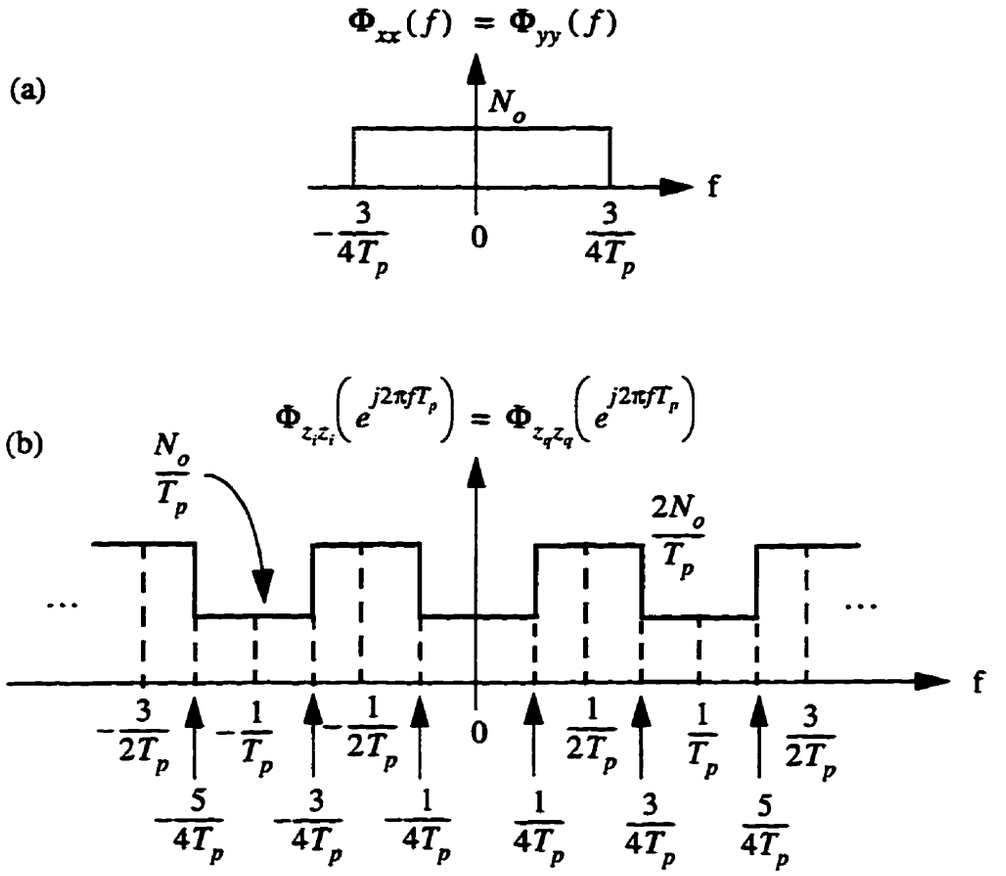

Figure 4.2.5 (a) Power density spectra of $x(t)$ and $y(t)$ for 50% excess bandwidth.
(b) Power density spectra of $z_i[n]$ and $z_q[n]$ for 50% excess bandwidth.

It is clear that the spectrum $\Phi_{z_i z_i}\left(e^{j2\pi fT_p}\right)$ is no longer flat and this result is consistent with the time domain investigation. In general, the two noise sequences $z_i[n]$ and $z_q[n]$ are not white processes for the signalling pulse having 0% (exclusive) to 100% (exclusive) excess bandwidth.

Case 3 : 100% excess bandwidth

With the signalling pulse having 100% excess bandwidth, the total lowpass bandwidth, W, is

$$W = \frac{2}{T_p} \tag{4.2.21}$$

Then the autocorrelation functions, $\phi_{xx}(\tau)$ and $\phi_{yy}(\tau)$, become

$$\phi_{xx}(\tau) = \phi_{yy}(\tau) = N_o \cdot \frac{\sin\left(\pi\frac{2\tau}{T_p}\right)}{\pi\tau} \tag{4.2.22}$$

These two functions are sketched in Figure 4.2.6.

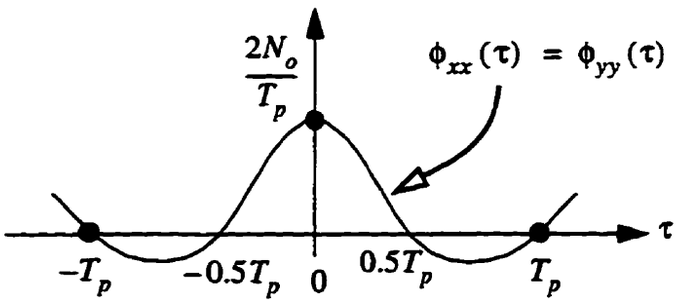

Figure 4.2.6 Autocorrelation functions $\phi_{xx}(\tau)$ and $\phi_{yy}(\tau)$ for 100% excess bandwidth.

Sampling this autocorrelation function with a sampling rate of $1/T_p$ yields $\phi_{z_i z_i}[k]$ and $\phi_{z_q z_q}[k]$ as,

$$\phi_{z_i z_i}[k] = \phi_{z_q z_q}[k] = \frac{2N_o}{T_p} \cdot \delta[k] \tag{4.2.23}$$

Since the autocorrelation functions equal to a scaled discrete-time delta function, both $z_i[n]$ and $z_q[n]$ are white random processes.

In the frequency domain, the power density spectra of $x(t)$ and $y(t)$ are given as,

$$\Phi_{xx}(f) = \Phi_{yy}(f) = \begin{cases} N_0 & |f| < \frac{1}{T_p} \\ 0 & otherwise \end{cases} \qquad (4.2.24)$$

By periodically replicating $\Phi_{xx}(f)$ with a period of $1/T_p$ and multiplying the spectrum by $1/T_p$, the power density spectra of $z_i[n]$ and $z_q[n]$ are obtained as

$$\Phi_{z_i z_i}\left(e^{j2\pi f T_p}\right) = \Phi_{z_q z_q}\left(e^{j2\pi f T_p}\right) = \frac{2N_o}{T_p} \qquad (4.2.25)$$

All of these four power density spectra are shown in Figure 4.2.7.

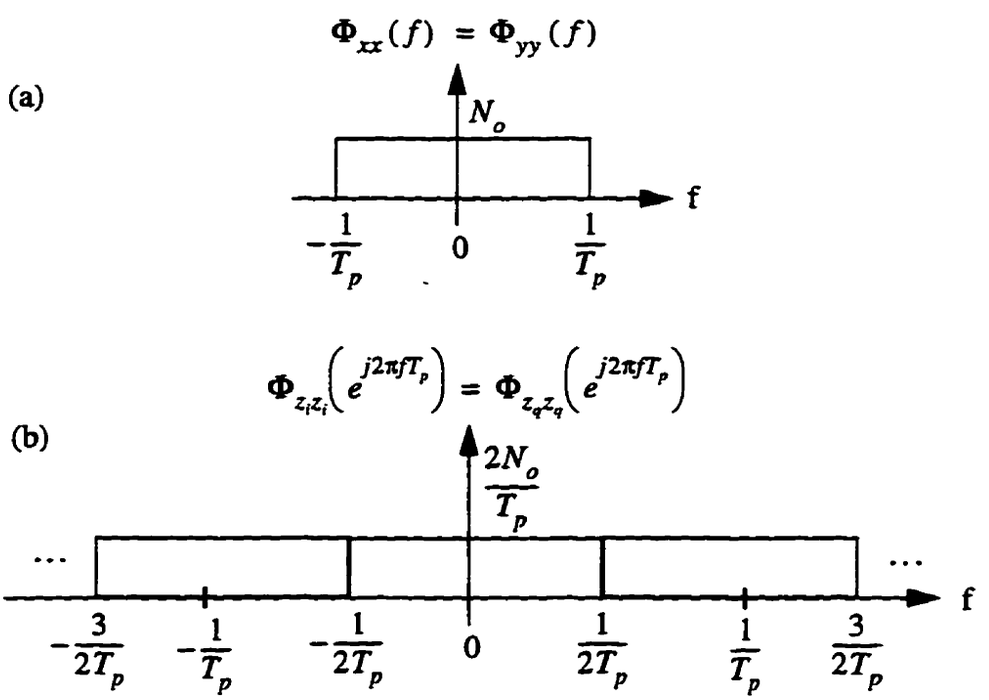

Figure 4.2.7 (a) Power density spectra of $x(t)$ and $y(t)$ for 100% excess bandwidth.
(b) Power density spectra of $z_i[n]$ and $z_q[n]$ for 100% excess bandwidth.

Again both $z_i[n]$ and $z_q[n]$ have flat power density spectra and as a result the noise sequences, $z_i[n]$ and $z_q[n]$, are white random processes.

In summary, the two noise sequences, $z_i[n]$ and $z_q[n]$ are white wide-sense stationary process for both 0% and 100% excess bandwidth signalling pulse. For any excess bandwidth ranging from 0% (exclusive) to 100% (exclusive), the two noise sequences are no longer white.

In addition to the autocorrelation function, another important parameter of a random process is its total average power. For a continuous-time random process, the total average power is equal to the autocorrelation function evaluated at zero time shift. Therefore,

$$\text{Total Average Power of } x(t) = \phi_{xx}(\tau = 0) = N_o \cdot W \qquad (4.2.26)$$

Similarly,

$$\text{Total Average Power of } y(t) = \phi_{yy}(\tau = 0) = N_o \cdot W \qquad (4.2.27)$$

For a discrete-time random process, the total average power is also equal to the autocorrelation function evaluated at zero time shift. Therefore,

$$\text{Total Average Power of } z_i[n] = \phi_{z_i z_i}[k = 0] = N_o \cdot W \qquad (4.2.28)$$

and

$$\text{Total Average Power of } z_q[n] = \phi_{z_q z_q}[k = 0] = N_o \cdot W \qquad (4.2.29)$$

Notice that the two discrete-time noise sequences, $z_i[n]$ and $z_q[n]$, have the same average power as the two continuous-time lowpass noise processes, $x(t)$ and $y(t)$. As

a result, as the bandpass noise propagates through the IF-sampling receiver, the noise is neither reduced nor enhanced. In other words, all noise power propagates through the IF-sampling receiver without modification.

The fourth investigated property is the cross-correlation function between $z_i[n]$ and $z_q[n]$. The cross-correlation function is defined as,

$$\phi_{z_i z_q}[n;n-k] = E\{z_i[n] \cdot z_q[n-k]\} \tag{4.2.30}$$

By substituting the expressions for $z_i[n]$ and $z_q[n]$ into the definition, the cross-correlation is expanded as,

$$\begin{aligned}\phi_{z_i z_q}[n;n-k] = \\ &E\left\{x(nT_p - t_d) \cdot x(nT_p - kT_p + 0.5T_p - t_d) \cdot \frac{1}{2}\sin\left(-\frac{2\pi t_d}{T_p} + 2\theta\right)\right\} \\ &+E\left\{x(nT_p - t_d) \cdot y(nT_p - kT_p + 0.5T_p - t_d) \cdot \cos^2\left(-\frac{\pi t_d}{T_p} + \theta\right)\right\} \\ &-E\left\{y(nT_p - t_d) \cdot x(nT_p - kT_p + 0.5T_p - t_d) \cdot \sin^2\left(-\frac{\pi t_d}{T_p} + \theta\right)\right\} \\ &-E\left\{y(nT_p - t_d) \cdot y(nT_p - kT_p + 0.5T_p - t_d) \cdot \frac{1}{2}\sin\left(-\frac{2\pi t_d}{T_p} + 2\theta\right)\right\}\end{aligned} \tag{4.2.31}$$

Since $\phi_{xy}(\tau) = 0$ for all τ, the middle two terms are equal to zero. Also since $x(t)$ and $y(t)$ have the same autocorrelation function, the first and the last terms cancel each other. Therefore the cross-correlation between $z_i[n]$ and $z_q[n]$ is always zero for any value of excess bandwidth and any time-shift.

$$\phi_{z_i z_q}[n;n-k] = \phi_{z_i z_q}[k] = 0 \tag{4.2.32}$$

The last statistical quantity being studied is the probability density functions of $z_i[n]$ and $z_q[n]$. Due to the fact that both $z_i[n]$ and $z_q[n]$ are linear combinations of two uncorrelated Gaussian processes, it follows that $z_i[n]$ and $z_q[n]$ are also Gaussian processes [2, pp.41].

In summary, the two discrete-time noise sequences are uncorrelated Gaussian processes with zero means. For the case of 0% and 100% excess bandwidths, these two processes are white. However, for any excess bandwidth ranging from 0% (exclusive) to 100% (exclusive), these two processes are no longer white.

4.3 The Equivalent Discrete-time Model

In addition to the bandpass communications system model shown in Figure 3.1, an equivalent discrete-time model can also be derived for the system. This discrete-time model summarizes the overall effect of the whole communications system (transmitter, channel and receiver) on the transmitted information symbols. It clearly shows the effects of any linear distortion affecting the symbols. Due to this capability, the equivalent discrete-time model is a useful tool for providing insight into the source of performance degradation and the solution for performance improvement.

4.3.1 The Equivalent Discrete-time Model for Any Signalling Pulse

The structure of the discrete-time model comes from the two expressions for the received inphase and quadrature symbols. These two expressions are given in Equations 3.3.11 and 3.3.12. By manipulating these two equations and substituting the definitions

of $z_i[n]$ and $z_q[n]$, these two equations can be rewritten as,

$$a[n] = Re\{ (I_n + jQ_n) \cdot e^{j\phi} \} \otimes g(nT_p - t_d) + z_i[n] \qquad (4.3.1)$$

and

$$b[n] = Im\{ (I_n + jQ_n) \cdot e^{j\phi} \} \otimes g(nT_p + 0.5T_p - t_d) + z_q[n] \qquad (4.3.2)$$

where $\phi = -\frac{\pi t_d}{T_p} + \theta$ and $\otimes$ denotes discrete-time convolution.

By representing these two equations in a block diagram as shown in Figure 4.3.1, the equivalent discrete-time model is obtained. Notice that since the derivation of these two equations makes no assumption on the signalling pulse, this discrete-time model is valid for any signalling pulse employed in the IF-sampling communication system. As summarized in the diagram, there are three distortions being introduced on the symbols :

1. Firstly, the transmitted complex symbols $I_n + jQ_n$ are rotated in a counter-clockwise direction by an amount ϕ which is defined above. The amount of rotation depends on both the phase offset, θ, of the local oscillator and the sampling timing error, t_d. Therefore even if the receiver complexity is increased to allow coherent downconversion, that is $\theta = 0$, the signal constellation is still rotated clockwise by $\pi t_d / T_p$. The only two situations in which the rotation vanishes are when the phase offset exactly counteracts the sampling error, that is $\theta = \pi t_d / T_p$ or when both θ and t_d are equal to zero. Note that this rotation is the only distortion which gives rise to the crossover (or crosstalk) between the I and Q channels. Thus a zero rotation implies zero crosstalk.

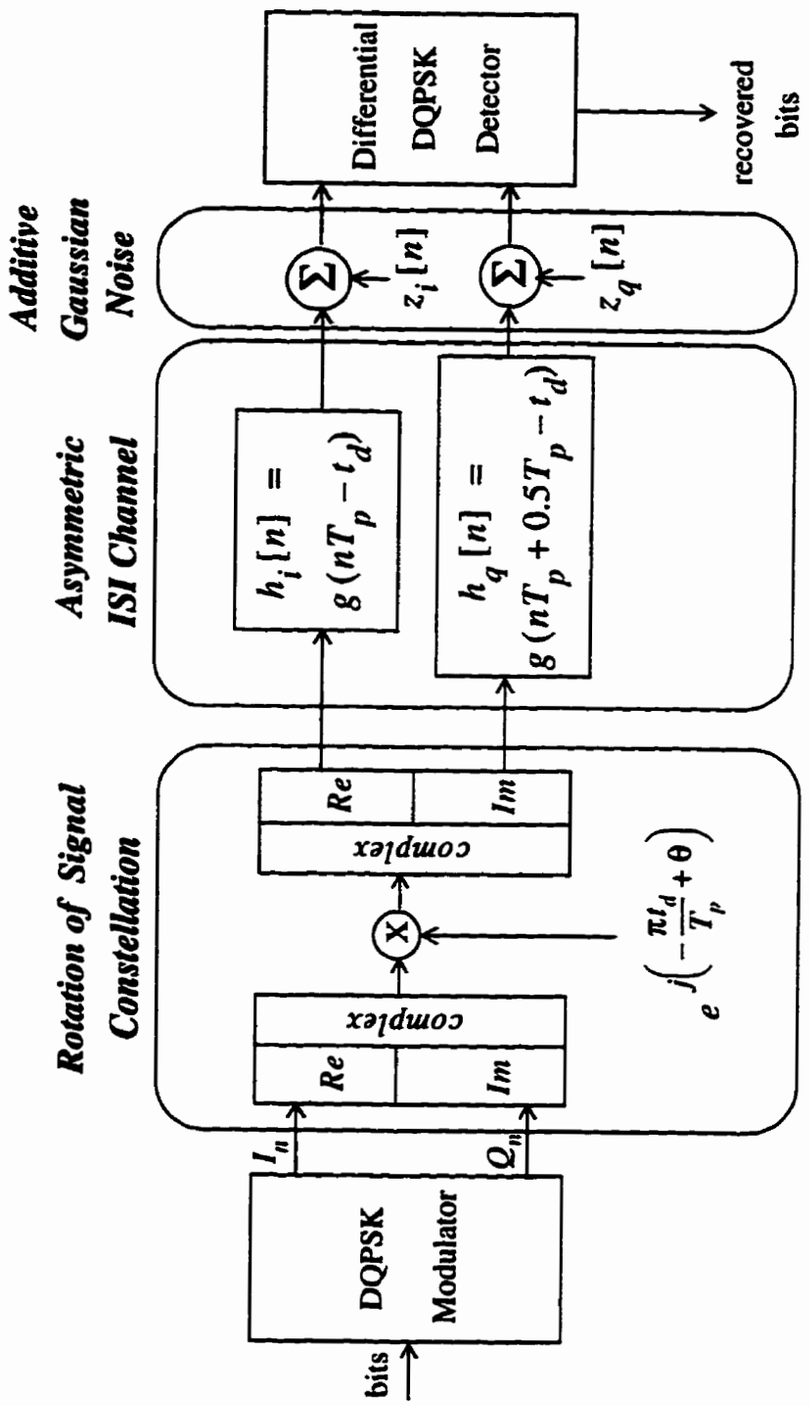

Figure 4.3.1 Equivalent discrete-time model for any signalling pulse.

2. The second distortion is the asymmetric intersymbol interference (ISI) channel. Inside this channel, the rotated I/Q symbols experience different forms of intersymbol interference. The effect of these two intersymbol interferences can be characterized by the two discrete-time filters with impulse responses denoted as $h_i[n]$ for the inphase channel and $h_q[n]$ for the quadrature channel. These two impulse responses are given as,

$$h_i[n] = g(nT_p - t_d) \tag{4.3.3}$$

and

$$h_q[n] = g(nT_p + 0.5T_p - t_d) \tag{4.3.4}$$

There are two different kinds of impairments combined to cause this asymmetric intersymbol interference. The first impairment is the sampling timing error which is responsible for causing the intersymbol interference. This is a typical distortion caused by the timing error and is common to any digital communications system. The second impairment, which is unique to the proposed IF-sampling receiver, is the timing misalignment mentioned earlier in chapter 2. Since the inphase and quadrature symbols are obtained at different times, different intersymbol interferences are introduced on the inphase and quadrature symbols. Therefore it is the timing misalignment which gives rise to the asymmetric nature of the intersymbol interference.

3. The third distortion is the addition of two noise sequences on inphase and quadrature symbols. The statistical properties of these two noises were covered in the last section. Notice that unlike the intersymbol interference, the inphase channel noise, $z_i[n]$ and the quadrature channel noise, $z_q[n]$ have the same statistical properties. Therefore the effects of noise on the inphase and quadrature channels are the same.

4.3.2 The Equivalent Discrete-time Model for Truncated 100% Excess Bandwidth Duobinary Pulse

This section focuses on the effect of the asymmetric intersymbol interference for the 100% excess bandwidth duobinary pulse. For simplicity, the term duobinary pulse is always referred to as the 100% excess bandwidth duobinary pulse. Similar to the raised cosine pulse, this duobinary pulse also has an infinite time duration in both positive and negative time axes. As a result, both filters in the asymmetric ISI channel have infinite number of taps in both positive and negative time axes. In order to obtain a simpler and more meaningful discrete-time model, an approximation is made on the duration of the duobinary pulse. Since the amplitude of the duobinary pulse decreases with $1/t^2$, where t is time and most of the energy is concentrated in the region from $t = -0.5T_p$ to $t = T_p$, the duobinary pulse is approximated by its truncated version, $g_T(t)$, which is defined as

$$g_T(t) = \begin{cases} \dfrac{0.25T_p^2 \cdot \sin(2\pi t/T_p)}{\pi t(0.5T_p - t)} & \text{for } -0.5T_p \le t \le T_p \\ 0 & \text{otherwise} \end{cases} \qquad (4.3.5)$$

By substituting this truncated duobinary pulse into the two filter impulse responses inside the asymmetric ISI channel, one can obtain the equivalent discrete-time models for different timing errors. The result is presented for three cases : (1) $t_d = 0$, (2) $0 \le t_d \le 0.25T_p$ and (3) $-0.25T_p \le t_d \le 0$.

Case 1 : $t_d = 0$

With $t_d = 0$, the sampling points coincide exactly with the zero-crossings of the infinitely long duobinary pulse. Therefore the impulse response of the inphase channel ISI filter becomes,

$$h_i[n] = g(nT_p - t_d) = g(nT_p) = \delta[n] \qquad (4.3.6)$$

whereas the impulse response of the quadrature channel ISI filter is,

$$h_q[n] = g(nT_p + 0.5T_p - t_d) = g(nT_p + 0.5T_p) = \delta[n] \qquad (4.3.7)$$

Since both ISI filters have the discrete-time delta function as their impulse responses, no distortion is introduced by these two filters. As a result, the effect of intersymbol interference vanishes and the remaining two distortions are constellation rotation and addition of Gaussian noises. The corresponding equivalent discrete-time model is shown in Figure 4.3.2. Notice that the above argument does not assume the duobinary pulse to have finite duration and therefore the discrete-time model shown in Figure 4.3.2 is valid for both the original and the truncated duobinary pulse. Also note that this result is consistent with the previous result obtained in the signal design for the proposed IF-sampling receiver.

Case 2 : $0 \le t_d \le 0.25T_p$

With the timing error (t_d) being not equal to zero, the sampling points no longer coincide with the zero-crossings of the duobinary pulse. As a result, an infinitely long intersymbol interference is introduced on the inphase and quadrature symbols. In addition, since the timing error (t_d) is greater than zero, the actual sampling points occur

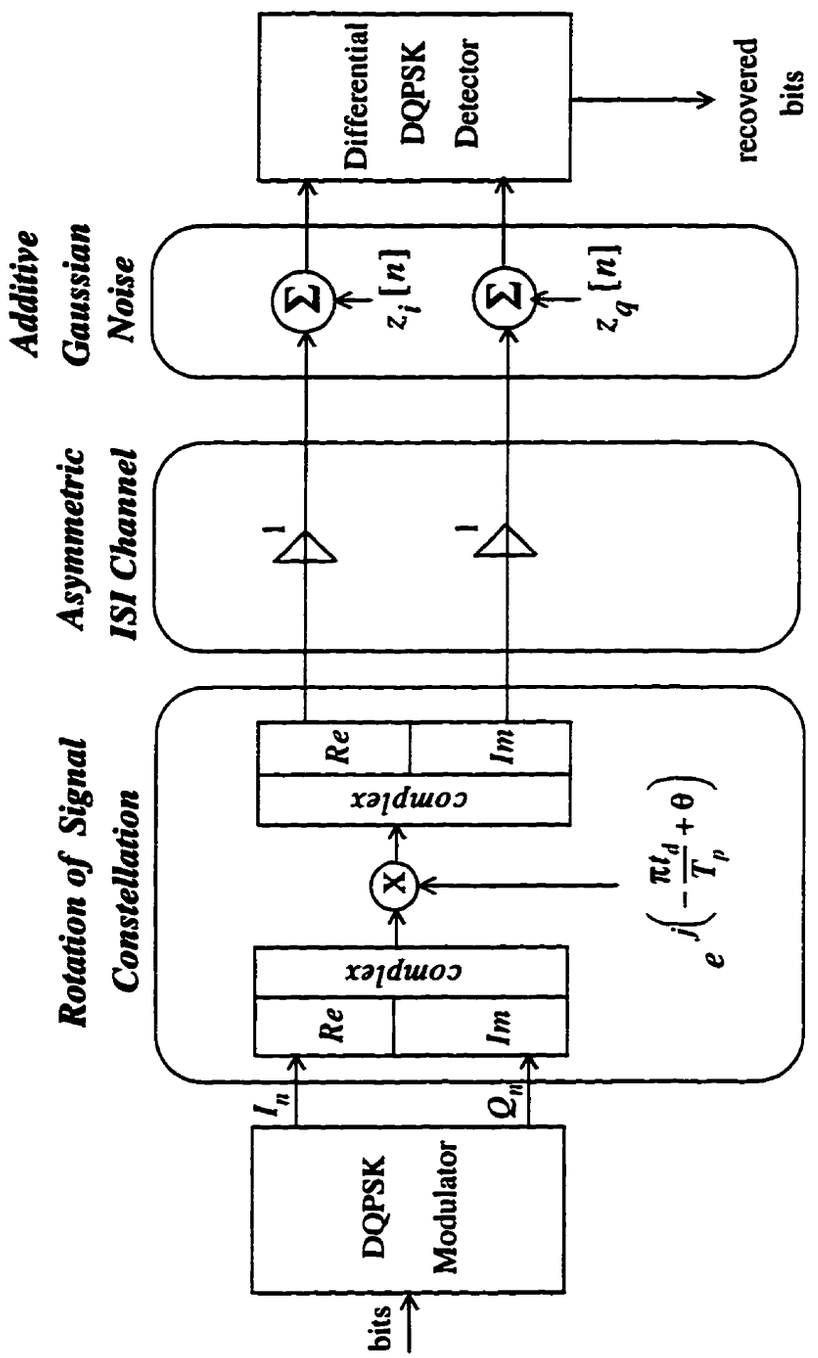

Figure 4.3.2 Equivalent discrete-time model for both original and truncated 100% excess bandwidth duobinary pulse and $t_d = 0$.

to the left of the optimal sampling points. Here optimal sampling points are referred to as the sampling points with $t_d = 0$. By replacing the original duobinary pulse with its truncated version, an approximation of the intersymbol interference is obtained and the result is presented as follows.

Approximating $g(t)$ with $g_T(t)$ in the inphase channel ISI filter yields,

$$h_i[n] \approx g_T(nT_p - t_d) \tag{4.3.8}$$

and substituting $0 \le t_d \le 0.25T_p$ into the equation of $g_T(t)$, the approximated impulse response of the inphase channel filter is found to be,

$$h_i[n] \approx A \cdot \delta[n] + B \cdot \delta[n-1] \tag{4.3.9}$$

where $A = g_T(-t_d)$

$B = g_T(T_p - t_d)$

By making the same approximation and substitution, the approximated impulse response of the quadrature channel filter is obtained as,

$$h_q[n] \approx g_T(nT_p + 0.5T_p - t_d) = C \cdot \delta[n] \tag{4.3.10}$$

where $C = g_T(0.5T_p - t_d)$

These two simplified impulse responses are incorporated into the asymmetric ISI channel and the result is shown in Figure 4.3.3. The values of the tap weights A, B and C are obtained by substituting different timing errors ranging from 0 to $0.25T_p$ into the truncated duobinary pulse specified in Equation 4.3.5 and the results are summarized in Table 4.3.1.

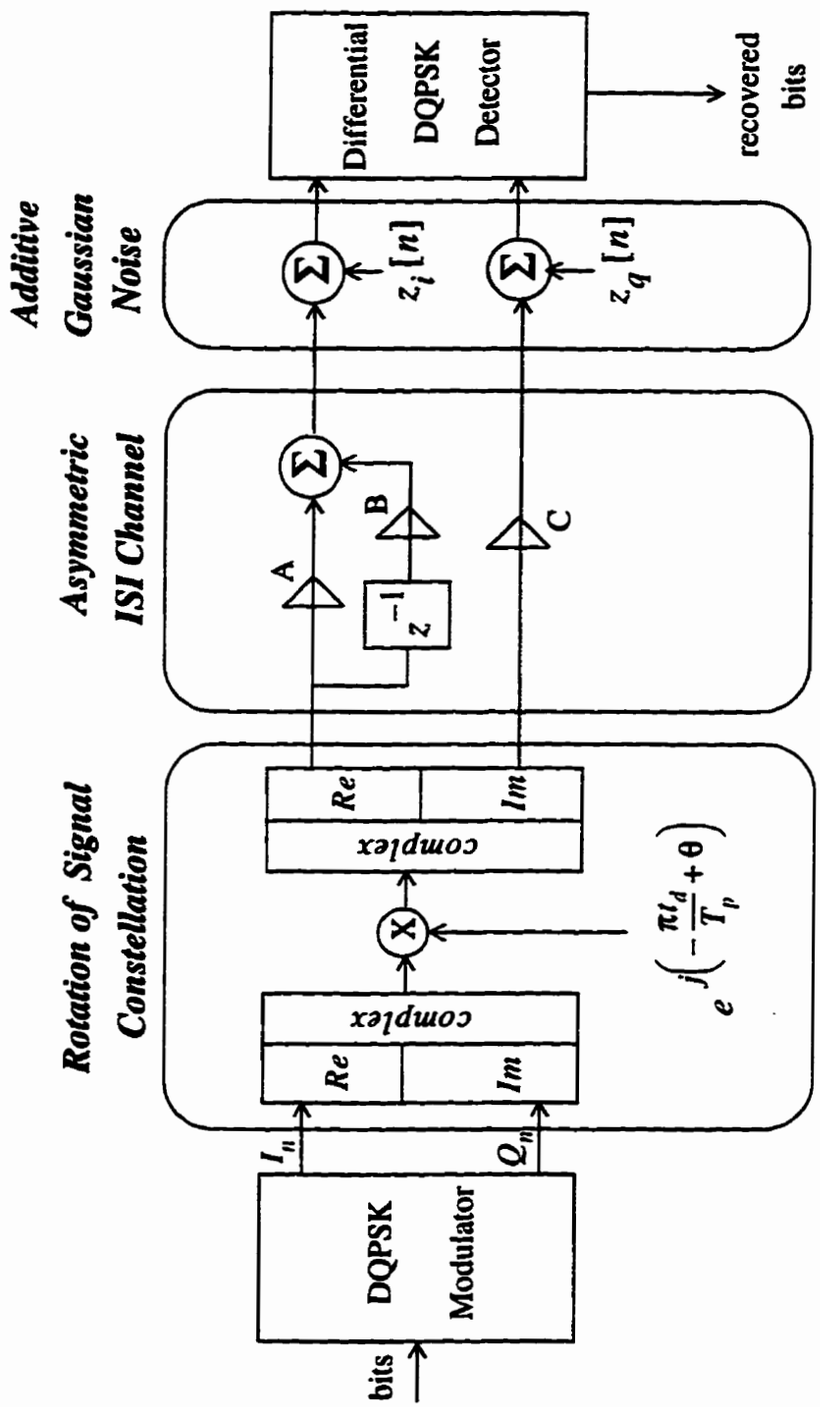

Figure 4.3.3 Equivalent discrete-time model for truncated 100% excess bandwidth duobinary pulse and $0 \leq t_d \leq 0.25T_p$.

t_d	A	B	C
0	1.0	0	1.0
$0.10T_p$	0.78	0.13	1.17
$0.15T_p$	0.66	0.216	1.23
$0.20T_p$	0.54	0.315	1.26
$0.25T_p$	0.424	0.424	1.27

Table 4.3.1 Table of tap weights A, B and C for $0 \le t_d \le 0.25T_p$.

Several observations can be made on the asymmetric ISI channel. Firstly, with the truncated duobinary pulse, the Q channel filter is simplified to having only one direct path scaled by the tap weight C. Since C ranges from 1.0 to 1.27, the Q symbols (after rotation) are always amplified by a factor of C. More importantly, since the Q channel filter does not have any second path, there is no intersymbol interference in the Q channel. On the other hand, the I channel filter is modelled as a two-path ISI channel with tap weight A representing the gain of the direct path and tap-weight B for the gain of the delayed path with one symbol delay. Due to the existence of the delayed path, intersymbol interference, which is caused by one past symbol, is introduced in the I channel. The amount of ISI is controlled by the ratio of direct path gain to the delayed path gain. From Table 4.3.1, it is clear that as timing error increases from 0 to $0.25T_p$, the direct path tap weight A decreases from 1 to 0.424 (a 58% drop) whereas the delayed path tap weight B increases from 0 to 0.424 (a 42% increase). Since both the drop in tap weight A and rise in tap weight B add up to enhance the ISI, an increase in timing error can significantly increase the amount of ISI in the I channel. It will be shown in

the next section that when the direct and delayed paths have the same gain, the system suffers severe performance degradation. The final comment on the I channel filter is regarding its z-transform transfer function which is obtained as

$$H_i(z) = A + B \cdot z^{-1} = \frac{A(z + B/A)}{z} \qquad \text{for} \quad |z| > 0 \qquad (4.3.11)$$

So $H_i(z)$ has one pole at $z = 0$ and one zero at $z = -B/A$. Except when $t_d = 0.25T_p$, A is always greater than B. This implies that when $0 \le t_d < 0.25T_p$, both zero and pole of $H_i(z)$ are inside the unit circle. Therefore $H_i(z)$ is a minimum phase system and its inverse system is always stable. When $t_d = 0.25T_p$, the zero is exactly on the unit circle and the inverse system of $H_i(z)$ is marginally stable.

Case 3 : $-0.25T_p \le t_d \le 0$

Similar to case 2, when the timing error (t_d) is not equal to zero, the sampling points no longer coincide with the zero-crossings of the duobinary pulse and infinitely long intersymbol interference occurs. However in this case, the timing error (t_d) is less than zero and therefore the actual sampling points occur to the right of the optimal sampling points. As will be shown below, this change in t_d makes a significant change in the characteristics of the asymmetric ISI channel.

Similar procedure is used to obtain the equivalent discrete-time model with the truncated duobinary pulse. By approximating $g(t)$ with $g_T(t)$ in the I channel ISI filter, and substituting $-0.25T_p \le t_d \le 0$ into the equation of $g_T(t)$, the approximated impulse response of the I channel filter is found to be,

$$h_i[n] \approx g_T(nT_p - t_d) = E \cdot \delta[n] \qquad (4.3.12)$$

where $E = g_T(-t_d)$

Similarly, the approximated impulse response of the Q channel filter is obtained as,

$$h_q[n] \approx g_T(nT_p + 0.5T_p - t_d) = F \cdot \delta[n+1] + G \cdot \delta[n] \qquad (4.3.13)$$

where $G = g_T(0.5T_p - t_d)$

$F = g_T(-0.5T_p - t_d)$

Notice that $h_q[n]$ is a noncausal filter with one element at $n = -1$. However, due to propagation delay through the channel, time delay in a communications system is inevitable. Thus an extra delay of one sample is added to both the inphase and quadrature channel filters to make $h_q[n]$ become causal. After the addition of this extra one sample delay, the two impulse responses become

$$h_i[n] \approx E \cdot \delta[n-1] \qquad (4.3.14)$$

where $E = g_T(-t_d)$

and

$$h_q[n] \approx F \cdot \delta[n] + G \cdot \delta[n-1] \qquad (4.3.15)$$

where $G = g_T(0.5T_p - t_d)$

and $F = g_T(-0.5T_p - t_d)$.

By incorporating these two simplified and delayed impulse responses into the asymmetric ISI channel, the equivalent discrete-time model is obtained and shown in Figure 4.3.4. The values of the tap weights E, F and G are obtained and summarized in Table 4.3.2.

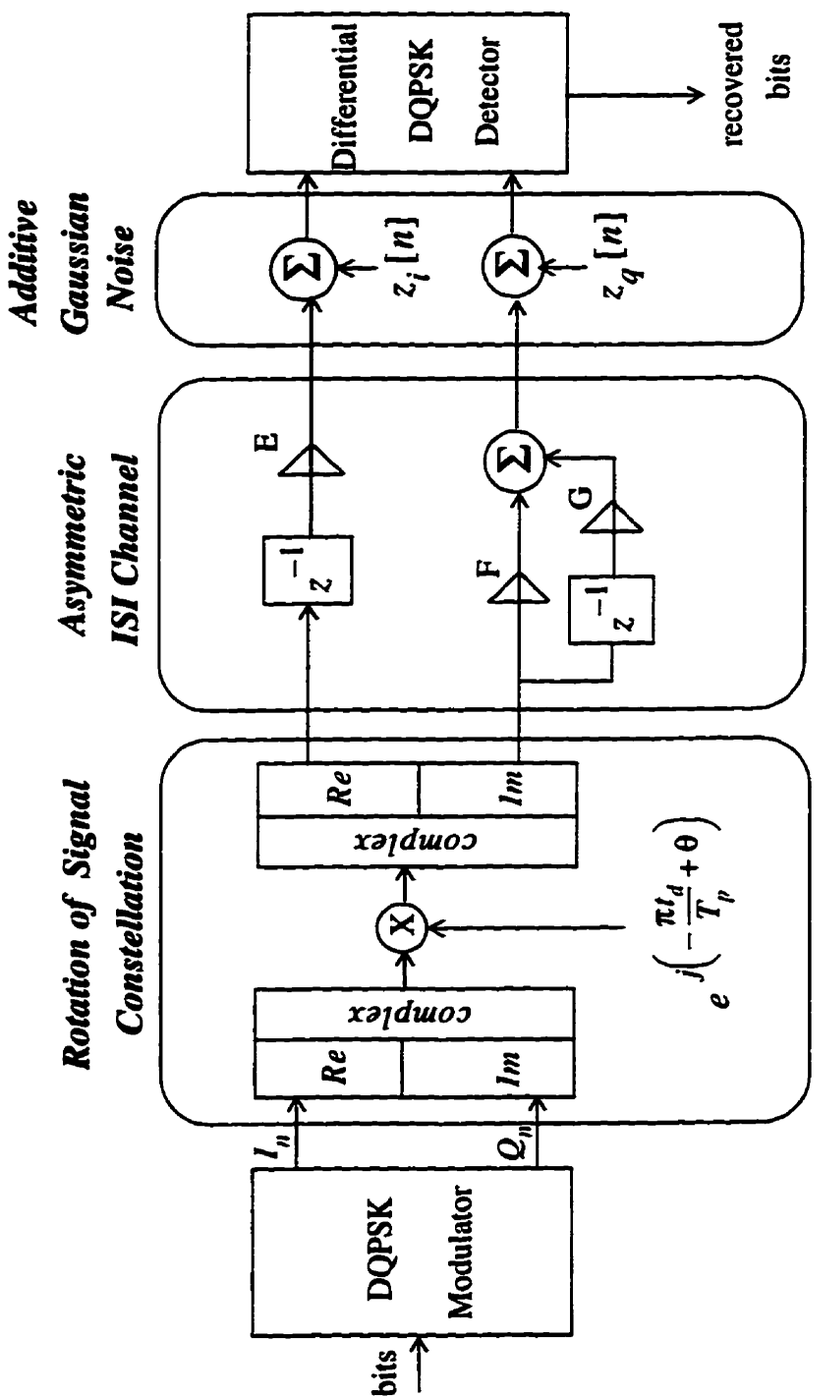

Figure 4.3.4 Equivalent discrete-time model for truncated 100% excess bandwidth duobinary pulse and $-0.25T_p \le t_d \le 0$.

t_d	E	F	G
0	1.0	0	1.0
$-0.10T_p$	1.17	0.13	0.78
$-0.15T_p$	1.23	0.216	0.66
$-0.20T_p$	1.26	0.315	0.54
$-0.25T_p$	1.27	0.424	0.424

Table 4.3.2 Table of tap weights E, F and G for $-0.25T_p \le t_d \le 0$.

Several observations can be made from the two simplified and delayed impulse responses. Firstly, unlike the I channel filter in case 2, this I channel filter shown in Figure 4.3.4 has only one path scaled by tap weight E. Since there is no second path in the filter, intersymbol interference is not introduced on the rotated I symbols. Also since E ranges from 1.0 to 1.27 as t_d increases from 0 to $0.25T_p$, the rotated I symbols are always amplified by a factor E. On the other hand, the Q channel filter is modelled as a two-path ISI channel with tap weight F in the direct path and tap weight G in the delayed path. Unlike the ISI in case 2 which is caused by one postcursor, the ISI in this case is produced by one precursor. Therefore the receiver should lock onto the delayed path symbols. The amount of ISI is controlled by the ratio of the delayed path gain to direct path gain. As the ratio decreases, the effect of ISI increases. From Table 4.3.2, it is clear that as t_d increases from 0 to $0.25T_p$, the tap weight F increases from 0 to 0.424 (a 42% increase) whereas the tap weight G decreases from 1.0 to 0.424 (a 58% decrease). Since both the increase in F and decrease in G raise the effect of ISI, an increase in timing error can significantly increase the amount of ISI in the system. A

final comment on the Q channel filter is regarding the z-transform of its impulse response. Taking the z-transform of $h_q[n]$ (given in Figure 4.3.7) yields

$$H_q(z) = F + G \cdot z^{-1} = \frac{F(z + G/F)}{z} \qquad \text{for} \quad |z| > 0 \qquad (4.3.17)$$

Note that since F equals to zero when t_d is zero, the above equation is only valid for $-0.25T_p \le t_d < 0$. Thus $H_q(z)$ has one pole at $z = 0$ and one zero at $z = G/F$. For $-0.25T_p < t_d < 0$, G is always greater than F and therefore the zero is always outside the unit circle. For the situation when $t_d = -0.25T_p$, the zero is exactly on the unit circle. Thus for $-0.25T_p < t_d < 0$, $h_q[n]$ is a maximum phase filter and its inverse system is an unstable system. When $t_d = -0.25T_p$, the inverse system is marginally stable.

4.4 Simulation of the IF-sampling system with 100% Excess Bandwidth Duobinary Pulse

In addition to the analysis of the bandpass and discrete-time models of the IF-sampling system, another important concern is the system's ability to transmit the data reliably through the channel. Typically the reliability is measured by the probability of bit error. In this thesis, the probability of bit error is obtained by computer simulation of the equivalent discrete-time model shown in Figure 4.3.1. The simulation program is written in C and all function calls are ANSI (American National Standards Institute) compatible. Therefore any C compiler that supports the ANSI standard is capable of compiling and linking the simulation program.

In the simulation program, the information bits are generated by a random

number generator whose source code can be found in [19, pp. 282]. This C function, named as 'ran2', generates a uniform random deviate between 0.0 and 1.0 (exclusive of the endpoint values) and has a long period of approximately 2×10^{18}. This generator is recommended by [19, pp. 286] if more than 10^8 random numbers are generated in a single calculation. In the simulation, the maximum number of random number of uniform deviates is around 3×10^9 and therefore this generator has a sufficiently long period to provide the randomness of the random number. By using this random number generator, the information bits are obtained by the following rule : the bit is 0 if the uniform random deviate is from 0 (exclusive) to 0.5 (inclusive) ; and the bit is 1 if the uniform random deviate is from 0.5 (exclusive) to 1.0 (exclusive). As a result, the bits (either 1 or 0) are equiprobable.

The signalling pulse being simulated is the duobinary pulse with a duration of 98 symbols, that is,

$$g(t) = \begin{cases} \dfrac{0.25T_p^2 \cdot \sin(2\pi t/T_p)}{\pi t(0.5T_p - t)} \cdot \dfrac{1}{\sqrt{T_p}} & \text{for } -49T_p \le t \le 49T_p \\ 0 & \text{otherwise} \end{cases} \qquad (4.4.2)$$

With this long duration, nearly all intersymbol interferences introduced by the tail of the duobinary pulse are taken into account. Notice that an extra scaling factor is added in the definition of $g(t)$. As will be shown later, this scaling factor is used to make the signal-to-noise ratio independent of the symbol duration T_p. Since $g(t)$ is a truncated duobinary pulse with a long duration, the Fourier transform of $g(t)$ can be approximated as,

$$G(f) = \begin{cases} T_p \cdot \cos\frac{\pi f T_p}{2} \cdot e^{-j\frac{\pi f T_p}{2}} \cdot \frac{1}{\sqrt{T_p}} & \text{for } |f| < \frac{1}{T_p} \\ 0 & \text{otherwise} \end{cases} \qquad (4.4.3)$$

By applying the Parseval's Theorem into the definition of energy of $g(t)$,

$$E_g = \int_{-\infty}^{\infty} g^2(t)\,dt = \int_{-\infty}^{\infty} |G(f)|^2 df \qquad (4.4.4)$$

the energy of g(t) is found to be,

$$E_g = \int_{-\frac{1}{T_p}}^{\frac{1}{T_p}} T_p \cdot \cos^2\left(\frac{\pi f T_p}{2}\right) df = 1 \qquad (4.4.5)$$

Therefore with the definition of g(t) as stated in Equation 4.4.2, the energy of $g(t)$ is equal to 1.

As already discussed in section 4.2, the two noise sequences $z_i[n]$ and $z_q[n]$ are uncorrelated white Gaussian processes with zero means. The total average powers of the two noise sequences are,

$$\phi_{z_i z_i}[0] = \phi_{z_q z_q}[0] = \frac{2N_o}{T_p} \qquad (4.4.6)$$

The system performance is plotted in a graph of the probability of bit error versus the signal-to-noise ratio (SNR) which is defined as,

$$SNR \equiv \frac{\text{Average power of transmitted bandpass signal}}{\text{Average power of in-band bandpass noise}} \qquad (4.4.7)$$

Referring to section 3.1, the transmitted bandpass signal $s(t)$ is given as :

$$s(t) = Re\{v(t) \cdot e^{j2\pi f_c t}\} \tag{4.4.8}$$

$$\text{where } v(t) = \sum_{m=-\infty}^{\infty} (I_m + jQ_m) \cdot g(t - mT_p)$$

It was shown that the lowpass equivalent signal $v(t)$ is a cyclostationary process with an average power density spectrum given by

$$\Phi_{vv}(f) = \frac{1}{T_p} \cdot |G(f)|^2 \cdot \frac{1}{2} \cdot E\{|I_n + jQ_n|^2\} \tag{4.4.9}$$

Since the total average power of $s(t)$ is the total area under $\Phi_{ss}(f)$ and

$$\Phi_{ss}(f) = \frac{1}{2} \cdot \Phi_{vv}(f - f_c) + \frac{1}{2} \cdot \Phi_{vv}(-f - f_c) \tag{4.4.10}$$

then

$$\text{Average power of } s(t) = \int_{-\infty}^{\infty} \Phi_{ss}(f)\, df \tag{4.4.11}$$

$$= \frac{1}{2} \cdot \int_{-\infty}^{\infty} \Phi_{vv}(f - f_c)\, df + \frac{1}{2} \cdot \int_{-\infty}^{\infty} \Phi_{vv}(-f - f_c)\, df$$

$$= \frac{1}{2} \cdot \int_{-\infty}^{\infty} \Phi_{vv}(f)\, df + \frac{1}{2} \cdot \int_{-\infty}^{\infty} \Phi_{vv}(f)\, df$$

$$= \int_{-\infty}^{\infty} \Phi_{vv}(f)\, df$$

$$= \frac{1}{2T_p} \cdot E\{|I_n + jQ_n|^2\} \cdot \int_{-\infty}^{\infty} |G(f)|^2 df$$

The last integral evaluates the energy of $g(t)$ which has already been shown to be unity. Also since the transmitted complex symbol, $I_n + jQ_n$, always resides on the unit circle, then

$$E\{|I_n + jQ_n|^2\} = E\{1\} = 1 \qquad (4.4.12)$$

Therefore the average power of $s(t)$ is obtained as,

$$\text{Average power of } s(t) = \frac{1}{2T_p} \qquad (4.4.13)$$

On the other hand, with the transmitted signal having 100% excess bandwidth, the average power of in-band bandpass noise is,

$$\text{Average power of in-band bandpass noise} = \frac{2N_o}{T_p} \qquad (4.4.14)$$

By substituting the results of the average signal power and average noise power into the definition of signal-to-noise ratio, then the signal-to-noise ratio is found to be,

$$SNR = \frac{1/(2T_p)}{2N_o/T_p} = \frac{1}{4N_o} \qquad (4.4.15)$$

Equivalently the signal-to-noise ratio expressed in decibel (dB) is,

$$SNR_{dB} = 10 \cdot \log_{10}\left(\frac{1}{4N_o}\right) \qquad (4.4.16)$$

Notice that the signal-to-noise ratio is independent of the symbol rate and therefore the symbol period is arbitrarily chosen to be 1 in the simulation, i.e.

$$T_p = 1 \qquad (4.4.17)$$

Simulation results are obtained to show the degradation caused by the three distortions which are rotation of signal constellation, asymmetric ISI channel and additive white Gaussian noise.

Firstly the degradation caused by different timing errors are shown in Figure 4.4.1. In the simulations, the phase shift ϕ is always set to 0. For timing error t_d equal to 0, the additive white Gaussian noise is the only distortion degrading the system performance. When the timing error is not zero, the system suffers distortions from both timing error and noise. The bit error rate curve corresponding to $t_d = 0$ serves as a reference for the investigation. At low signal-to-noise ratios, eg. from 2 dB to 6 dB, all the bit error rate curves are close to each other. This is because at low $SNRs$, the effect of noise dominates the timing error. Therefore the system suffers similar degradation for different timing errors. As the SNR increases, i.e. the noise power decreases, the system performance mainly depends on the timing error, or equivalently the asymmetric intersymbol interference. It is clear that the larger the timing error, the more severe the system performance degrades. For example, at the probability of bit error of 10^{-3}, which is the targeting bit error rate for voice transmission [20], the system suffers a significant SNR loss of approximately 7 dB as t_d increases from 0 to $0.1T_p$. The bit error rate becomes irreducible when t_d is greater than or equal to $0.15T_p$. Therefore with t_d greater than $0.15T_p$, the IF-sampling system becomes ineffective in transmitting data through the system.

The irreducible bit error curve for $t_d = 0.15T_p$ can also be analytically observed from the discrete-time model for truncated duobinary pulse shown in Figure 4.3.3. In this analysis, the noise sequences are assumed to be zero. As stated in Table 4.3.1, when $t_d = 0.15T_p$, the tap weights A, B and C are given as 0.66, 0.216 and 1.23 respectively.

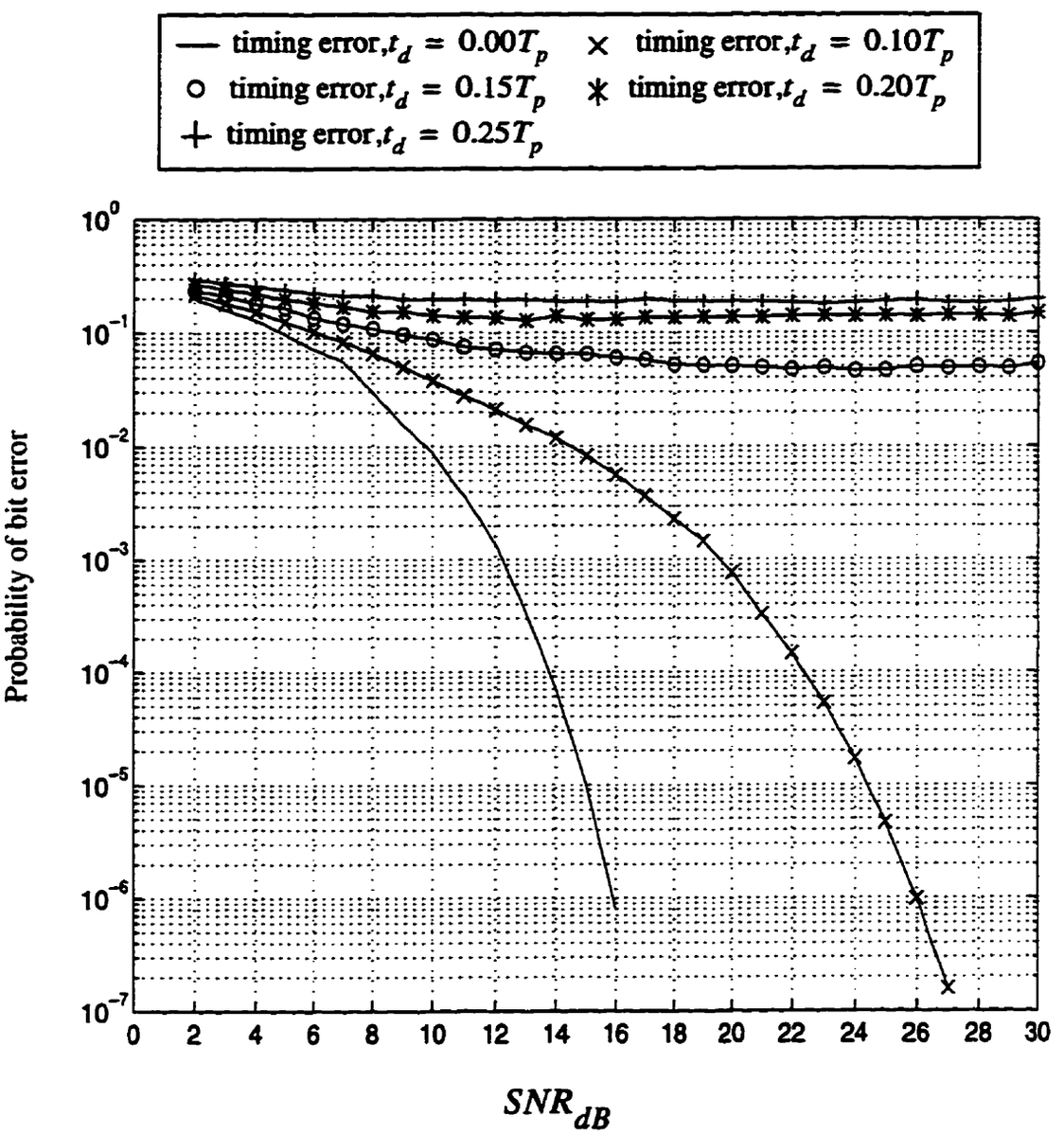

Figure 4.4.1 Bit error rate curves for different timing errors. For all cases, $\phi = 0$.

Since there is one symbol memory in the DQPSK modulation and another one symbol memory in the asymmetric ISI channel, three symbols are required to cover all possible cases. For example, if the three transmit complex symbols are,

$$\left[e^{j45^o}, e^{j45^o}, e^{j135^o}\right] \qquad (4.4.17)$$

where the first element in the vector corresponds to the first symbol, then the output of the asymmetric ISI channel is,

$$\left[e^{j45^o}, 1.07e^{j54.6^o}, 0.925e^{j109.8^o}\right] \qquad (4.4.18)$$

Here it is assumed that no symbol is transmitted before the first symbol and thus there is no intersymbol interference on the first symbol. However, both the second and third symbols are corrupted by the asymmetric ISI. For the transmit symbols, the phase change from the second to the third symbol is 90^o and therefore a dibit of '01' is transmitted in this case. On the other hand, at the output of the asymmetric ISI channel, the second and third symbols are $1.07e^{j54.6^o}$ and $0.925e^{j109.8^o}$. Therefore the detected phase transition is 55.2^o and the detected dibit is '01'. No error is made in this example.

However it is possible for the receiver to make an error even if the two noise sequences are zero. The occurrence of bit error mainly depends on the combination of the three transmit complex symbols. One possible combination is

$$\left[e^{j45^o}, e^{j135^o}, e^{j45^o}\right] \qquad (4.4.19)$$

Again substituting these three transmit symbols and the three tap weights corresponding to $t_d = 0.15T_p$ into the discrete-time model yields the output of the asymmetric ISI channel to be,

$$\left[e^{j45^\circ}, 0.92e^{j109.8^\circ}, 0.92e^{j70.2^\circ}\right] \qquad (4.4.20)$$

Since the phase transition of the second and third transmit symbol is -90°, the transmitted dibit is '10'. However, the phase transition of the second and third received symbol is -39.6° therefore forcing the detected dibit is '00'. As a result, one bit error is made in the detection. By stepping through all combinations of the three transmit complex symbols, it is found that the detector makes an error in the following patterns.

$$\text{Pattern 1}: \left[e^{j45^\circ}, e^{j135^\circ}, e^{j45^\circ}\right]$$

$$\text{Pattern 2}: \left[e^{j45^\circ}, e^{-j135^\circ}, e^{-j45^\circ}\right]$$

$$\text{Pattern 3}: \left[e^{j135^\circ}, e^{j45^\circ}, e^{j135^\circ}\right]$$

$$\text{Pattern 4}: \left[e^{j135^\circ}, e^{-j45^\circ}, e^{-j135^\circ}\right]$$

$$\text{Pattern 5}: \left[e^{-j135^\circ}, e^{j45^\circ}, e^{j135^\circ}\right]$$

$$\text{Pattern 6}: \left[e^{-j135^\circ}, e^{-j45^\circ}, e^{-j135^\circ}\right]$$

$$\text{Pattern 7}: \left[e^{-j45^\circ}, e^{j135^\circ}, e^{j45^\circ}\right]$$

$$\text{Pattern 8}: \left[e^{-j45^\circ}, e^{-j135^\circ}, e^{-j45^\circ}\right]$$

Note that in all cases, only one bit error is made and therefore the probability of bit error is determined as,

$$\begin{aligned} Pr(\text{bit error}) &= Pr(\text{bit error} \mid \text{wrong pattern}) \cdot Pr(\text{wrong pattern}) \\ &= \frac{8}{4 \times 4 \times 4} = 0.0625 \end{aligned} \qquad (4.4.21)$$

From Figure 4.4.1, the simulated bit error rate is about 0.05 which is close to the above result. The discrepancy between the analytical result and the simulation result stems from two factors : (1) A truncated duobinary pulse with a short duration of $1.5T_p$ is used in the analytical analysis whereas a much longer duration of $99T_p$ is used in the simulation ; (2) The two noise sequences are assumed to be zero in the analytical analysis whereas the noises are nonzero in the simulation.

Due to the presence of the asymmetric intersymbol interference, the phase shift ϕ also plays an important role in the system performance. The simulation results are shown in Figure 4.4.2. Again the bit error rate curve corresponding to $t_d = 0$ serves as a reference. For $t_d = 0.10T_p$ and a bit error rate of 10^{-3}, the system suffers a SNR loss of approximately 7 dB for $\phi = 0^o$ but only 2 dB for $\phi = 45^o$. So the performance difference between the two phase shifts is 5 dB. As t_d increases to $0.15T_p$, the bit error rate curve for $\phi = 0^o$ becomes irreducible. On the contrary, the bit error rate curve for $\phi = 45^o$ decreases monotonically with signal-to-noise ratio resulting in a 6 dB loss at a bit error rate of 10^{-3}. When t_d further increases to the worst case, which is $0.25T_p$, the bit error rate curves for both $\phi = 0^o$ and $\phi = 45^o$ are approximately the same.

The drastic difference between the two phase shifts can be explained by investigating the four constellations shown in Figure 4.4.3. These four diagrams are generated by transmitting 1000 bits through the discrete-time model shown in Figure 4.3.3. Without the noise, the top-left diagram shows the constellation of the I/Q symbols at the output of the rotation. Since $\phi = 0^o$, this constellation is exactly the same as that at the output of the DQPSK modulator.

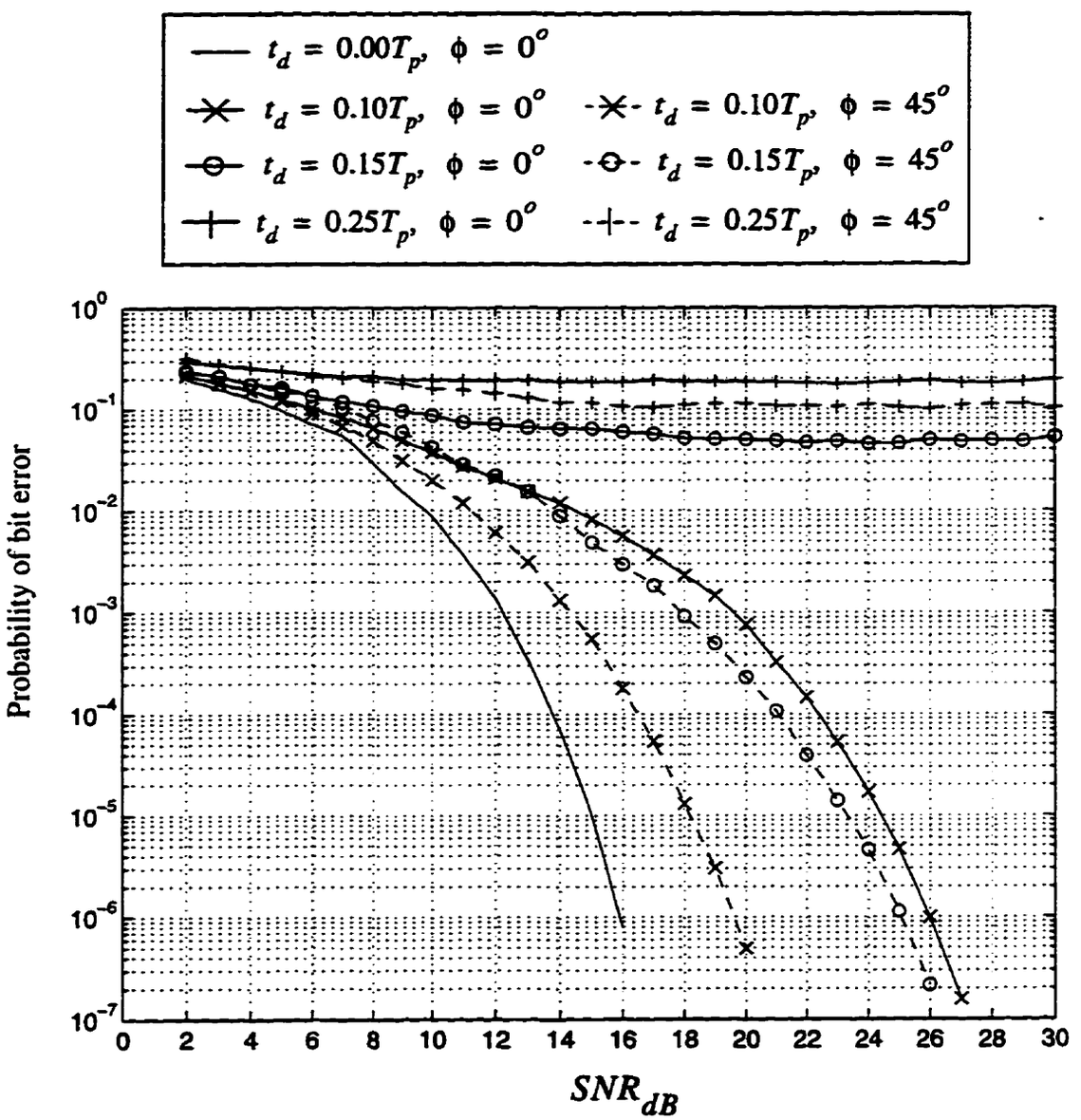

Figure 4.4.2 Bit error rate curves for different timing errors t_d and phase shifts ϕ.

As shown in the diagram, there are only four possible points corresponding to the transmit phases of 45°, 135°, -135°, -45°. After these symbols are distorted by the asymmetric ISI channel, the resulting constellation no longer contains four points. Instead, as shown in the top-right diagram, the constellation contains four clusters each containing more than one point. Notice that the two signal points inside any cluster are separated in horizontal direction only. This is because the intersymbol interference only occurs in the inphase channel (which corresponds to the horizontal axis) but not on the quadrature channel (the vertical axis). The irreducible bit error rate comes from the fact that some signal points in neighboring clusters are too close to each other. For example, the phases of the two signal points 'a' and 'b' in the top-right diagram only differ by 39.7°. Since the phase difference is between 45° and -45°, the differential detector decodes the dibits to be 00 which actually should be 01. As a result, a symbol error is made.

On the other hand, when $\phi = 45^{o}$, the constellations of both rotated and ISI corrupted symbols are shown in the bottom-left and bottom-right diagrams respectively. Although the ISI corrupted constellation also has clusters of signal points, the signals in different clusters are separated far enough such that the differential detector can always decode the dibits correctly. Therefore no symbol error is made with the absence of noise. In other words, with $\phi = 45^{o}$, the asymmetric ISI channel alone cannot cause any symbol error and as a result the bit error rate always depends on the noise power.

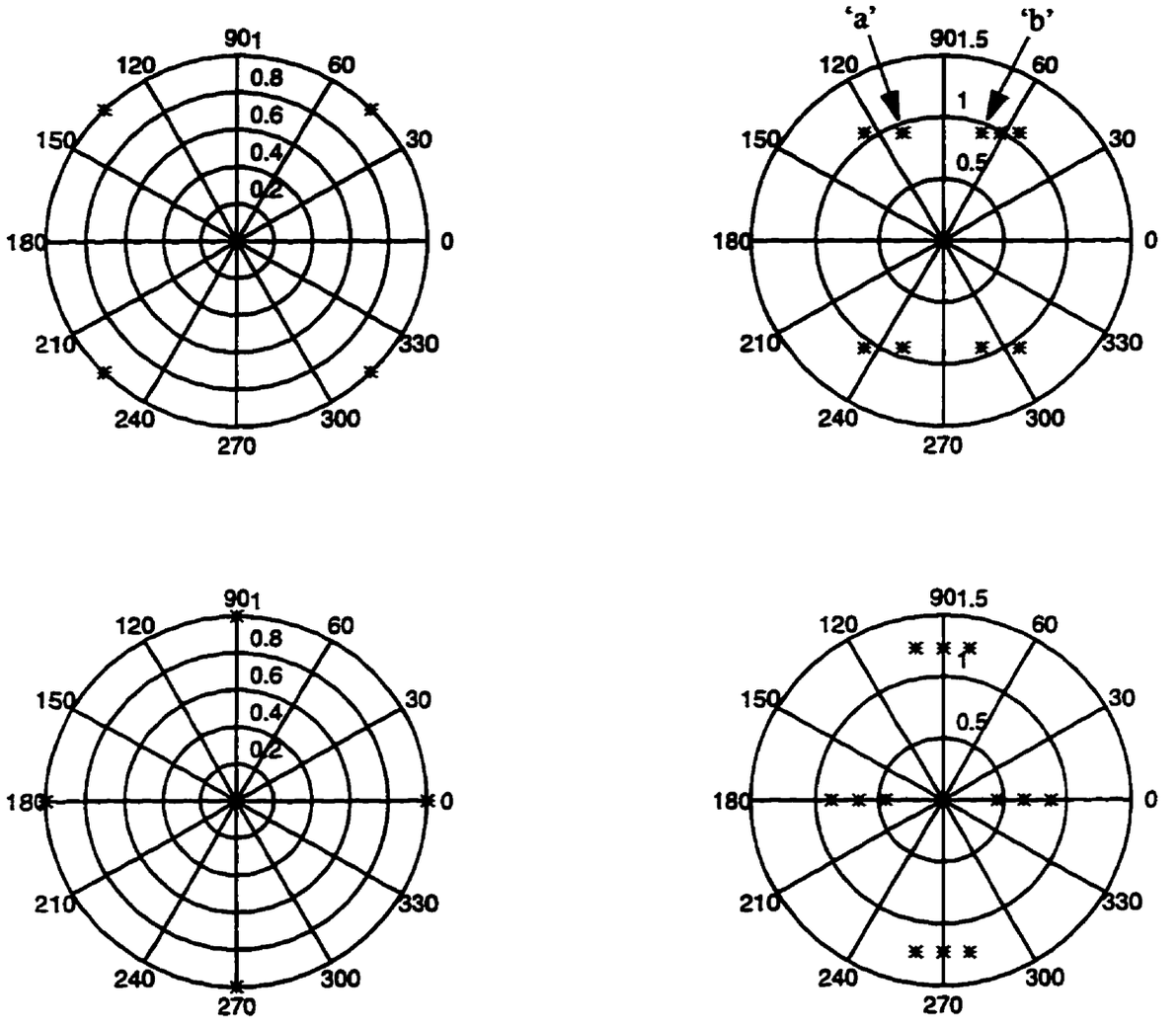

Figure 4.4.3

Top-left : Constellation of rotated symbols for $\phi = 0^o$ and $t_d = 0$.

Top-right : Constellation of asymmetric ISI channel output for $\phi = 0^o$ and $t_d = 0.15T_p$.

Bottom-left : Constellation of rotated symbols for $\phi = 45^o$ and $t_d = 0$.

Bottom-right : Constellation of asymmetric ISI channel output for $\phi = 45^o$ and $t_d = 0.15T_p$.

4.5

seque

exces

sever

to th

const

obser

Chapter 5 Two Solutions and Their Performance

In the last chapter, simulation results showed a severe performance degradation due to timing error. Two solutions are proposed to combat this timing error problem. The first solution is a direct-sequence spread-spectrum IF-sampling system. By using the autocorrelation property of a pseudonoise sequence, the asymmetric intersymbol interference can be alleviated by the spreading and the despreading processes. The second solution takes a different approach. It uses the 100% excess bandwidth duobinary pulse. By simply increasing the sampling rate to 4 samples per symbol and selecting the proper two samples, a considerable amount of intersymbol interference can be avoided. Simulation results are obtained for both systems to show their performance.

5.1 Solution 1 : Direct-Sequence Spread-Spectrum IF-sampling System

Pseudonoise (PN) sequences have been used extensively in many different areas [21]. Some of the examples are antijamming communications, multiple user random access communications with selective addressing capability, global positioning system (GPS) and accurate universal timing. In the area of point-to-point communications, the autocorrelation of the PN sequence is proven to be efficient in combating the intersymbol interference caused by the multipath channel. Since the timing error in the IF-sampling system also causes intersymbol interference, it is likely that the autocorrelation of the PN sequence is also capable of alleviating the intersymbol interference caused by the timing error. This is the main reason why a direct-sequence spread-spectrum system is chosen as a solution.

5.1.1 Autocorrelation of Barker Sequence

In the IEEE Draft Standard for Wireless LAN [22], the physical layer consists of a direct-sequence spread-spectrum (DS-SS) system employing an 11 chip Barker sequence. Due to its adoption by the proposed IEEE wireless LAN standard, this particular PN sequence is also used in this project. Note that the structures of both transmitter and receiver proposed in this solution are also applicable to other PN sequences. The 11 chip Barker sequence is given as :

$$+1, -1, +1, +1, -1, +1, +1, +1, -1, -1, -1 \qquad (5.1.1)$$

where the left most chip is transmitted first. The first chip is aligned at the start of a transmitted symbol and the symbol duration is exactly 11 chips long. Barker sequences are known to exist for only few short sequence lengths [23, pp. 564] [24, pp. 290]. So far only sequence lengths of 1, 2, 3, 4, 5, 7, 11 and 13 are found and it has been hypothesized that no longer Barker sequences exist. However, despite its short sequence length, a Barker sequence exhibits a special autocorrelation function which is very useful in a DS-SS system. In general, an aperiodic autocorrelation of a real-valued PN sequence is defined as [25],

$$C_x(l) = \begin{cases} \sum_{j=0}^{N-1-l} x_j x_{j+l} & ,0 \le l \le N-1 \\ \sum_{j=0}^{N-1+l} x_{j-l} x_j & ,1-N \le l \le 0 \\ 0 & ,|l| \ge N \end{cases} \qquad (5.1.2)$$

where N is the length of the PN sequence. It is found that [24, pp. 290] any Barker sequence has the following aperiodic autocorrelation :

$$C_x(l) = \begin{cases} N, & l = 0 \\ 0 \, or \pm 1, & otherwise \end{cases} \tag{5.1.3}$$

This aperiodic autocorrelation is useful in a situation in which the two consecutive symbols are different in polarity (for example, the first symbol is a +1 and the second symbol is a -1) and the locally generated PN sequence is not aligned with the received PN sequence. Although a rigorous proof is not given, this application is illustrated with an example in which the 11 chip Barker sequence is used and the two consecutive symbols are assumed to be +1 and -1. Thus, assuming there is no distortion in the channel, the received signal is :

$$r[n] = 1 \cdot p[n] + (-1) \cdot p[n-11] \tag{5.1.4}$$

where $p[n]$ is the 11 chip Barker sequence. By correlating the received signal $r[n]$ with another locally generated Barker sequence, the correlation output is

$$y[n] = \sum_{k=0}^{10} r[k] \cdot p[k-n] \tag{5.1.5}$$

where n can be interpreted as the time offset between the received Barker sequence and the local Barker sequence. The values of $y[n]$ are tabulated in Table 5.1.1 . When $n = 0$, the local Barker sequence is aligned with the first Barker sequence. Whenever $n \neq 0$, the correlation output always has a magnitude of 1 even when the two consecutive symbols are different in sign. This property ensures that the correlation output due to a delayed Barker sequence (the delay is assumed to be an integer multiple of chip) is always kept as low as ± 1 and this is useful in alleviating the effects of intersymbol interference.

Time Offset, n	$y[n]$
0	11
1	1
2	-1
3	1
4	-1
5	1
6	-1
7	1
8	-1
9	1
10	-1

Table 5.1.1 Values of $y[n]$ for different time offsets n.

5.1.2 The DS-SS IF-sampling Transmitter

In order to make use of the autocorrelation function of the Barker sequence, both the transmitter and the receiver in the IF-sampling system must be modified. Instead of passing the complex DQPSK symbols directly into the pulse-shaping filters, two additional blocks are added to preprocess these complex symbols. The combination of these blocks are commonly known as spreader [26] and the transmitter structure is shown in Figure 5.1.1 . Identical processing is performed on the inphase and the quadrature symbols independently. Firstly the spreader raises the sampling rate by the length of the Barker sequence. This is achieved by inserting 10 zeros between successive symbols. This ensures that all eleven chips of the Barker sequence carry the information of one symbol only and thus no intersymbol interference is introduced by

the spreader.

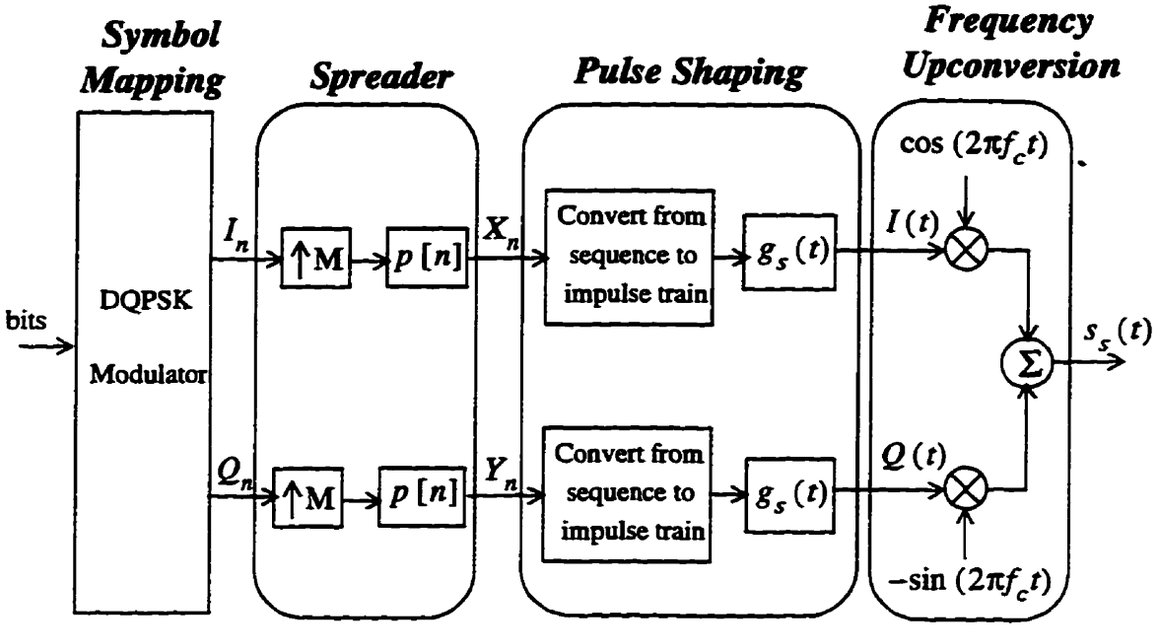

Figure 5.1.1 Transmitter in direct-sequence spread-spectrum IF-sampling system. $M = 11$ and $p[n]$ is the 11 chip Barker sequence.

Secondly the spreader imposes the Barker sequence onto the I/Q symbols by filtering the zero-filled symbol sequences with $p[n]$. The two output sequences of the spreader are :

$$X_n = \left\{ \sum_{k=-\infty}^{\infty} I_k \cdot \delta[n-kM] \right\} \otimes p[n] = \sum_{k=-\infty}^{\infty} I_k \cdot p[n-kM] \qquad (5.1.6)$$

$$Y_n = \left\{ \sum_{k=-\infty}^{\infty} Q_k \cdot \delta[n-kM] \right\} \otimes p[n] = \sum_{k=-\infty}^{\infty} Q_k \cdot p[n-kM] \qquad (5.1.7)$$

Due to the increase of the sampling rate by a factor of M, the transmission rate is also increased to the chip rate which is M times the symbol rate. The spreaded bandpass signal is given as,

$$s_s(t) = \sum_{m=-\infty}^{\infty} X_m \cdot g_s(t-mT_c) \cdot \cos(2\pi f_c t) - \sum_{m=-\infty}^{\infty} Y_m \cdot g_s(t-mT_c) \cdot \sin(2\pi f_c t) \quad (5.1.8)$$

where T_c is the chip period and $g_s(t)$ is the same 100% excess bandwidth duobinary pulse as in chapter 4 except that T_p is replaced by T_c. Thus,

$$g_s(t) = \frac{0.25T_c^2 \cdot \sin(2\pi t/T_c)}{\pi t(0.5T_c - t)} \quad (5.1.9)$$

Notice that by replacing T_p with T_c, the lowpass bandwidth is increased from $2/T_p$ to $2/T_c$. Therefore the transmission bandwidth must be increased M times to accommodate the spreaded signal.

5.1.3 The Channel

Similar to chapter 3, the channel is still assumed to corrupt the transmitted bandpass spreaded signal $s_s(t)$ by the additive bandpass white noise $n_s(t)$. Thus the received signal $r_s(t)$ is :

$$r_s(t) = s_s(t) + n_s(t) \quad (5.1.10)$$

All the statistical properties about the noise discussed in chapter 3 still apply and the bandwidth W is $2/T_c$ Hz.

5.1.4 The DS-SS IF-sampling Receiver

Due to the spreading in the transmitter, a reverse process known as despreading is also required and is implemented in the digital portion of the receiver. In other words, the complete architecture of the IF-sampling receiver (as shown in Figure 3.3.1) can be re-used and the only modification is to replace the symbol period T_p with the chip period T_c. Therefore the sampling rate of the sampler is raised by 11 times from 2 samples per symbol to 2 samples per chip. Also the two output sequences of the DS-SS IF-sampling receiver are no longer the inphase and quadrature symbols. But instead these two sequences are the inphase and quadrature chips. The architecture of the DS-SS IF-sampling receiver is shown in Figure 5.1.2 . The despreader takes the I/Q chips, processes them with 2 identical LTI systems with impulse response $p[-n+N_d]$ and reduces the sampling rate by a factor of M. Hence, the sampling rate at the output of the despreader is brought back to the symbol rate. The despreaded sequences are then multiplied by two different gains denoted as G_I and G_Q and the outputs are the recovered inphase and quadrature symbols. By passing these I/Q symbols into the differential DQPSK detector, the receiver can produce an estimate of the information bits.

In order to understand how the spreading/despreading processes alleviate the asymmetric ISI and determine the values of G_I, G_Q and N_d, it is required to obtain a discrete-time model for the DS-SS system as shown in Figure 5.1.3. Since both spreading and despreading processes are done in the digital section, the new discrete-time model would be the original discrete-time model with the addition of the spreader, despreader and the multiplication of G_I and G_Q on the I and Q channels. Also T_p is replaced with T_c in the original model. N_d is the timing parameter used to compensate the time shift due to the asymmetric ISI channel.

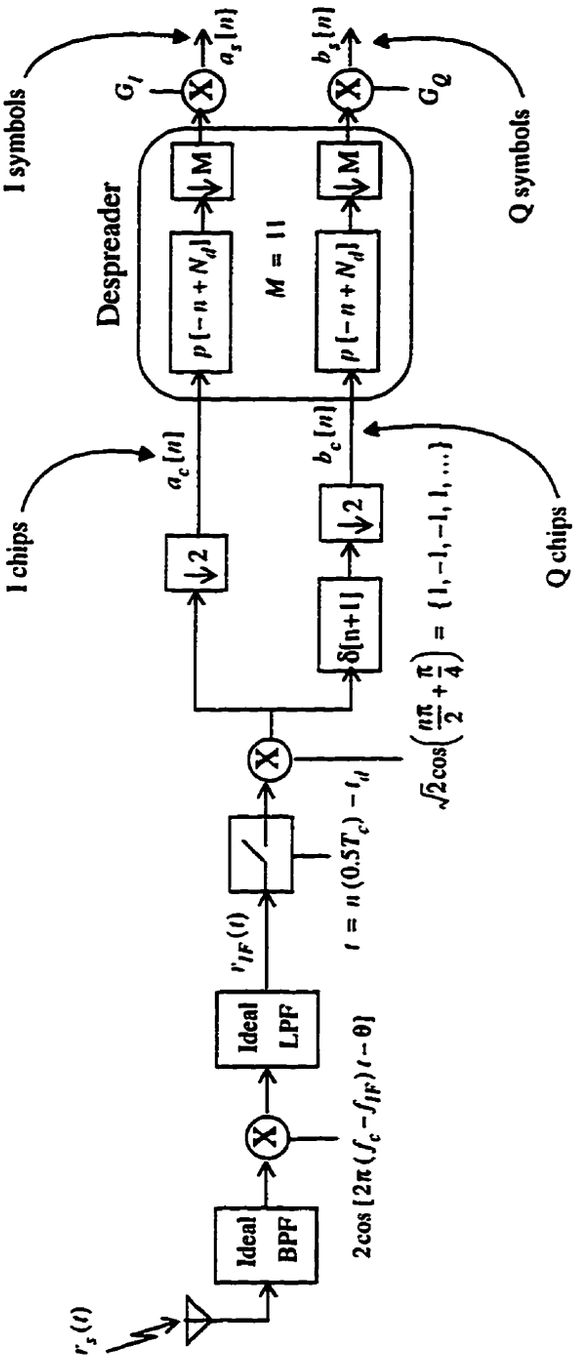

Figure 5.1.2 Architecture of the IF-sampling receiver for DS-SS system.

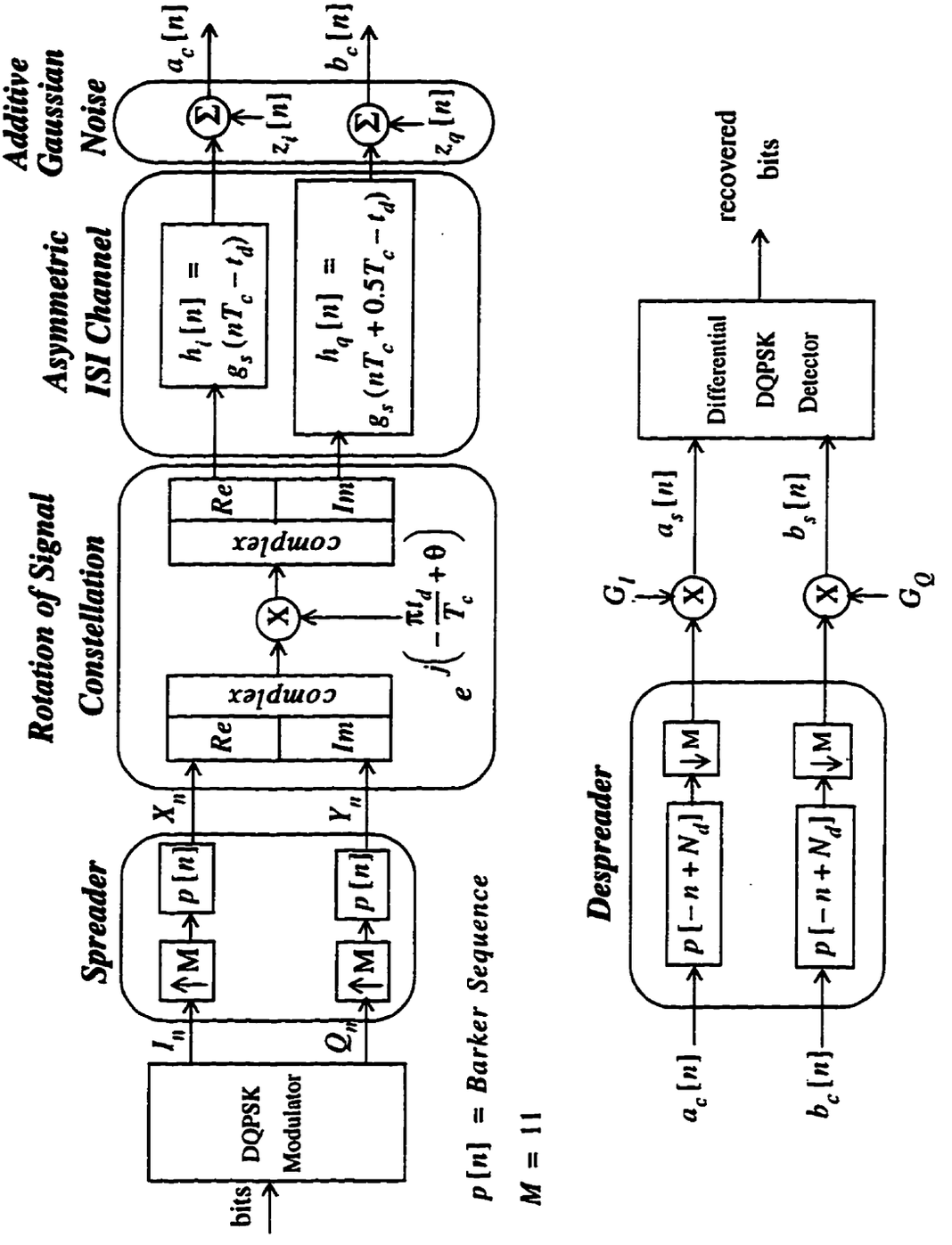

Figure 5.1.3 Discrete-time Model of the DS-SS IF-sampling system.

Similar to the previous approach, the two filters inside the asymmetric ISI channel are approximated by the truncated duobinary pulse with definition similar to Equation 4.3.5,

$$g_s(t) = g_{s,T}(t) = \begin{cases} \dfrac{0.25T_c^2 \cdot \sin(2\pi t/T_c)}{\pi t(0.5T_c - t)} & \text{for } -0.5T_c \le t \le T_c \\ 0 & \text{otherwise} \end{cases} \qquad (5.1.11)$$

The values of G_I , G_Q and N_d depend on the timing error t_d and the results are presented in three cases : (1) $t_d = 0$, (2) $0 \le t_d \le 0.25T_c$ and (3) $-0.25T_c \le t_d \le 0$. In these three cases, both the two noise sequences and the phase shift are assumed to be zero.

Case 1 : $t_d = 0$

With the sampling error equal to zero, both the I and Q channel ISI filters are simplified to the discrete-time delta functions :

$$h_i[n] = g_s(nT_c - t_d) = g_s(nT_c) = \delta[n] \qquad (5.1.12)$$

$$h_q[n] = g_s(nT_c + 0.5T_c - t_d) = g_s(nT_c + 0.5T_c) = \delta[n] \qquad (5.1.13)$$

Then

$$a_c[n] = \sum_{k=-\infty}^{\infty} I_k \cdot p[n - kM] \qquad (5.1.14)$$

$$b_c[n] = \sum_{k=-\infty}^{\infty} Q_k \cdot p[n - kM] \qquad (5.1.15)$$

In general, the recovered I/Q symbols obtained at the output of the multiplication of G_I and G_Q are found to be,

$$a_s[n] = G_I \cdot \sum_{m=-\infty}^{\infty} a_c[m] \cdot p[m - nM + N_d] \tag{5.1.16}$$

$$b_s[n] = G_Q \cdot \sum_{m=-\infty}^{\infty} b_c[m] \cdot p[m - nM + N_d] \tag{5.1.17}$$

By substituting $a_c[n]$ into Equation 5.1.16 and setting the gains, G_I and G_Q, to 1 and N_d to 0, the recovered I symbol becomes,

$$a_s[n] = \sum_{m=-\infty}^{\infty} \sum_{k=-\infty}^{\infty} I_k \cdot p[m - kM] \cdot p[m - nM] \tag{5.1.18}$$

Since $p[n]$ has a duration from $n = 0$ to $n = M$, the product $p[m - kM] \cdot p[m - nM]$ would be zero if $n \neq k$. Therefore, the nonzero contribution of $p[m - kM] \cdot p[m - nM]$ comes from $n = k$. Thus,

$$a_s[n] = I_n \cdot \sum_{m=-\infty}^{\infty} p[m - nM] \cdot p[m - nM] = I_n \cdot M \tag{5.1.19}$$

Note that the synchronization is assumed to be perfect such that the received Barker sequence and the local Barker sequence are perfectly aligned. The receiver can always extract the autocorrelation peak. By following the same arguments, the Q symbols are recovered as,

$$b_s[n] = Q_n \cdot M \tag{5.1.20}$$

Therefore, when $t_d = 0$, the two gains G_I and G_Q should be set to 1 while N_d should be 0.

Case 2 : $0 \le t_d \le 0.25T_c$

For the case where $t_d \neq 0$, the I/Q symbols experience asymmetric intersymbol interference. In order to simplify the analysis, both the inphase and quadrature channel ISI filters are approximated by the truncated duobinary pulse. Thus,

$$h_i[n] \approx g_{s,T}(nT_c - t_d) = A_s \cdot \delta[n] + B_s \cdot \delta[n-1] \qquad (5.1.21)$$

$$h_q[n] \approx g_{s,T}(nT_c + 0.5T_c - t_d) = C_s \cdot \delta[n] \qquad (5.1.22)$$

where $A_s = g_{s,T}(-t_d)$

$$B_s = g_{s,T}(T_c - t_d)$$

$$C_s = g_{s,T}(0.5T_c - t_d)$$

The values of A_s, B_s and C_s are tabulated in Table 5.1.2.

t_d	A_s	B_s	C_s
0	1.0	0	1.0
$0.10T_c$	0.78	0.13	1.17
$0.15T_c$	0.66	0.216	1.23
$0.20T_c$	0.54	0.315	1.26
$0.25T_c$	0.424	0.424	1.27

Table 5.1.2 Table of tap weights A_s, B_s and C_s for $0 \le t_d \le 0.25T_c$.

At the output of the asymmetric ISI channel, the two discrete-time sequences are,

$$a_c[n] = A_s \cdot \sum_{k=-\infty}^{\infty} I_k \cdot p[n-kM] + B_s \cdot \sum_{k=-\infty}^{\infty} I_k \cdot p[n-1-kM] \qquad (5.1.23)$$

$$b_c[n] = C_s \cdot \sum_{k=-\infty}^{\infty} Q_k \cdot p[n-kM] \qquad (5.1.24)$$

Due to the presence of a delayed path in the I channel, there are two copies of the spreaded inphase symbols at the output of the ISI channel. The main purpose of the despreader is to enhance one copy while suppressing the other one. This is achieved by the autocorrelation of the Barker sequence. Since A_s is always greater than or equal to B_s, the first term in Equation 5.1.23 is intended to be enhanced while the second term is suppressed.

By despreading $a_c[n]$ and multiplying the despreaded signal with G_I, the recovered inphase symbol is,

$$a_s[n] = G_I \cdot \sum_{m=-\infty}^{\infty} a_c[m] \cdot p[m-nM+N_d] \qquad (5.1.25)$$

In order to keep the A_s component, the receiver should lock onto the first path and thus,

$$N_d = 0 \qquad (5.1.26)$$

Then

$$\begin{aligned} a_s[n] = {} & G_I \cdot \sum_{m=-\infty}^{\infty} \sum_{k=-\infty}^{\infty} A_s \cdot I_k \cdot p[m-kM] \cdot p[m-nM] \\ & + G_I \cdot \sum_{m=-\infty}^{\infty} \sum_{k=-\infty}^{\infty} B_s \cdot I_k \cdot p[m-1-kM] \cdot p[m-nM] \end{aligned} \qquad (5.1.27)$$

The first term in Equation 5.1.27 is the same as Equation 5.1.18 except of the scaling factor $G_I \cdot A_s$. Therefore the first term is simplified as $G_I \cdot A_s \cdot M \cdot I_n$. The second term represents the autocorrelation of the Barker sequence with a time offset of 1 chip. Due to the good autocorrelation property of Barker sequence and I_k is always either +0.707 or -0.707, the second term reduces to $G_I \cdot B_s \cdot (\pm 1) \cdot I_n$. Therefore the final expression for $a_s[n]$ is,

$$a_s[n] = G_I \cdot A_s \cdot M \cdot I_n + G_I \cdot B_s \cdot (\pm 1) \cdot I_n \qquad (5.1.28)$$

Since M is 11 and $A_s \geq B_s$, then the second term in Equation 5.1.28 is comparatively small and thus,

$$a_s[n] \approx G_I \cdot A_s \cdot M \cdot I_n \qquad (5.1.29)$$

For the Q channel, since there is only one path, the despreaded signal would consist of a single term only and the result is very similar to the previous case except for a scaling factor. Therefore,

$$b_s[n] = G_Q \cdot C_s \cdot M \cdot Q_n \qquad (5.1.30)$$

Notice that there is a gain imbalance between $a_s[n]$ and $b_s[n]$. The goal of G_I and G_Q is to correct the gain imbalance and so the following settings are chosen,

$$G_I = 1/A_s \qquad (5.1.31)$$

$$G_Q = 1/C_s \qquad (5.1.32)$$

Although the above analysis is based on the assumption of a zero phase shift, the values of N_d, G_I and G_Q are also applicable to a nonzero phase situation.

Case 3 : $-0.25T_c \le t_d \le 0$

Similar to case 2, asymmetric ISI also appears in this case and the two ISI channel filters are also approximated as,

$$h_i[n] = E_s \cdot \delta[n-1] \tag{5.1.33}$$

$$h_q[n] = F_s \cdot \delta[n] + G_s \cdot \delta[n-1] \tag{5.1.34}$$

where $E_s = g_{s,T}(-t_d)$

$F_s = g_{s,T}(-0.5T_c - t_d)$

$G_s = g_{s,T}(0.5T_c - t_d)$

The values of E_s, F_s and G_s are given in Table 5.1.3.

t_d	E_s	F_s	G_s
0	1.0	0	1.0
$-0.10T_c$	1.17	0.13	0.78
$-0.15T_c$	1.23	0.216	0.66
$-0.20T_c$	1.26	0.315	0.54
$-0.25T_c$	1.27	0.424	0.424

Table 5.1.3 Table of tap weights E_s, F_s and G_s for $-0.25T_c \le t_d \le 0$.

Notice that an extra delay of 1 chip is added to both channels so that the quadrature channel ISI filter becomes causal. The output sequences of the asymmetric ISI channel are,

$$a_c[n] = E_s \cdot \sum_{k=-\infty}^{\infty} I_k \cdot p[n-1-kM] \tag{5.1.35}$$

$$b_c[n] = F_s \cdot \sum_{k=-\infty}^{\infty} Q_k \cdot p[n-kM] + G_s \cdot \sum_{k=-\infty}^{\infty} Q_k \cdot p[n-1-kM] \quad (5.1.36)$$

Note that $G_s \geq F_s$ and thus the receiver should keep the second term in Equation 5.1.36 and suppress the first term. In order to achieve this, the parameter N_d should be,

$$N_d = -1 \quad (5.1.37)$$

By despreading $b_c[n]$ and multiplying the despreaded signal by G_Q, the quadrature symbols are recovered as,

$$\begin{aligned} b_s[n] = {} & G_Q \cdot F_s \cdot \sum_{m=-\infty}^{\infty} \sum_{k=-\infty}^{\infty} Q_k \cdot p[m-kM] \cdot p[m-1-nM] \\ & + G_Q \cdot G_s \cdot \sum_{m=-\infty}^{\infty} \sum_{k=-\infty}^{\infty} Q_k \cdot p[m-1-kM] \cdot p[m-1-nM] \end{aligned} \quad (5.1.38)$$

With $n = k$, the double summation in the first term is the autocorrelation of the Barker sequence with a time offset of 1 chip. Therefore the first term reduces to $G_Q \cdot F_s \cdot (\pm 1) \cdot Q_n$. On the other hand, the double summation in the second term is the autocorrelation of the Barker sequence with zero time offset and it can be simplified as $G_Q \cdot G_s \cdot M \cdot Q_n$. Thus the final expression for $b_s[n]$ is,

$$b_s[n] = G_Q \cdot F_s \cdot (\pm 1) \cdot Q_n + G_Q \cdot G_s \cdot M \cdot Q_n \quad (5.1.39)$$

Again, $G_s M$ is larger than F_s and thus the recovered quadrature symbols are approximated as,

$$b_s[n] \approx G_Q \cdot G_s \cdot M \cdot Q_n \quad (5.1.40)$$

For the inphase channel, the recovered inphase symbols are,

$$a_s[n] = G_I \cdot E_s \cdot M \cdot I_n \tag{5.1.41}$$

Similar to the previous case, there is a gain imbalance between the inphase and quadrature symbols. By having the following settings of G_I and G_Q,

$$G_I = 1/E_s \tag{5.1.42}$$

$$G_Q = 1/G_s \tag{5.1.43}$$

the receiver can correct the gain imbalance. Similarly, although the above analysis assumes zero phase shift, the design parameters N_d, G_I and G_Q are also applicable to the non-zero phase.

5.1.5 Performance of the DS-SS IF-sampling system

The performance of the DS-SS IF-sampling system is obtained using a simulation based on the discrete-time model shown in Figure 5.1.3. The signal-to-noise ratio is defined as in Equation 4.4.15,

$$SNR = \frac{1}{4N_o} \tag{5.1.44}$$

This is true since the SNR is independent of the data rate which is either the symbol rate or the chip rate. The simulation results are shown in Figure 5.1.4. Note that the phase shift, $-(\pi t_d/T_c) + \theta$, is set to zero for all cases. By comparing the performance curves of the IF-sampling system and the DS-SS IF-sampling system for $t_d = 0$, it is clear that both systems give the same performance under the absence of intersymbol interference. When $t_d \neq 0$, the system suffers distortion caused by the timing error and the

performance degradation is clearly shown in the simulation. Again the bit error rate for $t_d = 0$ is used as a reference. At bit error rate of 10^{-3}, the DS-SS system suffers about 1 dB loss for $t_d = 0.10T_c$ (as opposed to 7 dB in the IF-sampling system). As t_d increases to the worst case of $0.25T_c$, the degradation is increased to a 7 dB loss.

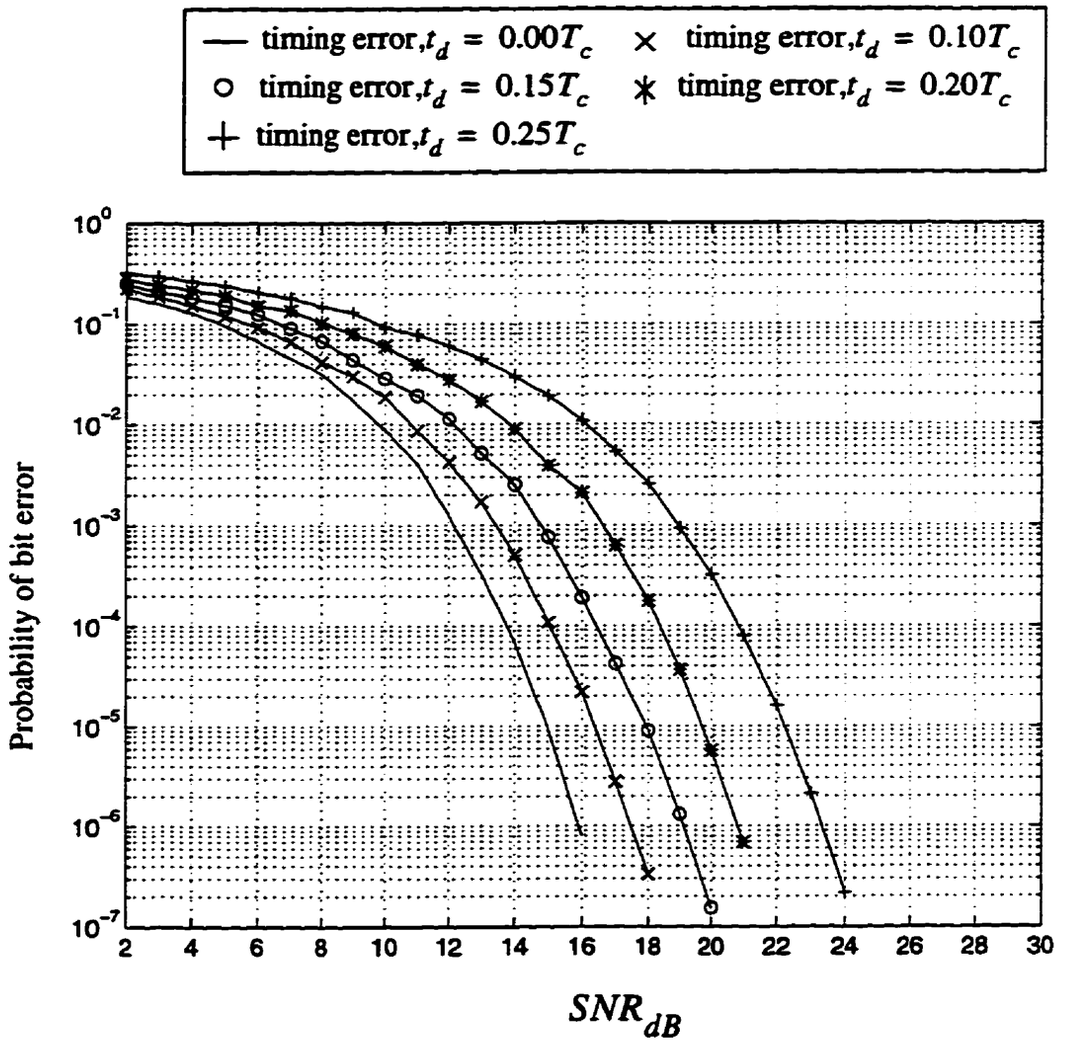

Figure 5.1.4 Simulated performance of the DS-SS IF-sampling system. Note that the phase shift, $-(\pi t_d/T_c) + \theta$, is zero for all cases.

The performance degradation mainly comes from three sources : (1) the residual intersymbol interference, (2) the discard of signal power in the delayed path and (3) the gain imbalance between the two noise sequences. Since the autocorrelation of the Barker sequence is not exactly zero for nonzero time shift (Table 5.1.1), the interfering paths are suppressed but not completely removed. Therefore a residual amount of ISI still exists at the output of the despreader and degrades the performance. Another factor is the discard of signal power in the delayed path. Instead of using the signal power from the delayed path, the despreader simply suppresses or discards it to alleviate ISI. For example, at $t_d = 0.25T_c$, the signal power is split equally into the direct path and the delayed path. Since the delayed path is discarded, half of the signal power is lost. The third degrading factor is the gain imbalance between the two noise sequences. Refer to the discrete-time model shown in Figure 5.1.3, the two noise sequences, $z_i[n]$ and $z_q[n]$ are also multiplied by G_I and G_Q respectively. Unless the two gains are exactly the same, gain imbalance is introduced on these two noise sequences. Only when $t_d = 0$, these two gains are exactly the same.

Although the DS-SS system still suffers degradation from timing error, the system performance is improved for all t_d and more importantly, the system no longer suffers irreducible bit error rate even when $t_d = 0.25T_c$. Thus the spreading and despreading processes are shown to be effective in alleviating the asymmetric ISI caused by the timing error.

5.2 Solution 2 : IF-sampling System with 4 Samples Per Symbol

In the first solution, the spreading/despreading in the DS-SS system was shown to be able to suppress the asymmetric intersymbol interference. In this section, an alternative approach is proposed to avoid the asymmetric ISI by simply doubling the sampling rate to 4 samples per symbol.

The idea behind this approach is based on the special shape of the 100% excess bandwidth duobinary pulse. This is illustrated in Figure 5.2.1 in which three truncated duobinary pulses are plotted with a delay of one symbol period relative to each other.

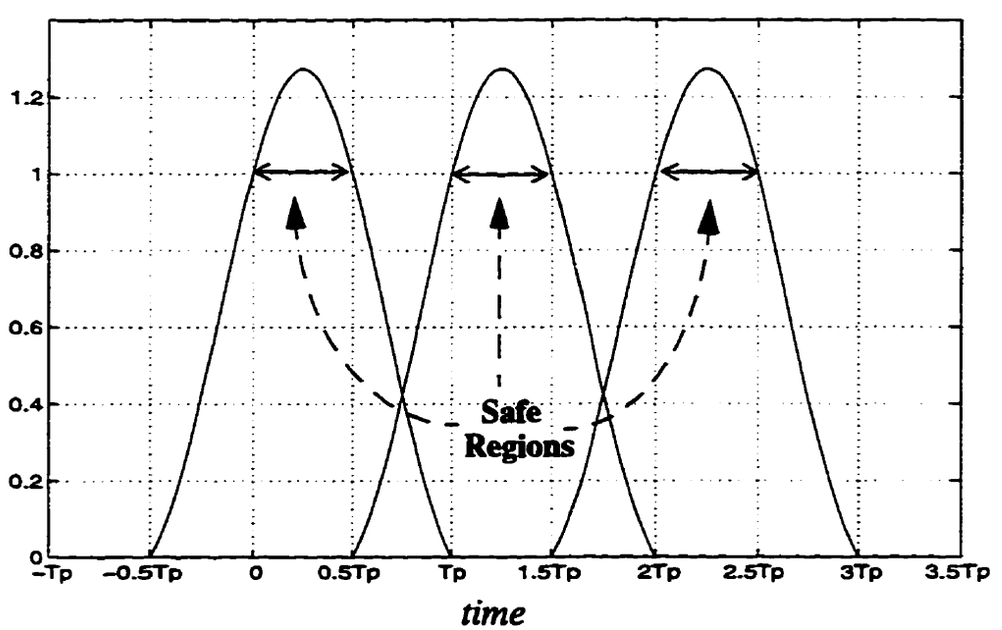

Figure 5.2.1 Illustration of the safe region for 100% excess bandwidth duobinary pulse.

Notice that by ignoring the tail of the duobinary pulse, there is a region which is free of ISI and has a duration of $0.5T_p$. This observation implies that even if the timing error is

not zero, a considerable amount of ISI can be avoided as long as the receiver can obtain the I/Q symbols within this safe region. In order to achieve this goal, the receiver has to sample the IF signal with 4 samples per symbol and selects the proper two samples out of four samples within one symbol period. With this approach, the selected two samples suffer only a small amount of ISI introduced by the tails of the duobinary pulse. Also notice that this approach does not require modification to the transmitter and thus all the discussions in chapter 3 about the transmitter and the channel still apply in this section.

5.2.1 IF-sampling Receiver with 4 Samples Per Symbol

In order to take advantage of the safe region, modifications are required to the digital portion of the receiver. Depending on the timing error, the receiver has to change from one architecture into a slightly different one.

Case 1 : $0 \le t_d \le 0.25T_p$

The receiver architecture for $0 \le t_d \le 0.25T_p$ is shown in Figure 5.2.2.

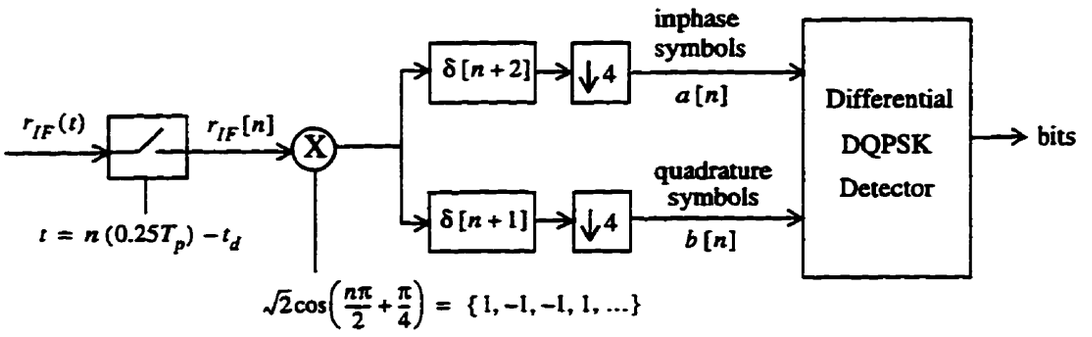

Figure 5.2.2 Architecture of the IF-sampling receiver with 4 samples per symbol and $0 \le t_d \le 0.25T_p$.

The downconverted IF signal $r_{IF}(t)$ is sampled with a new sampling rate of 4 samples per symbol,

$$F_s = \frac{4}{T_p} \; Hz \tag{5.2.1}$$

Since the IF center frequency depends on the sampling rate, the IF center frequency also takes a new value,

$$f_{IF} = \frac{F_s}{4} = \frac{1}{T_p} \; Hz \tag{5.2.2}$$

With this new IF center frequency, the negative and positive spectra of the IF signal do not overlap unless the bandwidth is greater than 100% excess bandwidth. The donwconverted IF signal is given as,

$$\begin{aligned} r_{IF}(t) = & \sum_{m=-\infty}^{\infty} I_m \cdot g(t-mT_p) \cdot \cos(2\pi f_{IF} t + \theta) \\ & - \sum_{m=-\infty}^{\infty} Q_m \cdot g(t-mT_p) \cdot \sin(2\pi f_{IF} t + \theta) \\ & + x(t) \cdot \cos(2\pi f_{IF} t + \theta) \\ & - y(t) \cdot \sin(2\pi f_{IF} t + \theta) \end{aligned} \tag{5.2.3}$$

By substituting the sampling time,

$$t = n(0.25T_p) - t_d \tag{5.2.4}$$

and the new value of f_{IF} into $r_{IF}(t)$, the sampled IF signal $r_{IF}[n]$ is obtained as,

$$
\begin{aligned}
r_{IF}[n] = & \sum_{m=-\infty}^{\infty} I_m \cdot g(n0.25T_p - t_d - mT_p) \cdot \cos\left(\frac{n\pi}{2} + \phi\right) \\
& - \sum_{m=-\infty}^{\infty} Q_m \cdot g(n0.25T_p - t_d - mT_p) \cdot \sin\left(\frac{n\pi}{2} + \phi\right) \\
& + x(n0.25T_p - t_d) \cdot \cos\left(\frac{n\pi}{2} + \phi\right) \\
& - y(n0.25T_p - t_d) \cdot \sin\left(\frac{n\pi}{2} + \phi\right) \\
& \text{where } \phi = -\frac{2\pi t_d}{T_p} + \theta
\end{aligned}
\tag{5.2.5}
$$

By performing the operations described in Figure 5.2.2, both the inphase symbols $a[n]$ and the quadrature symbols $b[n]$ are found to be,

$$
\begin{aligned}
a[n] = & \sum_{m=-\infty}^{\infty} I_m \cdot g(nT_p - mT_p + 0.5T_p - t_d) \cdot \cos\phi \\
& - \sum_{m=-\infty}^{\infty} Q_m \cdot g(nT_p - mT_p + 0.5T_p - t_d) \cdot \sin\phi \\
& + x(nT_p + 0.5T_p - t_d) \cdot \cos\phi \\
& - y(nT_p + 0.5T_p - t_d) \cdot \sin\phi
\end{aligned}
\tag{5.2.6}
$$

$$
\begin{aligned}
b[n] = & \sum_{m=-\infty}^{\infty} I_m \cdot g(nT_p - mT_p + 0.25T_p - t_d) \cdot \sin\phi \\
& + \sum_{m=-\infty}^{\infty} Q_m \cdot g(nT_p - mT_p + 0.25T_p - t_d) \cdot \cos\phi \\
& + x(nT_p + 0.25T_p - t_d) \cdot \sin\phi \\
& + y(nT_p + 0.25T_p - t_d) \cdot \cos\phi
\end{aligned}
\tag{5.2.7}
$$

By representing these two equations with a diagram, a discrete-time model is obtained and shown in Figure 5.2.3. The observation of the safe region can also be made from these two equations. Recall that the truncated 100% excess bandwidth duobinary pulse is defined as,

$$g_T(t) = \begin{cases} \dfrac{0.25T_p^2 \cdot \sin(2\pi t/T_p)}{\pi t(0.5T_p - t)} & \text{for } -0.5T_p \le t \le T_p \\ 0 & \text{otherwise} \end{cases} \tag{5.2.8}$$

By approximating $g(t)$ with $g_T(t)$, it follows that

$$g(nT_p - mT_p + 0.5T_p - t_d) = \begin{cases} g_T(0.5T_p - t_d) & \text{for n = m} \\ 0 & \text{otherwise} \end{cases} \tag{5.2.9}$$

and

$$g(nT_p - mT_p + 0.25T_p - t_d) = \begin{cases} g_T(0.25T_p - t_d) & \text{for n = m} \\ 0 & \text{otherwise} \end{cases} \tag{5.2.10}$$

By substituting these two approximations into $a[n]$ and $b[n]$, the received inphase and quadrature symbols can be simplified as,

$$\begin{aligned} a[n] &= A_4 \cdot (I_n \cdot \cos\phi - Q_n \cdot \sin\phi) \\ &\quad + x(nT_p + 0.5T_p - t_d) \cdot \cos\phi \\ &\quad - y(nT_p + 0.5T_p - t_d) \cdot \sin\phi \end{aligned} \tag{5.2.11}$$

$$\begin{aligned} b[n] &= B_4 \cdot (I_n \cdot \sin\phi + Q_n \cdot \cos\phi) \\ &\quad + x(nT_p + 0.25T_p - t_d) \cdot \sin\phi \\ &\quad + y(nT_p + 0.25T_p - t_d) \cdot \cos\phi \end{aligned} \tag{5.2.12}$$

where $A_4 = g_T(0.5T_p - t_d)$ and $B_4 = g_T(0.25T_p - t_d)$

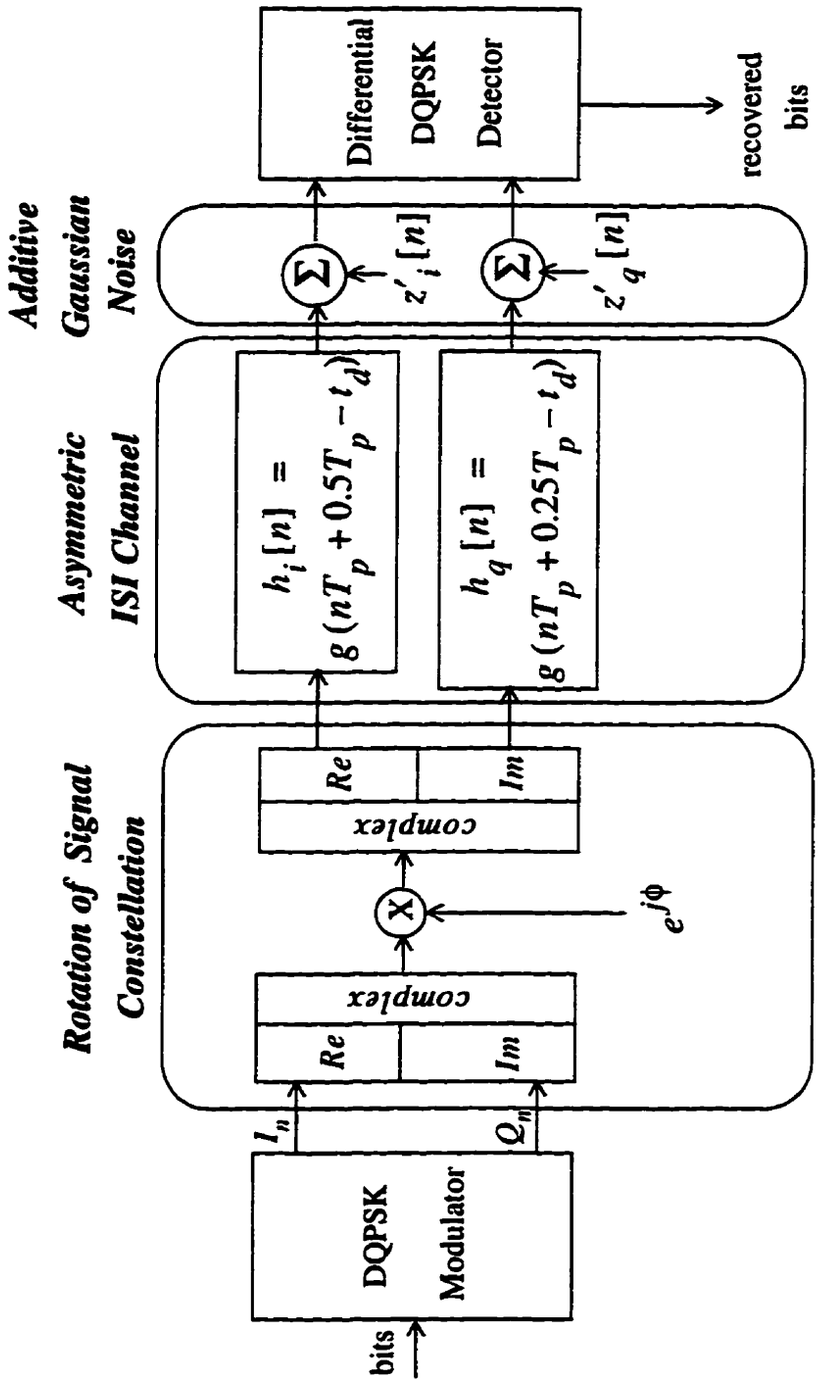

Figure 5.2.3 Equivalent discrete-time model for IF-sampling system with 4 samples per symbol and $0 \le t_d \le 0.25T_p$.

The values of A_4 and B_4 are listed in Table 5.2.1 for different timing errors.

t_d	A_4	B_4
0	1.0	1.27
$0.10T_p$	1.17	1.23
$0.125T_p$	1.20	1.20
$0.15T_p$	1.23	1.17
$0.20T_p$	1.26	1.09
$0.25T_p$	1.27	1.0

Table 5.2.1 Values of A_4 and B_4 for $0 \le t_d \le 0.25T_p$.

As clearly shown in Equations 5.2.11 and 5.2.12, both received inphase and quadrature symbols consist only of the present I/Q symbols and noise. Therefore, with the assumption of using a truncated 100% excess bandwidth duobinary pulse, intersymbol interference no longer exists in the system. Also notice that for any t_d, both A_4 and B_4 are always greater than or equal to 1.0 . Thus the I/Q symbols are always amplified by A_4 and B_4. However, when the gains on I channel (A_4) and Q channel (B_4) are different, the system suffers from the gain imbalance. From Table 5.2.1, the gain imbalance is worst at the two end-points of t_d, that is, when $t_d = 0$ or when $t_d = 0.25T_p$. As t_d increases from 0, the gain imbalance decreases and eventually vanishes when $t_d = 0.125T_p$. When t_d increases further, the gain imbalance becomes severe again and finally reaches the worst value at $t_d = 0.25T_p$. It will be shown later that the gain imbalance plays a significant role in determining the system performance.

In addition to the signal, the statistics of the two new discrete-time noise

sequences are also analyzed. From Equations 5.2.6 and 5.2.7, the two new noise sequences, $z'_i[n]$ and $z'_q[n]$, are defined as

$$z'_i[n] = x(nT_p + 0.5T_p - t_d) \cdot \cos\phi - y(nT_p + 0.5T_p - t_d) \cdot \sin\phi \quad (5.2.13)$$

and

$$z'_q[n] = x(nT_p + 0.25T_p - t_d) \cdot \sin\phi + y(nT_p + 0.25T_p - t_d) \cdot \cos\phi \quad (5.2.14)$$

The autocorrelation of $z'_i[n]$ is defined as,

$$\phi_{z'_i z'_i}[n;n-k] = E\{z'_i[n] \cdot z'_i[n-k]\} \quad (5.2.15)$$

Substituting the definition of $z'_i[n]$ into Equation 5.2.15 yields,

$$\begin{aligned}\phi_{z'_i z'_i}[n;n-k] = E\{ & x(nT_p + 0.5T_p - t_d) \cdot x(nT_p - kT_p + 0.5T_p - t_d) \cdot \cos^2\phi \\ & - x(nT_p + 0.5T_p - t_d) \cdot y(nT_p - kT_p + 0.5T_p - t_d) \cdot \cos\phi \cdot \sin\phi \\ & - x(nT_p - kT_p + 0.5T_p - t_d) \cdot y(nT_p + 0.5T_p - t_d) \cdot \cos\phi \cdot \sin\phi \\ & + y(nT_p + 0.5T_p - t_d) \cdot y(nT_p - kT_p + 0.5T_p - t_d) \cdot \sin^2\phi \}\end{aligned} \quad (5.2.16)$$

Since $\phi_{xy}(\tau) = 0$ for all time τ, the middle two terms are zero. Also $\phi_{xx}(\tau) = \phi_{yy}(\tau)$ for all time τ. Therefore the autocorrelation of $z'_i[n]$ is simplified as

$$\phi_{z'_i z'_i}[n;n-k] = \phi_{z'_i z'_i}[k] = \phi_{xx}(kT_p) = \frac{2N_o}{T_p} \cdot \delta[k] \quad (5.2.17)$$

In order to have the last equality of the above equation to be valid, the signal bandwidth is assumed to be 100% excess bandwidth. It is clear that the autocorrelation of $z'_i[n]$ depends only on k and is nonzero only when $k = 0$. Thus $z'_i[n]$ is a wide-sense stationary white process.

By repeating the above argument, the autocorrelation of $z'_q[n]$ is obtained as,

$$\phi_{z'_q z'_q}[n;n-k] = \phi_{z'_q z'_q}[k] = \phi_{xx}(kT_p) = \frac{2N_o}{T_p} \cdot \delta[k] \qquad (5.2.18)$$

So $z'_q[n]$ is also a wide-sense stationary white process.

The cross-correlation of $z'_i[n]$ and $z'_q[n]$ is defined as,

$$\phi_{z'_i z'_q}[n;n-k] = E\{z'_i[n] \cdot z'_q[n-k]\} \qquad (5.2.19)$$

Substituting the definitions of $z'_i[n]$ and $z'_q[n]$ into the above equation yields,

$$\begin{aligned}\phi_{z'_i z'_q}[n;n-k] = E\{&x(nT_p + 0.5T_p - t_d) \cdot x(nT_p - kT_p + 0.25T_p - t_d) \cdot \cos\phi \cdot \sin\phi \\ &+ x(nT_p + 0.5T_p - t_d) \cdot y(nT_p - kT_p + 0.25T_p - t_d) \cdot \cos^2\phi \\ &- x(nT_p - kT_p + 0.25T_p - t_d) \cdot y(nT_p + 0.5T_p - t_d) \cdot \sin^2\phi \\ &- y(nT_p + 0.5T_p - t_d) \cdot y(nT_p - kT_p + 0.25T_p - t_d) \cdot \cos\phi \cdot \sin\phi\}\end{aligned} \qquad (5.2.20)$$

Again the middle two terms are zero because $\phi_{xy}(\tau) = 0$ for all τ. Since $\phi_{xx}(\tau) = \phi_{yy}(\tau)$ for all τ, the first and the last terms cancel each other and therefore,

$$\phi_{z'_i z'_q}[n;n-k] = \phi_{z'_i z'_q}[k] = 0 \qquad \text{for all k} \qquad (5.2.21)$$

Finally since $x(t)$ and $y(t)$ are uncorrelated Gaussian processes and $z'_i[n]$ and $z'_q[n]$ are linear combinations of $x(t)$ and $y(t)$, therefore $z'_i[n]$ and $z'_q[n]$ are also Gaussian processes. In summary, both $z'_i[n]$ and $z'_q[n]$ are discrete-time wide-sense stationary uncorrelated Gaussian processes.

Case 2 : $-0.25T_p \le t_d \le 0$

When the timing error t_d takes a negative value from 0 to $-0.25T_p$, the positions of the two proper samples are shifted to the beginning of a symbol period. This change is reflected in a slightly different receiver architecture shown in Figure 5.2.4.

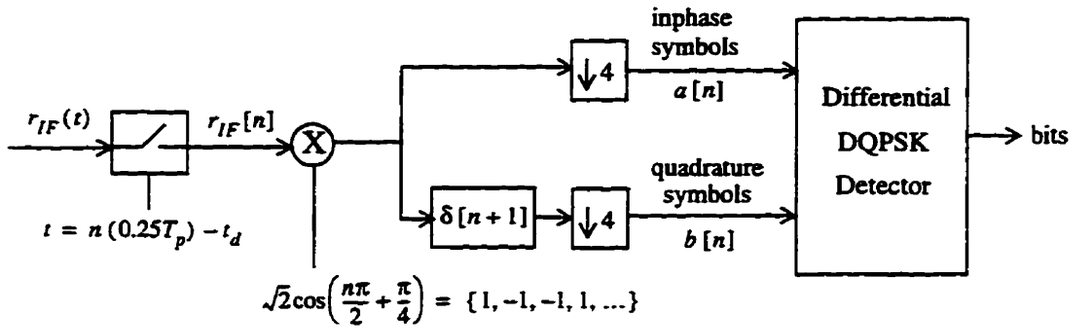

Figure 5.2.4 Architecture of the IF-sampling receiver with 4 samples per symbol and $-0.25T_p \le t_d \le 0$.

Notice that the only modification is the time delay on the inphase and quadrature

channels. By having zero delay on the inphase channel, the receiver can extract the first sample and assign it as the received inphase symbol. On the other hand, by having an time advance on the quadrature channel, the receiver extracts the second sample and assigns it as the received quadrature symbol. The mathematical expressions for $a[n]$ and $b[n]$ are obtained by processing $r_{IF}(t)$ (Equation 5.2.3) as shown in Figure 5.2.4. It is found that

$$\begin{aligned} a[n] = & \sum_{m=-\infty}^{\infty} I_m \cdot g(nT_p - mT_p - t_d) \cdot \cos\phi \\ & - \sum_{m=-\infty}^{\infty} Q_m \cdot g(nT_p - mT_p - t_d) \cdot \sin\phi \\ & + x(nT_p - t_d) \cdot \cos\phi \\ & - y(nT_p - t_d) \cdot \sin\phi \end{aligned} \tag{5.2.22}$$

and

$$\begin{aligned} b[n] = & \sum_{m=-\infty}^{\infty} I_m \cdot g(nT_p - mT_p + 0.25T_p - t_d) \cdot \sin\phi \\ & + \sum_{m=-\infty}^{\infty} Q_m \cdot g(nT_p - mT_p + 0.25T_p - t_d) \cdot \cos\phi \\ & + x(nT_p + 0.25T_p - t_d) \cdot \sin\phi \\ & + y(nT_p + 0.25T_p - t_d) \cdot \cos\phi \end{aligned} \tag{5.2.23}$$

These two equations are represented by the discrete-time model shown in Figure 5.2.5.

Again, by approximating $g(t)$ with the truncated 100% excess bandwidth duobinary pulse, Equations 5.2.22 and 5.2.23 are simplified as,

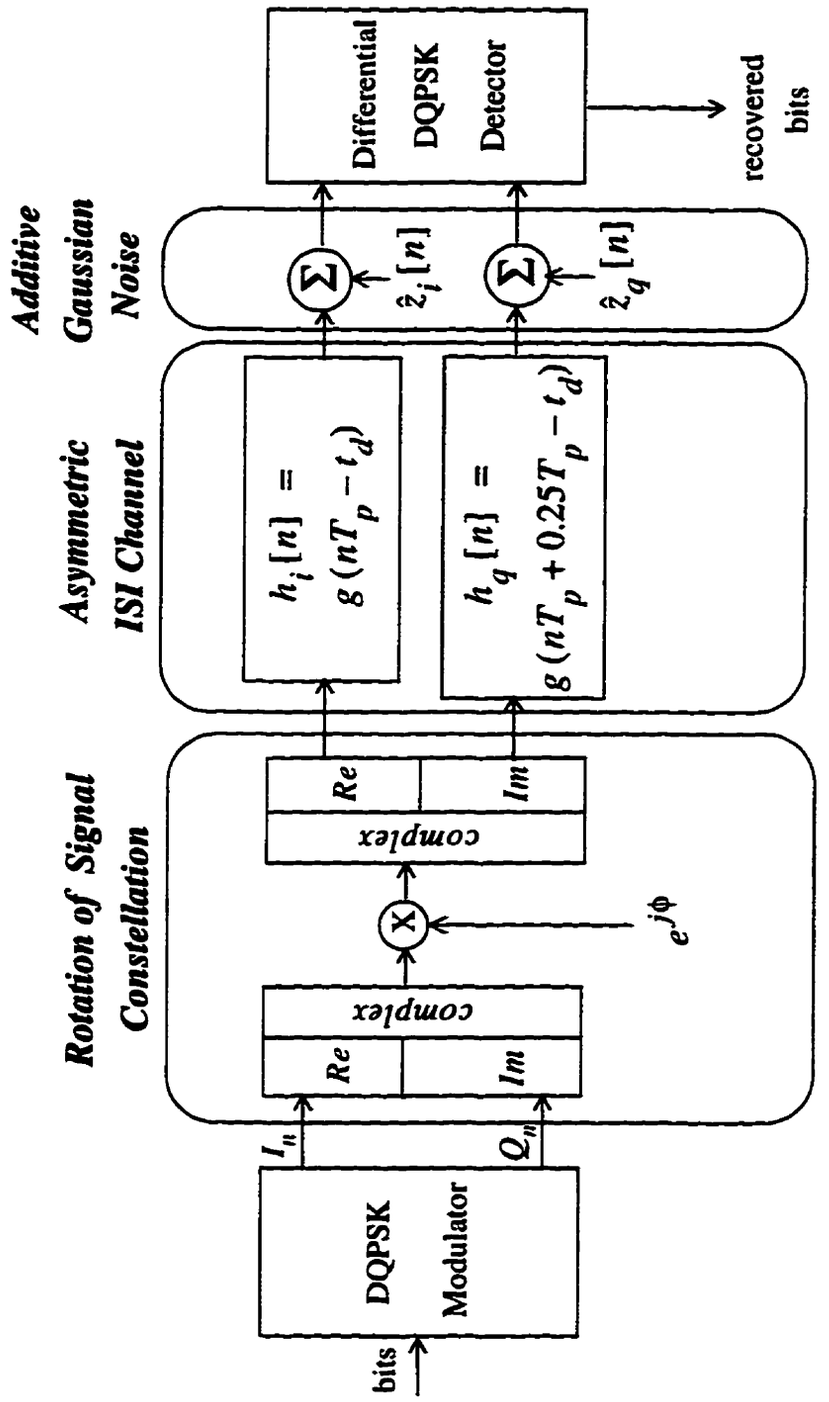

Figure 5.2.5 Equivalent discrete-time model for IF-sampling system with 4 samples per symbol and $-0.25T_p \le t_d \le 0$.

$$\begin{aligned} a[n] &= C_4 \cdot (I_n \cdot \cos\phi - Q_n \cdot \sin\phi) \\ &\quad + x(nT_p - t_d) \cdot \cos\phi \\ &\quad - y(nT_p - t_d) \cdot \sin\phi \end{aligned} \tag{5.2.24}$$

and

$$\begin{aligned} b[n] &= D_4 \cdot (I_n \cdot \sin\phi + Q_n \cdot \cos\phi) \\ &\quad + x(nT_p + 0.25T_p - t_d) \cdot \sin\phi \\ &\quad + y(nT_p + 0.25T_p - t_d) \cdot \cos\phi \end{aligned} \tag{5.2.25}$$

where $C_4 = g_T(-t_d)$ and $D_4 = g_T(0.25T_p - t_d)$

The values of C_4 and D_4 are tabulated in Table 5.2.2.

t_d	C_4	D_4
0	1.0	1.27
$-0.10T_p$	1.17	1.23
$-0.125T_p$	1.20	1.20
$-0.15T_p$	1.23	1.17
$-0.20T_p$	1.26	1.09
$-0.25T_p$	1.27	1.0

Table 5.2.2 Values of C_4 and D_4 for $-0.25T_p \le t_d \le 0$.

The two new discrete-time noise sequences namely $\hat{z}_i[n]$ and $\hat{z}_q[n]$ are,

$$\hat{z}_i[n] = x(nT_p - t_d) \cdot \cos\phi - y(nT_p - t_d) \cdot \sin\phi \qquad (5.2.26)$$

and

$$\hat{z}_q[n] = x(nT_p + 0.25T_p - t_d) \cdot \sin\phi + y(nT_p + 0.25T_p - t_d) \cdot \cos\phi \qquad (5.2.27)$$

The two autocorrelation functions for $\hat{z}_i[n]$ and $\hat{z}_q[n]$ are found to be,

$$\phi_{\hat{z}_i\hat{z}_i}[n;n-k] = \phi_{\hat{z}_i\hat{z}_i}[k] = \phi_{xx}(kT_p) = \frac{2N_o}{T_p} \cdot \delta[k] \qquad (5.2.28)$$

$$\phi_{\hat{z}_q\hat{z}_q}[n;n-k] = \phi_{\hat{z}_q\hat{z}_q}[k] = \phi_{xx}(kT_p) = \frac{2N_o}{T_p} \cdot \delta[k] \qquad (5.2.29)$$

It is clear that both autocorrelation functions depend only on the time shift k and therefore the two noise sequences are wide-sense stationary. Also when the signal bandwidth is 100% excess bandwidth, the autocorrelation functions are equal to a scaled discrete-time delta function and therefore the two noise sequences are also white.

In addition to the autocorrelation functions, the cross-correlation function is determined as,

$$\phi_{\hat{z}_i\hat{z}_q}[n;n-k] = \phi_{\hat{z}_i\hat{z}_q}[k] = 0 \qquad \text{for all k} \qquad (5.2.30)$$

Thus the two processes are uncorrelated for all time shifts k. Besides, since both noise processes are linear combination of two uncorrelated Gaussian processes, $\hat{z}_i[n]$ and $\hat{z}_q[n]$ are also Gaussian processes. Note that the statistics of the two noise sequences are exactly the same for both cases of t_d.

5.2.2 Performance of the IF-sampling system with 4 Samples Per Symbol

The performance of the IF-sampling with 4 samples per symbol is simulated using the discrete-time model shown in Figure 5.2.3. Here it is assumed that $0 \le t_d \le 0.25T_p$ and $\phi = 0$. Since modification is made only in the receiver, the definition of signal-to-noise ratio defined in Equation 4.4.15 still applies.

$$SNR = \frac{1}{4N_o} \tag{5.2.31}$$

Note that the same definition of SNR is used for all three systems.

The simulation results are shown in Figure 5.2.6. Two important points are observed from the simulation. Firstly, by using the bit error rate curve for the IF-sampling system with 2 samples per symbol and zero timing error as a reference, the simulation shows that the IF-sampling system with 4 samples per symbol can generate a better performance (from 2 dB to 16 dB) for some timing errors. In other words, instead of degrading the performance, a certain timing error can actually improve the performance in this second solution system. For example, at a bit error rate of 10^{-3}, any timing error ranging from $0.1T_p$ to $0.2T_p$ generates a better performance than the one corresponding to 2 samples per symbol, and the best improvement is about 1 dB.

Secondly, the simulation results are consistent with the argument that the system performance is mainly controlled by the gain imbalance between the received I/Q symbols. From Table 5.2.1, it is clear that the gain imbalance starts with the worst value at $t_d = 0$. As t_d increases to $0.125T_p$, the gain imbalance decreases and eventually drops to zero at $t_d = 0.125T_p$. However, as t_d further increases to $0.25T_p$, the gain

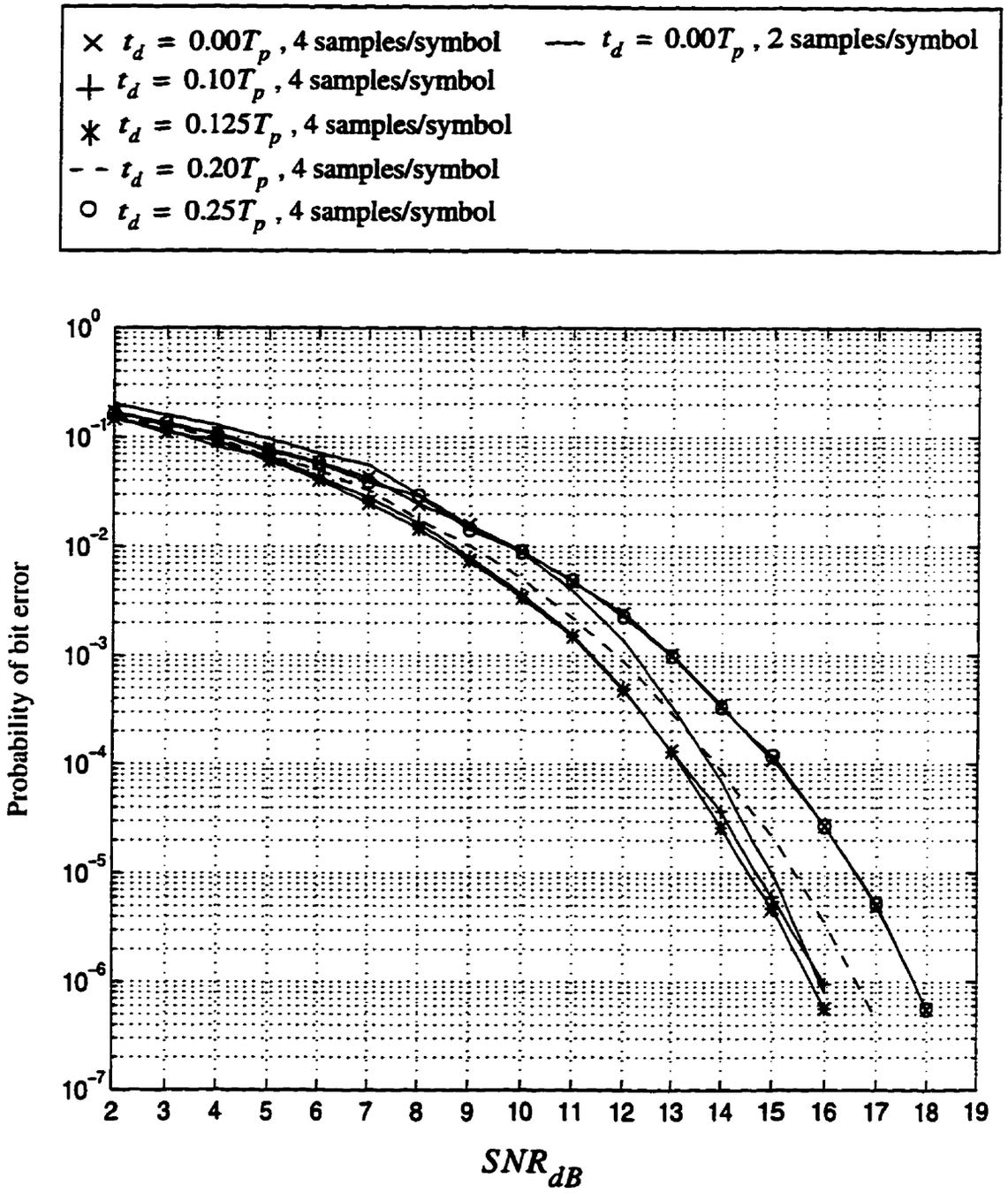

Figure 5.2.6 Simulated performance of the IF-sampling system with 4 samples per symbol. Note that $\phi = 0$.

imbalance increases and eventually reaches the worst value at $t_d = 0.25T_p$. The same pattern is observed in the simulation results. The timing errors of 0 and $0.25T_p$ give the same and worst performance. At the error rates of 10^{-3} and 10^{-6} , the performance degradations (compared with the 2 samples per symbol system and $t_d = 0$) are about 0.8 dB and 2 dB respectively. As t_d becomes closer to $0.125T_p$, the performance is getting better. The best performance occurs at $t_d = 0.125T_p$ and the improvements at error rates of 10^{-3} and 10^{-6} are about 1 dB and 0.2 dB respectively.

However a little inconsistency is also shown in the bit error rate curves for $t_d = 0.1T_p$ and $t_d = 0.125T_p$. These two timing errors generate an almost identical performance from 2 dB to 13 dB. Only when the *SNR* is greater than 13 dB, then $t_d = 0.125T_p$ gives a slightly better performance than $t_d = 0.1T_p$.

5.3 Summary

In order to combat the timing error problem, two solutions were proposed in this chapter. The first solution is a DS-SS IF-sampling system with 11 chip Barker sequence. This system uses the autocorrelation of the Barker sequence to suppress the delayed path and thus alleviates the asymmetric intersymbol interference. In order for the system to operate properly, the three system parameters (G_I, G_Q and N_d) must be modified in real-time for the variation of t_d. As t_d increases from 0 to $0.25T_c$, the system performance is gradually degraded from 1 dB loss to 7 dB loss at a bit error rate of 10^{-3} .

In the second solution, the special pulse shape of the 100% excess bandwidth duobinary pulse is used to avoid the intersymbol interference. In this system, the sampling rate is raised to 4 samples per symbol. The system performance also depends on the timing error but with a different trend. As t_d increases from 0 to $0.125T_p$, the performance is gradually improved from 0.8 dB loss to 1 dB gain. As t_d increases further to $0.25T_p$, the performance is downgraded from 1 dB gain back to 0.8 dB loss. Another unique characteristics of this system is that certain timing errors can actually improve the performance of the receiver and the best performance occurs at $t_d = 0.125T_p$. Overall the second solution outperforms the first solution in terms of performance and complexity.

Chapter 6 Conclusion and Future Work

In chapter 2, two important concepts have served as the foundations for the design of the proposed IF-sampling receiver. With the first concept, $F_s/4$ downconversion, the receiver can use a very simple digital structure to extract the inphase and quadrature samples from the continuous-time bandpass IF signal. In order to employ this technique, the receiver must satisfy one requirement : the IF center frequency must be an odd integer multiple of a quarter of the sampling rate. In other words, this technique specifies the IF center frequency and provides the idea for the architecture of the IF-sampling receiver. The second concept involves three sampling theorems which are (1) the Nyquist sampling theorem, (2) the bandpass sampling theorem and (3) the sampling theorem for linearly modulated signals with zero intersymbol interference. The objective of the first two theorems is to avoid spectral overlap of the sampled signal. However, in the demodulation of a linearly modulated signal, a certain form of spectral overlap is desired and thus a lower sampling rate is allowed. It is found that the minimum sampling rate for the recovery of the inphase and quadrature symbols is 2 samples per symbol. This sampling rate is adopted in the proposed IF-sampling receiver.

Based on the ideas from the two concepts, the architecture of the IF-sampling receiver is derived in chapter 3. The receiver samples the IF signal with 2 samples per symbol and extracts the inphase and quadrature symbols using a simple structure. In addition to the receiver, both the transmitter and the channel are also specified. The transmitter performs a typical linear modulation scheme while the channel is assumed to be an additive bandpass white Gaussian noise channel. No channel fading is considered in this thesis. With the proposed IF-sampling receiver, both the time and frequency domain criteria for zero intersymbol interference are derived. By using the frequency domain criterion, one can prove that the minimum bandwidth for achieving zero

intersymbol interference is $2/T_p$ Hz. Any bandwidth less than $2/T_p$ Hz must generate ISI. In addition to the minimum bandwidth, the actual signalling pulse for zero ISI and minimum bandwidth is also derived and the result is a 100% excess bandwidth duobinary pulse.

With the IF-sampling receiver, the effect of the bandpass white Gaussian noise is studied. Both the first and second order statistics are obtained for the two noise sequences at the output of the IF-sampling receiver. In addition to the study of noise, an equivalent discrete-time model is also derived for the IF-sampling communications system. This model is shown to be useful for analyzing the effect of the complete system on the information symbols. Besides, the discrete-time model is also used as a simulation model to obtain the system performance. Simulation results show that the timing error can severely degrade the system performance and cause irreducible bit error rate. Also due to the presence of the asymmetric intersymbol interference, a phase shift can cause significant variation in the system performance.

Two solutions are suggested to combat the severe degradation caused by the timing error. The first solution is a DS-SS IF-sampling system with an 11 chip Barker sequence. By using the autocorrelation of the Barker sequence, the system can suppress the delayed paths in the asymmetric ISI channel. Inside this system, there are three parameters, G_I, G_Q and N_d, depending on the timing error and therefore the system must be able to modify these three parameters in real-time. Simulation results show that as t_d increases from 0 to $0.25T_p$, the system performance is gradually degraded from 1 dB loss (best performance) to 7 dB loss (worst performance) at error rate of 10^{-3}.

A different approach is used in the second solution which takes advantage of the special pulse shape of the 100% excess bandwidth duobinary pulse. By sampling the

continuous-time IF signal with 4 samples per symbol and selecting the proper two samples, the system can actually avoid a considerable amount of ISI. One unique characteristics of this system is that certain timing errors can actually produce performance improvement. As t_d increases from 0 to $0.125T_p$, the performance is improved from 0.8 dB loss to 1 dB gain. As t_d increases further to $0.25T_p$, the performance is degraded from 1 dB gain back to 0.8 dB loss. Therefore the best performance occurs at $t_d = 0.125T_p$ whereas the worst performance is at both $t_d = 0$ and $t_d = 0.25T_p$. It is also found that this performance trend is consistent with the gain imbalance introduced by the 100% excess bandwidth duobinary pulse. In terms of both system complexity and performance, the second solution outperforms the first solution.

Several issues are not being considered in this project. Firstly, the modulation scheme is restricted to be linear in this project. Therefore all three systems mentioned in this thesis cannot be used for nonlinear modulation schemes, such as continuous phase frequency shift keying (CPFSK) or continuous phase modulation (CPM). Further research is required for the design of the IF-sampling receiver for nonlinear modulation schemes. Secondly, equalizer (either linear or nonlinear) can also be used to alleviate the asymmetric intersymbol interference. However, due to the asymmetric nature of the intersymbol interference, a conventional equalizer structure may not be adequate. Further work needs to be done in this area.

References

[1] A.V. Oppenheim and R.W. Schafer, "Discrete-Time Signal Processing", Prentice-Hall, Englewood Cliffs, New Jersey 07632, 1989.

[2] J.G. Proakis, "Digital Communications", 3rd Edition, McGraw Hill Inc., 1995.

[3] J.K. Cavers and M.W. Liao, "Adaptive Compensation for Imbalance and Offset Losses in Direct Conversion Transceivers", IEEE Transactions on Vehicular Technology, vol. 42, pp. 581-588, no. 4, November 1993.

[4] G.J. Saulnier, C.M. Puckette, IV, R.C. Gaus, JR., R.J. Dunki-Jacobs, and T.E. Thiel, "A VLSI Demodulator for Digital RF Network Applications: Theory and Results", IEEE Journal on Selected Areas in Communications, vol. 8, pp. 1500-1511, no. 8, October 1990.

[5] E.O. Brigham, "The Fast Fourier Transform and its Applications", Englewood Cliffs, N.J. : Prentice-Hall, 1988.

[6] S. Benedetto, E. Biglieri, and V. Castellani, "Digital Transmission Theory", Prentice-Hall, Englewood Cliffs, New Jersey 07632, 1987.

[7] J.H. Lodge, "Digital Implementation of Narrowband Radio", Report from Communications Research Centre, 1989.

[8] A. Bateman and D.H. Haines, "Direct Conversion Transceiver Design for Compact Low-Cost Portable Mobile Radio Terminals", Proc. IEEE Vehicular Technology Conference, San Franciso, CA, May 1989.

[9] H. Samueli and B.C. Wong, "A VLSI Architecture for a High-Speed All-Digital Quadrature Modulator and Demodulator for Digital Radio Applications", IEEE Journal on Selected Areas in Communications, vol. 8, pp. 1512-1519, no. 8, October 1990.

[10] E. Patton, "Hardware Implementation of the Digital Rake Transceiver", Master Thesis, pp. 39-58, University of Calgary, 1993.

[11] H. Meyr and R. Subramanian, "Advanced Digital Receiver Principles and Technologies for PCS", IEEE Communications Magazine, pp. 68-78, January 1995.

[12] C.L. Liu, and K. Feher, "Noncoherent Detection of π/4-QPSK Systems in a CCI-AWGN Combined Interference Environment", Proc. IEEE Vehicular Technology Conference, San Franciso, CA, May 1989.

[13] D.A. Shnidman, "A Generalized Nyquist Criterion and an Optimum Linear Receiver for a Pulse Modulation System", The Bell System Technical Journal, vol. 46, pp. 2163-2177, no. 9, November 1967.

[14] S. Chennakeshu, and G.J. Saulnier, "Differential Detection of π/4-Shifted-DQPSK for Digital Cellular Radio", IEEE Transactions on Vehicular Technology, vol. 42, pp. 46-57, no. 1, February 1993.

[15] Y. Akaiwa, and Y. Nagata, "Highly Efficient Digital Mobile Communications with a Linear Modulation Method", IEEE Journal on Selected Areas in Communications, vol. SAC-5, pp. 890-895, June 1987.

[16] P.C. Wong and P.T. Mathiopoulos, "Nonredundant Error Correction Analysis and Evaluation of Differentially Detected pi/4-Shift DQPSK Systems in a Combined CCI and AWGN Environment", IEEE Transactions on Vehicular Technology, vol. 41, pp. 35-48, no. 1, February 1992.

[17] C.S. Ng, T.T. Tjhung, F. Adachi and K.M. Lye, "On the Error Rates of Differentially Detected Narrowband pi/4-DQPSK in Rayleigh Fading and Gaussian Noise", IEEE Transactions on Vehicular Technology, vol. 42, pp. 259-265, no. 3, August 1993.

[18] K.A. Hamied and G.L. Stuber, "An Adaptive Truncated MLSE Receiver for Japanese Personal Digital Cellular", IEEE Transactions on Vehicular Technology, vol. 45, pp. 41-50, no. 1, February 1996.

[19] W.H. Press, S.A. Teukolsky, W.T. Vetterling, and B.P. Flannery, "Numerical Recipes in C : The Art of Scientific Computing", 2nd Edition, Cambridge University Press, 1992.

[20] F.J. Casadevall, and A. Valdovinos, "Performance Analysis of QAM Modulations Applied to the LINC Transmitter", IEEE Transactions on Vehicular Technology, vol. 42, pp. 399-406, no. 4, November 1993.

[21] R.L. Pickholtz, D.L. Schilling, and L.B. Milstein, "Theory of Spread-Spectrum Communications — A Tutorial", IEEE Transcations on Communications, vol. com-30, pp. 855-884, no. 5, May 1982.

[22] "Draft Standard IEEE 802.11 Wireless LAN", pp. 267-276, 1 December 1994.

[23] J.K. Holmes, "Coherent Spread Spectrum Systems," 1990 Robert E. Krieger Publishing Company, Inc. , pp. 564, 618

[24] G.R. Cooper, C.D. McGillem, "Modern Communications and Spread Spectrum," 1986 McGraw-Hill, pp. 290 .

[25] D.V. Sarwate, and M.B. Pursley, "Crosscorrelation Properties of Pseudorandom and Related Sequences", Proceedings of the IEEE, vol. 68, pp. 593-619, no. 5, May 1980.

[26] G.W. Wornell, "Emerging Applications of Multirate Signal Processing and Wavelets in Digital Communications", Proceedings of the IEEE, vol. 84, no. 4, April 1996.

[27] R. Subramanian, "Advanced Digital Receiver Design for Paging", Communication Systems Design, vol. 2, pp. 53-64, no. 6, June 1996.

[28] J.K. Cavers and S.P. Stapleton, "A DSP-Based Alternative to Direct Conversion Receivers for Digital Moible Communications", in Proc. IEEE Global Telecommun. Conf., San Diego, CA, Dec 1990.

[29] P. Estabrook and B.B. Lusignan, "The Design of a Mobile Radio Receiver using a Direct Conversion Architecture", Proc. IEEE Vehicular Technology Conference, San Franciso, 1989, pp. 63-72.

[30] "HSP43216 Manual of Harris Semiconductor", Jan 1994, pp. 3-43 to 3-59.

[31] "Z2000 Spread-Spectrum Transceiver Manual of Zilog", pp. A-1 to A-11.